CRANFIELD UNIVERSITY

Pongpun Othaganont

Optimisation Methods for Battery Electric Vehicle Powertrain

School of Aerospace Transport and Manufacturing
PhD in Transport systems

PhD Thesis
Academic Year: 2017

Supervisor: Dr Daniel J. Auger
Dr James F. Whidborne
July 2017

CRANFIELD UNIVERSITY

School of Aerospace Transport and Manufacturing
PhD in Transport systems

PhD Thesis

Academic Year 2017

Pongpun Othaganont

Optimisation Methods for Battery Electric Vehicle Powertrain

Supervisor: Dr Daniel J. Auger
Dr James F. Whidborne
July 2017

This thesis is submitted in partial fulfilment of the requirements for the degree of PhD

ABSTRACT

The battery electric vehicle (BEV) is considered to be one of the solutions for reducing greenhouse gasses and an alternative means of transportation. However, some current limitations such as higher powertrain costs, limited driving range and negative perceptions of that range, have reduced BEVs' popularity.

This thesis aims to improve the tank-to-wheel energy consumption of the BEV by presenting possible powertrain architectures and developing new tools for powertrain analysis. The study has two main objectives; the first is to evaluate different possible powertrain topologies. The selected topologies include the single-motor single-axle, the double-motor double-axle, the in-wheel-motor single-axle and the in-wheel-motor double-axle. Models of these powertrains have been modified from the Quasi-Static toolbox, using vehicle parameters from the Nissan Leaf and subject to state assumptions. The multi-objective optimisation method has been applied to establish the costs/benefits of energy consumption, acceleration performance and powertrain cost. The results show that each topology presents its own benefits as the in-wheel types are good at energy efficiency and drivability, while the cost of the powertrain is the major drawback. The non-in-wheel-motor vehicle provides sufficient energy efficiency and driveability with lower powertrain cost.

The second objective is to evaluate a possible alternative tool for BEV powertrain modelling and optimisation. The tool consists of four methodologies: sensitivity analysis, differential flatness, the Chebfun computational tool and the multi-disciplinary optimisation method. The study presents a possible alternative optimisation tool which may perhaps benefit the designer. This new tool may not be as convenient as the previous one; however, the new tool may give the designer greater understanding and insight into the BEV powertrain.

Keywords: battery electric vehicle, multi-objective optimisation, powertrain topologies, sensitivity analysis, differential flatness, Chebfun, multi-disciplinary optimisation.

ACKNOWLEDGEMENTS

I would like to express my sincere gratitude to all my thesis supervisors, Dr Daniel Auger, Dr James Whidborne, Professor Francis Assadian, Dr James Marco and Professor Patrick Luk. This thesis would not have been possible without their teaching, guidance and encouragement throughout the completion of my study. I also want to acknowledge Professor Stephen James, Dr Marko Tirovic and Dr Glenn Sherwood for whose valuable suggestions during this study.

Thank you to the proofreader, Heather Simpkins, to my supervisors, Dr Daniel Auger and Dr James Whidborne, for helping me by checking my English and suggesting improvements.

I would like to offer my special thanks to my co-authors of published papers on both sensitivity analysis and powertrain topologies.

I would like to thank the Ministry of Science & Technology, Naresuan University, Thailand, and Cranfield University, UK, for the funding that supported this work.

I would like to thank Morris family, Robert, Aom and Joyce for the cosy accommodation during my study.

I would also like to thank you both of examiners, Professor Keith Burnham and Dr Stefano Longo for providing constructive feedback to improve my thesis.

Finally, I would like to thank my parents, families and friends who have always supported me throughout this study.

TABLE OF CONTENTS

LIST OF FIGURES

LIST OF TABLES

LIST OF ABBREVIATIONS

ABS	Anti-Lock Braking System
BEV	Battery Electric Vehicle
BLISS	Bi-Level Integrated System Synthesis
CO	Collaborative Optimisation
CSSO	Concurrent Subspace Optimisation
CVT	Continuously Variable Transmission
DM-DA	Double-Motor Double-Axle
EMF	Electromotive Force
EPA	The US Environmental Protection Agency
EV	Electric Vehicle
HEV	Hybrid Electric Vehicles
IDF	Individual Disciplinary Feasible
IWM-DA	In-Wheel Motor Double-Axle
IWM-SA	In-Wheel Motor Single-Axle
MDF	Multidisciplinary Feasible
NEDC	New European Driving Cycle
PI	Proportional-Integral
SM-SA	Single-Motor Single-Axle
SOC	State of Charge

1 Introduction

Environmental concerns and the fossil fuel shortage crisis have become global issues recently. In particular, the automobile is regarded as one of the major sources of air pollution and most of them still require fossil fuel as an energy source. One target that the UK needs to achieve is to cut greenhouse gas emissions by 80% by 2050 [1]. In the transport section, the electric vehicle (EV) will be a necessary key to this achievement. In addition, to reach the target more quickly, electricity, which will supply the EVs, should be generated from low-carbon energy sources [2] and components may produce from bio-materials [3].

To encourage people, the UK Department of Transport has announced promotions for road users, some examples include: tax benefits for ultra-low emission vehicles [4], free parking spaces for EVs [5] and subsidised home charging units for EV users [6].

However, pure EVs still suffer from some limitations such as[1]

- High cost of the vehicle due to the battery cost,
- Limited range between recharges,
- Longer recharge time, and
- Small number of recharging infrastructures.

1.1 Background

Early stages of EV

Battery electric vehicles (BEVs) were first invented in the early 19th century which was around 50 years earlier than the first petrol-powered engine was built [7]. However, the BEV did not draw a large amount of attention due to its lower on-board energy storage. At that time, the use of the lead-acid battery with its specific energy at around 0.03 kWh/kg, was hardly comparable with petrol and diesel fuel which provided their specific energy at around 46.4 and 48 MJ/kg (12.8 and 13 kWh/kg) respectively. As a result, this led to the use of the EV being inconvenient as they only afforded a short driving range when compared to internal combustion vehicles and required a long time for recharging.

However, due to the oil crisis in the Middle East in the late 20th century, energy shortages and environmental issues became a global concern. The automotive industry then had to look for an alternative technology in order to use fossil fuel more efficiently and emit less pollution. These approaches challenged the automotive designers to develop sustainable powertrain technology. Thus, EVs were considered as possible solutions for the above concerns and will become one of the candidates for road vehicles in the 21st century [8], [9].

Transition from internal combustion vehicles to pure EV

The hybrid electric vehicle (HEV) is a suitable option at the present time. The HEV combines the advantages of using two or more sources of energy. Two of those generally used are the internal combustion engine and the electric machine. The key advantage of this type of vehicle is its greater fuel efficiency compared with that of the conventional internal combustion vehicles, although the HEV still requires energy from fossil fuel and produces pollution while being driven on the roads. This has led to the need for a vehicle that uses pure electric energy, has its alternative on board energy storage [10] and produces zero tailpipe emissions such the BEV. Furthermore, it will be beneficial if this electricity is generated from low-carbon sources or renewable energy.

Powertrain conversion

The traditional BEV is converted from an internal combustion vehicles by replacing the internal combustion engine with an electric machine and the fuel tank with an electric energy storage unit [11]. However, the transmission system, including clutch, shaft drive, multi ratio gearbox and differential, is still used. As a result, this affects overall transmission efficiency and vehicle weight. Consequently, the electric machine provides a maximum torque at low speed, unlike an internal combustion engine that provides maximum torque when the engine reaches a certain speed. It is possible that an EV can be operated with a single or double ratio transmission rather than the five speed transmission of the internal combustion vehicles. A simplified and higher efficiency transmission, e.g. single-ratio transmission, is possible to use in the BEV as there are many

examples of production BEVs, such as well the Tesla Roadster and the Nissan Leaf.

BEVs available in the market

BEVs tend to be produced more now and are being sold in the marketplace. Several automobile companies have introduced a new BEV, such as the Nissan Leaf [12], the Mitsubishi MiEV [13], the Tesla Model S, X [14], the BMWi [15], the Smart Fortwo electric drive [16], and the BYD e6 [17]. It is quite likely that the BEV will become an everyday-use car since the battery capacity is sufficient for use on a regular daily basis. As Loft (2014) [18] suggested, a range of 150 km is required to cover at least 95% of all daily distances by a car in both the UK and Germany. This is possible within the range per charge provided by most BEVs, such as the Nissan Leaf, Tesla Roadster.

Alternative powertrain topologies

The major advantage of the BEV over the internal combustion vehicles is their flexibility of powertrain arrangement. The possible BEV powertrain topologies are: a single electric machine as in the Nissan Leaf [12], front and rear independent motors as used in the Tesla Model X [14], rear-wheel-drive by twin traction motor with a single speed reduction gearbox as in the Lightning GT [19], [20] and in-wheel motors as presented in most of the concept vehicles.

Benefits and limitations of the flexible powertrain

By using electric machines as the traction power source, around 80% of energy is delivered to the wheels whereas only around 20% efficiency is obtained from internal combustion engines because of much energy being lost as heat [1]. In addition, mechanical parts such as the mechanical differential can be replaced by an electronic one. Eliminating mechanical parts and transferring energy by wire can reduce vehicle weight and mechanical losses. This results in less complexity in terms of mechanical layout, possible device arrangement and more space.

However, some BEV topologies, such as an independent wheel drive using an electronic differential, increases the complexity of the non-linear control which requires an attention to be paid to the design for stability and safety [21], [22]. In addition, the integrated motor to the wheel (hub motor) can add weight to an unsprung mass, which needs to be considered in vehicle handling dynamics and motor vibration [23].

1.2 Problem statement

BEVs provide zero tailpipe-emissions and use energy more efficiently. However, it may not possible to switch immediately from internal combustion vehicles to BEV due to the many limitations of the BEV, such as energy storage capacity, charging facilities [24] and perception of range anxiety.

Guzzella stated some approaches to improving the tank-to-wheel efficiency for EVs in [25] which may increase the attention being paid to the BEV and can be described briefly as:

i. To improve the components' peak efficiency
ii. To improve components' part-load efficiency
iii. To improve a kinetic energy recuperative system
iv. To optimise the structure and parameters of the propulsion system, and
v. To take advantage of the appropriate supervisory control algorithms.

Since the first three issues are beyond the scope of this study, the rest are of more concern; however, this thesis mainly focuses on the fourth issue, which is structure and parameter optimisation.

1.3 Thesis aims, objectives and scope

This thesis aims to improve the tank-to-wheel energy consumption by using the methodology of BEV powertrain components sizing and powertrain system optimisation.

The objectives of this thesis consist of two main concerns; the first objective is to develop a methodology to evaluate different possible BEV powertrain topologies using multi-objective optimisation.

The second objective is to construct and evaluate alternative modelling/ optimisation methodologies for BEV powertrain design. The approaches to be explored include sensitivity analysis, consideration of differential flatness, Chebfun-based methods and multi-disciplinary optimisation.

This thesis is scope to longitudinal vehicle dynamics, considers only BEV powertrain, and focuses on the C-segment passenger car. However, many of the methods could be applied more generally.

1.4 Thesis structure

In Chapter 2, the fundamentals of the BEV powertrain model simulation will be presented and their components will be mathematically described. The implementation of the BEV model for estimating the energy consumption by using the quasi-static backward simulation method will be explained. This chapter is aimed at introducing the general idea of the simulation technique which is generally used for powertrain sizing and optimisation.

Chapter 3 presents the use of a modelling technique as presented in Chapter 2 to optimise the single-motor single-axle (SM-SA) type BEV. The Nissan leaf, SM-SA BEV, as it is equipped with a single traction motor and front-wheel drive, will be used as a benchmark for the optimisation. Results from this chapter will be used to construct the model of different BEV powertrain topologies.

Chapter 4 presents the multi-objective optimisation between three objective functions for four different types of BEV powertrain architectures which are: the SM-SA, double-motor double-axle (DM-DA), in-wheel motor single-axle (IWM-SA) and the in-wheel motor double-axle (IWM-DA). This chapter aims to present a comparative study of some possible BEV topologies. This study is based on a system level design and optimisation from which some assumptions will be included and introduced. Finally, the results will show the merits and limitations of energy efficiency, driveability performance and cost between selected powertrain architectures.

Chapter 5 will present an insight into the BEV powertrain parameters by determining which of those parameters affect the energy consumption the most.

The sensitivity analysis technique will be implemented by starting with first order sensitivity analysis to determine the most sensitive parameter in the BEV powertrain. Then, the second order sensitivity analysis will also be implemented to explore the cross-coupling effect between a pair of powertrain parameters. In other words, the first order sensitivity analysis will present the most important parameter for the energy consumption and the second order sensitivity analysis will determine which pair of parameters have a significant effect on energy consumption. These techniques will be applied to the SM-SA BEV and again the Nissan Leaf is the case study vehicle.

Chapter 6 investigates the differential flatness of the BEV powertrain model. Differential flatness is a property of the system dynamics which means that if an output is flat, the system dynamics can be inverted so that the system input can be calculated from the flat output and its derivatives without iteration. This chapter presents the background to the simulation techniques used for powertrain modelling then introduces the differential flatness and compares them. The results will show the advantages and limitations of the differential flatness for BEV powertrain modelling and optimisation.

Chapter 7 presents an alternative technique for BEV powertrain optimisation. The technique is comprised of sensitivity analysis, presented in Chapter 5, the differential flatness, presented in Chapter 6, and the technique of multi-disciplinary optimisation with a new computation tool, Chebfun [26]. Moreover, the sensitivity analysis technique will be implemented using Chebfun and a new result visualisation is presented.

The final chapter summarises the thesis, indicates the findings, and presents the conclusion, contributions and suggestions for future work.

1.5 Thesis contributions

The main contribution points of this thesis are in Chapters 4, 5, 6 and 7 and are as follows:

- To evaluate cost and benefit of different powertrain topologies of the BEV.

- To develop the second order sensitivity analysis technique to investigate the cross-coupling parameters in the BEV powertrain.
- To determine that the differential flatness property is useful for modelling the BEV powertrain for the purpose of components sizing and optimisation, and indicate its merits and limitations.
- To develop and encourage the use of the alternative methodology of BEV powertrain sizing and optimisation using the Chebfun computational tool and multi-disciplinary optimisation methods.

1.6 Publications in due course

Journal publications

1. Othaganont, P.; Assadian, F.; Auger, D. Sensitivity Analyses for Cross-Coupled Parameters in Automotive Powertrain Optimization. *Energies* 2014, *7*, 3733-3747.
2. Pongpun Othaganont, Francis Assadian and Daniel J. Auger Multi-objective optimization for battery electric vehicle powertrain topologies, Proceedings of the Institution of Mechanical Engineers, Part D: Journal of Automobile Engineering 0954407016671275, published on October 6, 2016

Conference publications

1. Othaganont, P., Assadian, Francis and Marco, James (2012) Battery electric vehicle powertrain simulation to optimise range and performance. In: Powertrain Modelling and Control conference, University of Bradford, UK, 4-6 Sep 2012
2. Othaganont, P. Assadian., F.; Auger, D., *Cycle-based optimisation of multi-speed transmission for battery electric vehicles*, in *Future Powertrain Conference*: National Motorcycle Museum, Solihull, UK, 25–26 February 2014

2 Battery electric vehicle powertrain components and simulation

The model and its simulation are considered to be an indispensable process for concept evaluation, developing a prototype and analysis of a road vehicle. Especially for developing EV, where more electrical components, such as electric machine, power electronics and battery, are required to be developed simultaneously with the mechanical components. These integrations among various engineering disciplines increase the complexity of designing and analysing the powertrain system [27], [28].

Consequently, computational modelling and simulation may be considered as a design tool to decrease development time and cost [27] and shorten the product life cycle. The complexity of the model is dependent on the level of expected results. For example, modelling a powertrain of the road vehicle can be steady-state, quasi-steady or dynamic. Examples of modelling techniques can be further studied in [27].

For developing a longitudinal dynamic of the BEV, generally, performance, cost and safety may be considered as key factors in designing the product. Customers expect the high performance of a vehicle while the automotive company aims to minimise costs while retaining satisfactory performance and safety. As a result, model and simulation is a tool used that predicts performance by requiring less investment.

This chapter will describe a model for BEV. A brief introduction of the motor and its type will be included. BEV components that are used in this simulation and optimisation will be explained in this chapter.

2.1 Vehicle modelling structure

When the energy consumption of a passenger car is considered, in an early stage, the energy estimates of a road vehicle can be found using computer models; these can be used to calculate the amount of energy required to complete a given cycle without needing a physical prototype. This modelling

process can be carried out using computer software, as described in the literature [27]. There are various free vehicle simulation software packages available on the market, such as ADVISOR [29] and the quasi-static toolbox [30]. By using these tools, many properties such as energy consumption, vehicle performance, drivability and cost of the powertrain can be predicted, all before a prototype is created. If the energy consumption is considered, one of the most important things to identify before simulating the model is how the vehicle will be used. For example, a vehicle used in urban or highway traffic consumes energy differently. Therefore, the sequence of vehicle simulation for energy estimation is normally started by choosing the speed profiles for testing the vehicle – called the driving cycle.

2.1.1 Driving cycle

The driving cycle is a standard profile of speed and elevation (and perhaps gear shift for a manual transmission vehicle) which are used as a reference to compare the emissions of the test vehicle. Driving cycles were originally introduced for the comparison of vehicle fuel consumption as measured in dynamometer tests [25], [31]. Several commonly used test cycles applied in Europe are NEDC and Artemis.

- **New European Driving Cycle (NEDC)**

The NEDC is the standard velocity reference for testing light-duty vehicles in Europe. It contains four-repeated cycles of ECE15 that represent urban driving and is followed by the EUDC which represents extra-urban driving under high speed conditions. Table 2-1 [32] and Figure 2-1 present information and plot the NEDC. The details of this driving cycle and legislative emission testing procedures can be found in [33].

Table 2-1 Details of NEDC driving cycle

	ECE 15 x 4	EUDC	NEDC
Distance (km)	4.05	7	11.05
Duration (s)	780	400	1180
Average Speed (km/h)	18.7	62.6	33.6
Max Speed (km/h)	50	120	129

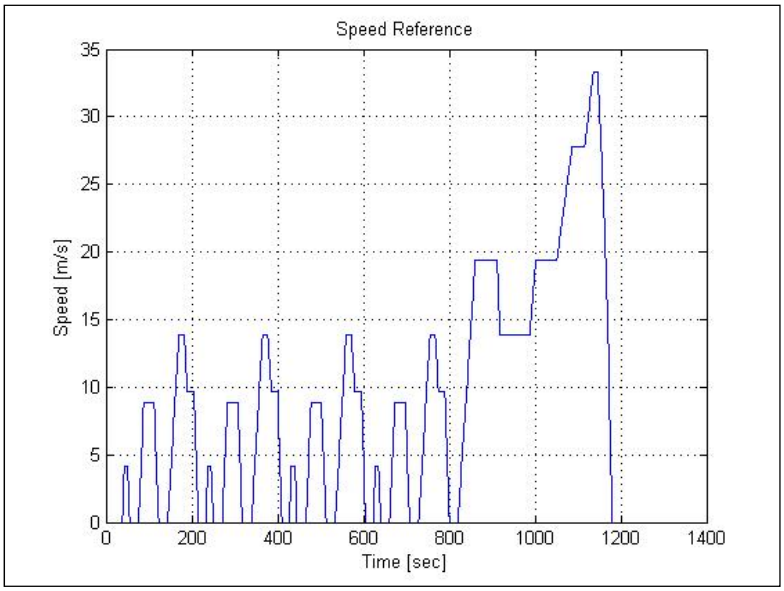

Figure 2-1 NEDC driving cycle

- **The Artemis driving cycle**

The NEDC contains a smooth and gentle acceleration, while under real road conditions more frequent start, stop and rapid acceleration may be required. The Artemis driving cycle was developed under the European Artemis project to produce a more realistic real-world driving cycle. This driving cycle was created from actual driving data collected from Europe [34]. The Artemis speed profile includes urban and rural roads, and motorways, details of which are presented in Table 2-2 [35]. In this work, simulations have used a “combined” Artemis cycle made from two cycles of the “urban” segment followed by two cycles of the “rural” segment, then one cycle of the “motorway” segment as presented in Figure 2-2.

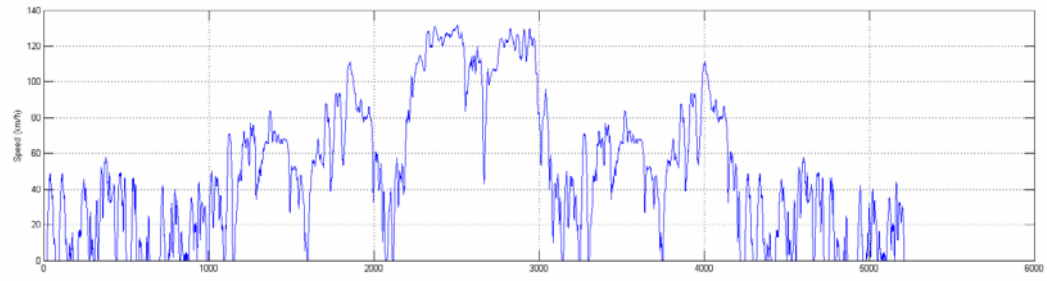

Figure 2-2 Combined Artemis velocity reference

Table 2-2 Details of Artemis driving cycle			
	Urban	Rural	Motorway
Duration (sec)	920	1081	1067
Distance (km)	4.47	17.27	28.74
Average speed (km/h)	17.5	57.5	97
Maximum speed (km/h)	58	112	132
Speed Distribution (%)			
Idle (0 km/h)	29	3	2
Low Speed (0-50 km/h)	69	31	15
Medium Speed (50-90 km/h)	2	59	13
High Speed (90-132 km/h)	0	7	70

2.1.2 The simulation technique

There are generally two types of technique for vehicle powertrain simulation: forward-facing simulation and quasi-static backward simulation. The literature in [29], [36] discusses the advantages and disadvantages of these two simulation methods, and a brief description is provided in the following sections.

- **Forward-facing simulation**

forward-facing simulation presents a realistic approach to vehicle simulation as it uses a driver model to control the vehicle speed, similarly to a driver controlling a car. Figure 2-3 illustrates the structure of a generic forward-facing simulation. Starting from the driver model, the reference speed and actual vehicle speed are compared giving an “error” signal, and this is used to generate a control signal to control the torque to power the vehicle. (Driver models normally use proportional-integral (PI) controllers). In practice, the source of power of the BEV is an electric machine, so a model of this is used to translate throttle and brake commands from the driver into torque and mechanical braking signals. Torque will transmit from the motor through the transmission and applied as a force at the wheels. For this application, to estimate energy consumption, the vehicle is usually assumed to simulate the effect of the longitudinal vehicle dynamic only. As a result, the effects of the two-dimensional vehicle dynamics are ignored.

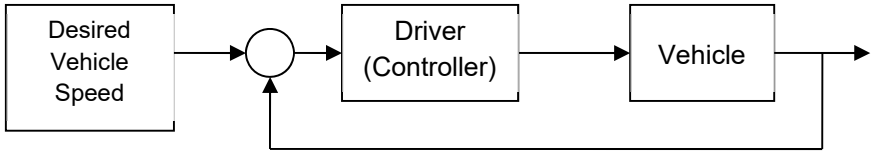

Figure 2-3 Vehicle forward-facing model

The advantage of the forward-facing simulation is that it is highly realistic, contains many details (dynamics) and normally uses small simulation time-steps. This method is used for designing vehicle hardware and detailed control development. However, this has to be a trade-off against the computational time-consuming.

- **Quasi-static backward simulation**

A quasi-static backward simulation, uses an opposite simulation approach compared to forward-facing simulation by using speed references (driving cycle) as an input rather than controlling the vehicle to follow the desired velocity, as in forward-facing simulation. One assumption made with the quasi-static backward simulation is that the vehicle will perfectly follow the driving cycle, a diagram of quasi-static backward simulation is presented in Figure 2-4. The traction forces of the vehicle are calculated from the environmental resistant forces which are dependent on the vehicle parameters and the driving cycle. The principle of conservation of power is applied from one component to the others; for example resultant forces and speeds between tyre and road contact are converted to torque and angular velocity to the gearbox. Then power required from the gearbox, including gearbox losses, is transferred to the electric machine and battery model. As a result, a driver model is not required for this simulation.

The electric machine in the quasi-static backward simulation as presented in [30] is typically modelled using a motor efficiency map. This map is a look-up table of the efficiencies, which are a function of the required torque and speed of the motor. These data are collected from the testing of a real electric machine at steady-state. This simulation type may not represent the real dynamical behaviour of the component, as in the forward-facing simulation. However, for the

energy consumption estimation and optimisation, the quasi-static backward simulation requires less time and less computational resources compared to those of forward-facing simulation.

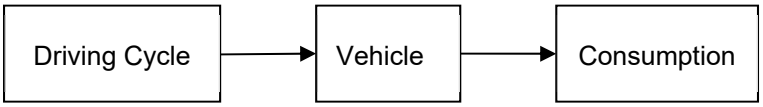

Figure 2-4 Backward-facing simulation

2.2 Component descriptions

Two types of common vehicle simulation technique were described briefly in the previous section. This section will present mathematical equations to describe the fundamental system of BEV, including power flow in the powertrain and components of the BEV.

2.2.1 Vehicle body and environmental resistance

Environmental resistant forces for the road vehicle typically include aerodynamic drag force, rolling resistant force and force due to the vehicle climbing a slope, as presented in Figure 2-5. In order to estimate the energy consumption, these forces will be converted to the force required for the vehicle traction.

The linear traction force, $F_{t,i}$ will be converted to torque at wheels, T_w, by

$$T_{w,i} = F_{t,i} \cdot r_d \quad \textbf{(2-1)}$$

and the angular velocity at the wheels, ω_w, can be calculated by

$$\omega_{w,i} = \frac{v_i}{r_d} \quad \textbf{(2-2)}$$

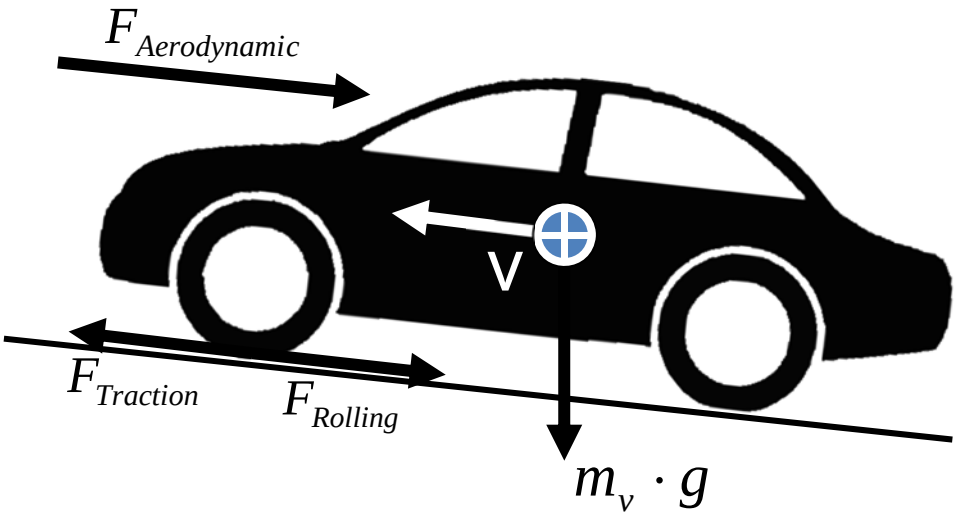

Figure 2-5 Vehicle body and resistant forces

Losses from the environmental force result from aerodynamic, tyre rolling resistance and the vehicle climbing the slope as described by

$$F_{t,i} = \frac{1}{2}\rho \cdot C_d \cdot A \cdot v_i^2 + C_r \cdot m_v \cdot g \cdot \cos(\alpha) + m_v \cdot g \cdot \sin(\alpha) + m\frac{dv_i}{dt} \qquad \textbf{(2-3)}$$

where v is vehicle velocity, r_d the effective tyre radius, ρ the air density, C_d the drag coefficient, A the vehicle frontal area, C_r the rolling resistant coefficient, g the gravitational acceleration, M_v the body mass, v the vehicle velocity and α the road angle. Figure 2-6 summarises the vehicle model.

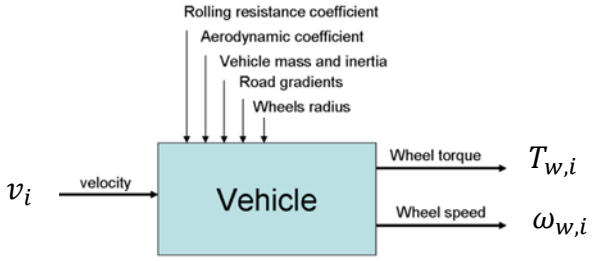

Figure 2-6 Quasi-static backward simulation model of the vehicle model

2.2.2 Transmission

The purpose of transmission is to transform a mechanical power quantity at certain speeds with certain torques to different speeds and torques. Transmission in a BEV powertrain usually includes the gearbox and final drive. However, this model has assumed that the gear ratios associated with the transmission and final drive are included in a single unit, as shown in Figure 2-7. This simulation is applied to both single speed transmission and two-speed transmission.

In general, electric machine provides a constant torque from zero speed to base speed and supplies constant power after the base speed, as seen in Figure 3-2. Because of the benefits of this torque-speed characteristic, it is possible that an EV can be used in a constant ratio transmission as can be seen from most of the pure EVs, such as the Nissan Leaf, Mitsubishi i-MiEv and Tesla roadster [37],[13],[14]. Moreover, single transmission can also benefit the minimisation of the drivetrain weight, volume, efficiency losses cost and complexity of the control system [38], [39]. The single transmission used in this simulation is described below.

- **Single speed transmission**

For a single motor BEV, in order to achieve high efficiency and reduce weight, it is possible for the BEV to use a high speed motor and high reduction single speed gearbox to reduce motor speed and increase torque. The equations for transmission are expressed by

$$\omega_{m,i} = \omega_{w,i} \cdot i_g \tag{2-4}$$

$$T_{m,i} = \frac{T_{w,i}}{i_g \cdot \eta_g} \tag{2-5}$$

where ω_m and ω_w are angular velocity at motor and wheel, T_m and T_w are torque at motor and wheel, η_g is efficiency of the transmission.

However, several researches have introduced a multiple speed gearbox and automatic transmission to increase the efficiency of a pure EV. Xi et al. [40]

present the use of automatic manual transmission (AMT) for a pure electric bus that was used in China. A three-speed AMT with transmission ratios of 4.03, 2.446 and 1.507 for the first to third gears respectively was used. Gear changes can be performed while the vehicle is in drive without using a clutch. In addition, the shift schedule can be determined by vehicle speed and throttle position. The results show that when using an AMT system, energy consumption decreases by 9% and acceleration time is shortened by 18%.

- **Two-speed transmission**

While a motor has the capability to drive an EV by using only a single transmission ratio, a two-speed gearbox probably increases the vehicle's performance in other aspects. The motor peak torque drops after the base speed as a result, therefore it is possible that a 2nd gear may help to increase wheel torque after the 1st gear reaches the base speed, which may result in increased acceleration performance and improve slope climbing ability. While the vehicle is running at low speed, a 1st gear will keep the motor running at high speed to maintain higher efficiency. In contrast, when the vehicle is running at high speed, a 2nd gear ratio can also reduce the motor speed to keep the motor operating at its most efficient and keep the motor within a motor speed limit [39],[41].

The mathematical expression used in the two-speed transmission is similar to the previous one for single speed, as stated in equations (2-4) and (2-5). However, the additional switching routine, which is a function of vehicle speed, is used to select a gear ratio and can be described by

$$i_{g,i} = f(v_i) \quad \textbf{(2-6)}$$

A specific velocity that makes a decision to change between the lower and upper gears is called the shift point. Gear ratio and shift point are selected to find the optimum point between acceleration performance and energy consumption over the driving cycle. A lower gear (higher number gear ratio e.g. 8:1) is used for increased available traction force. This results in improved acceleration performance. Moreover, for the gradient test, this gear ratio will also improve hill

climbing. For the higher gear (lower number gear ratio e.g. 5:1), this gear will reduce the speed of the motor when the vehicle speed is high. As a result, more torque is available at the higher vehicle speed and provides better overtaking performance at high speed.

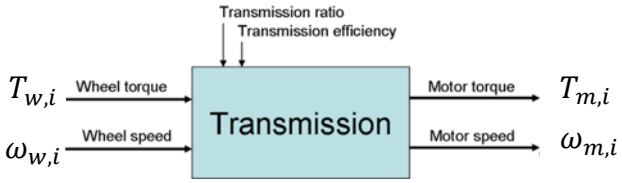

Figure 2-7 Backward-facing simulation of transmission model

2.2.3 Electric machine

The electric machine is the sole source of traction torque in a BEV. There are various possible choices of selecting an electric machine. Factors which are used in the consideration include performance, packaging and maintenance [42].

- **Electric machine type for BEV applications**
  - **Brush motor**

One of the motor types that can be used as an EV traction motor is a simple brushed DC motor [43]. Because of its simple structure, the motor is equipped with permanent magnets as a stator and a rotating wire coil inside as an armature. This motor is named a brush type because of the current flow to the rotor by brushes that connect to the commutator. As a result, this type of motor is simple and less expensive because of the uncomplicated electronics controls. However, there are some disadvantages that make this motor not applicable in an EV [43]. Since the motor is a brush type, there is friction between brushes and the commutator that generates heat and energy loss. Brush wearing is the main problem that affects the maintenance. More importantly, the coil is located in the middle of the motor which also generates heat and is difficult to remove.

- **Brushless motor**

By using an electronic commutator to replace a mechanical one, the problem of brush wearing can be eliminated. Moreover, using a magnetic field that is generated by the coil at the outer stator, heat is removed more easily and the size of the motor is also reduced. Because of these advantages, the brushless motor is preferred to the EV traction motor. Three possible brushless motors for traction motors include the induction motor, permanent magnet synchronous motor and switched reluctance motor [43].

- **Induction motor**

Induction motor is widely used for industry and capable for EV application. This is because of their mature technology, low cost, light weight and high reliability. However, there are some losses due to the current induced in the rotor. This results in 1-2% less efficiency than other brushless types [43]. This induction motor is used in production BEVs, such as the Tesla Roadster [44].

- **Permanent magnet motor**

Permanent magnet synchronous motor has torque-speed characteristics similar to the brush DC motor; however, using an electronic commutator makes permanent magnet synchronous motor preferable in EV application. Due to the lower inertia, higher power density, higher efficiency and smaller size, permanent magnet synchronous motor becomes more attractive for EVs when compared to the induction motor. When the speed of the motor increases, back electromotive force (EMF) is also increased, which reduces the motor current. As a result, this motor is more efficient at higher speed; however, the torque reduces due to the reduction of magnetic field strength. The maximum speed is limited to the supply voltage because back EMF cannot be greater than the supply voltage. In terms of motor cost, permanent magnet synchronous motor needs strong magnets that are more expensive than other brushless motors [43].

- **Switched reluctance motor**

The switched reluctance motor is considered to be one of the attractive candidates for the EV traction motor because of its better efficiency over a wider

torque-speed range compared to the permanent magnet synchronous motor. Thus, its rotor is made from soft iron. This results in low cost and higher speed operation. Additionally, no back EMF leads to higher power density. Nonetheless, critical disadvantages are difficulty in control and noisy torque ripples [43].

- **Electric machine modelling**

The role of an electric machine is to provide the traction torque during acceleration as a motor and to capture the kinetic energy losses during deceleration as a generator. The motor power can be calculated from motor torque and speed as described by

$$P_{m,i} = T_{m,i} \cdot \omega_{m,i} \,/\, \eta_{m,i} \tag{2-7}$$

where P_m and η_m are power and efficiency of motor

Power in the mechanical domain (torque and speed) transfers to electrical power by a fraction of motor efficiency, which is the function of motor torque, speed and size, as shown in

$$\eta_{m,i} = f(T_{m,i}, \omega_{m,i}, \phi_M) \tag{2-8}$$

where ϕ_M is motor size in kW.

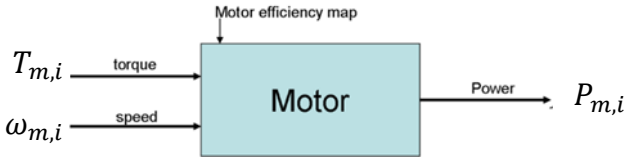

Figure 2-8 Quasi-static backward simulation of an electric machine model

- **Electric motor modelling using a motor efficiency map**

Significant factors which affect the efficiency of electric machines include size, mass and motor cooling. Different powertrain architectures use different numbers of motors and motor sizes. For the same power requirement, the SM-SA type needs a single high powered electric machine. On the other hand, the independent drive considers two or four small motors, the total power of which is

equal to that of requirement. As a result, size, mass and method of motor cooling may influence the powertrain design. In general, increases in motor power also increase motor efficiency [43]. A high speed motor is more likely to have a better efficiency than a lower one [43]. This is because the losses in the motor are directly proportional to the motor current which is related to torque rather than power. Hence motor at which same power rating, a low speed, high torque motor is more likely to dissipate higher losses. Similarly, in terms of motor size, a high speed motor is likely to be smaller than a low speed, high torque motor [43].

Guzzella et al. [30] developed a quasi-static toolbox that provided a scalable motor efficiency map for the generic motor. This toolbox contains a look-up table of the electric machine efficiency in both motor and generator mode. A scaled motor map depends on the size of the motor results in modified motor efficiency, peak torque and maximum power. The quasi-static motor efficiency map modified the torque axis to match the peak power of the permanent magnet synchronous motor, as shown in Figure 2-9.

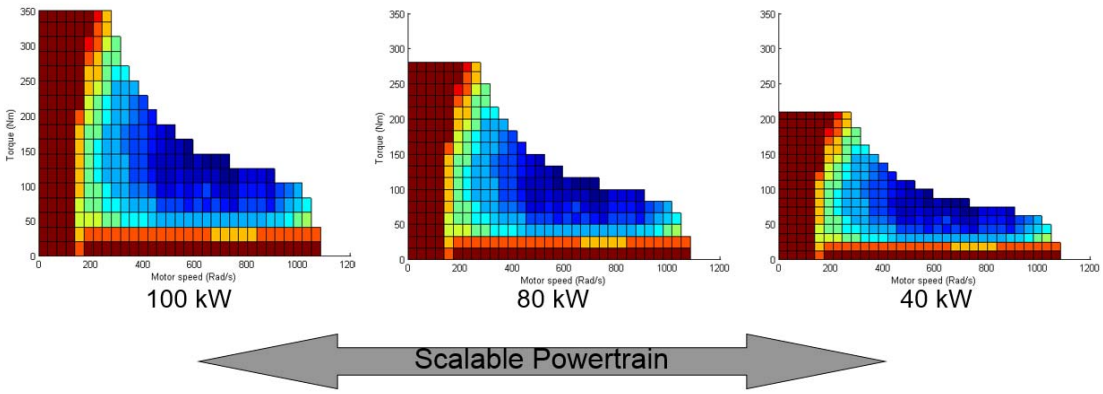

Figure 2-9 Scalable Motor MAP for Permanent Magnet Synchronous Motor

2.2.4 Battery

The battery is the only source of energy for the BEV. It is an electrochemical device that stores electrical energy in the form of chemicals. In this chapter, a simple battery model is utilised. A static model of battery consists of an open

circuit voltage source and internal resistance is utilised. The battery model for quasi-static backward simulation is presented in Figure 2-11.

- **Battery state of charge**

Battery state of charge (SOC), a quantity describing the amount energy available in the battery, is calculated from the charge Q_i remaining related to the maximum capacity of the battery Q_0 as described by

$$SOC = {Q_i}/{Q_0} \tag{2-9}$$

$$Q_i = Q_0 - \int_{t_0}^{t} I_{BT}\, dt \tag{2-10}$$

where Q_i is an charge available of the battery, I_{BT} is the terminal current of the battery. Positive current is the discharge and negative current is the charge of the battery. Current at the terminal of the battery can be calculated as a function of power that is required from the battery and the terminal voltage of the battery, as described by.

$$I_{BT,i} = {P_{m,i}}/{V_{BT}} \tag{2-11}$$

where V_{BT} is a terminal voltage calculated from the open circuit voltage V_{ocv} and internal cell resistance $R_{B,i}$ as described by

$$V_{BT} = V_{ocv} - I_{BT} \cdot R_{B,i} \tag{2-12}$$

By substituting current $I_{BT,i}$ from equations (2-11) to (2-12), the terminal voltage can be calculated as the function of power, open circuit voltage and internal resistance as in

$$V_{BT}^2 - V_{ocv} \cdot V_{BT} + P_{m,i} \cdot R_{B,i} = 0 \tag{2-13}$$

$$V_{BT} = \frac{V_{ocv} \pm \sqrt{V_{ocv}^2 - 4 \cdot P_{m,i} \cdot R_{B,i}}}{2} \tag{2-14}$$

- **Battery pack calculation**

Battery terminal voltage and battery capacity are calculated from the series stacks of a battery cell, as shown in Figure 2-10 [45].

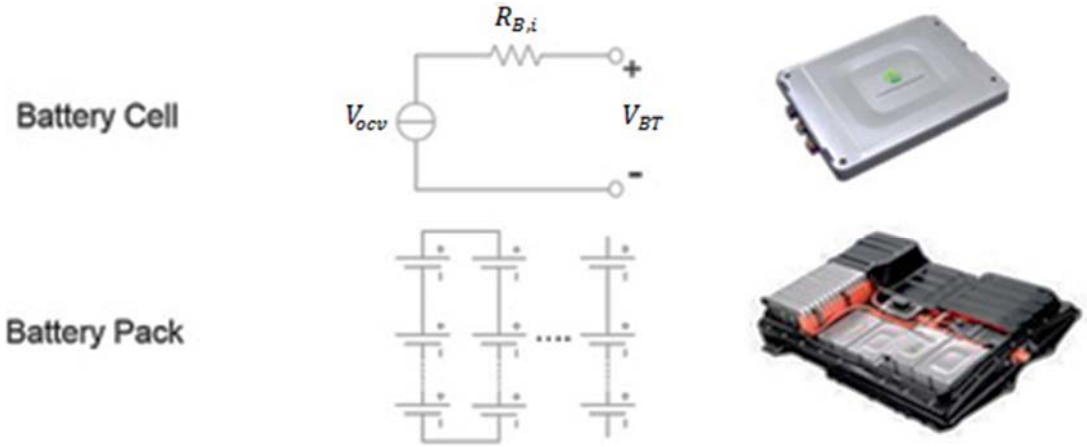

Figure 2-10 Battery cell and battery pack for EV

The open circuit voltage of a battery pack is calculated from the open circuit voltage cell and the number of cells in series, as shown by

$$V_{BT} = V_{ocv} \cdot N_C \quad \textbf{(2-15)}$$

where N_C is a battery series stack and the model of the battery can be illustrated by Figure 2-11.

Figure 2-11 Quasi-static backward simulation of battery model

2.3 Battery electric vehicle integrated descriptions

As mentioned earlier, concerning the quasi-static backward simulation for BEV, Figure 2-12 shows the power flow from the driving cycle to the energy

consumption of the battery. This section will describe the integration of BEV powertrain components, the method of energy calculation, how weight and cost of the powertrain are estimated, the regenerative braking control algorithm and vehicle acceleration time calculation.

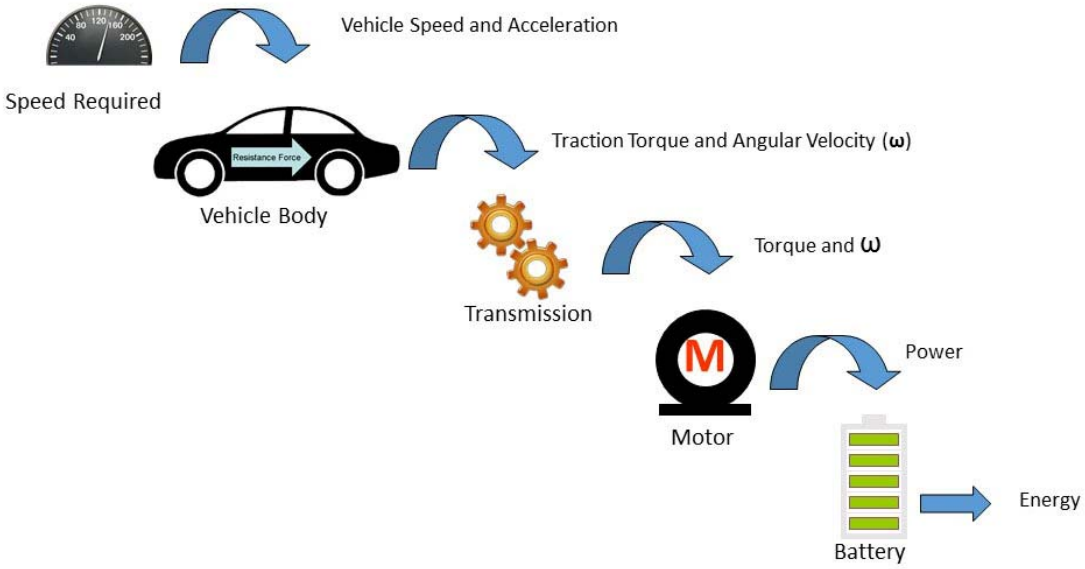

Figure 2-12 Power flow of vehicle backward-facing model

2.3.1 Energy consumption

Energy consumption is one of the key objective factors for this study. The energy consumption, E, calculates the amount of required energy to traction the vehicle over a speed profile. Energy consumption can be calculated by the integral of power required at the battery terminal over a specific time period as described by

$$E = \int_{t_0}^{t} V_{BT}(t) \cdot I_{BT}(t)\, dt \tag{2-16}$$

However, in a discrete time simulation, the integration is replaced by

$$E = \sum_{i}^{n} V_{BT,i} \cdot I_{BT,i} \tag{2-17}$$

where the positive power ($V_{BT,i} \cdot I_{BT,i}$) indicates power is required from the battery. On the other hand, negative power means power is captured from regenerative braking and it is being charged to the battery.

2.3.2 Powertrain weight estimation

Estimation of powertrain weight is described in this section. These equations are based on the information using a long-term assumption from [46].

- **Electric Motor weight estimation**

Weight of the motor, W_{Motor} , can be calculated by

$$W_{\text{Motor}} = 0.532 \times \text{P}_{\text{Motor,kW}} + 21.6 \quad \textbf{(2-18)}$$

- **Transmission weight assumption**

Weight of transmission for an SM-SA is assumed to be constant for all sets of gear ratio. However, for the other type of BEV, the assumptions made will be described in a later chapter.

- **Battery weight estimation**

Battery weight is simply calculated from the number, N, of battery cells and battery cells' weight, including battery accessories such as cables and battery cooling devices. The equation to estimate battery weight can be described as

$$W_{\text{Battery}} = N_{\text{cells,seies,Battery}} \times N_{\text{cells,parellel,Battery}} \times W_{\text{cell,Battery}} \quad \textbf{(2-19)}$$

where $W_{\text{cell,Battery}}$ is weight of a battery cell.

- **Weight of powertrain integration**

The weight of the powertrain is the combined weight of the motor and battery in the powertrain, as presented by

$$W_{\text{Powertrain}} = W_{\text{Motor}} + W_{\text{Battery}} \quad \textbf{(2-20)}$$

2.3.3 Powertrain cost estimation

The cost of the powertrain is estimated by the cost of the motor and the cost of the battery. The cost of the motor can be estimated by [46]

$$\mathrm{Cost}_{\mathrm{Motor},\$} = 16 \cdot P_{\mathrm{Motor,kW}} + 385 \quad \textbf{(2-21)}$$

The cost of the battery can be estimated as presented in

$$\mathrm{Cost}_{\mathrm{cell,Battery},\$/\mathrm{kWh}} = 11.1 \times \left({}^{P}/_{E}\right) + 221.1 \quad \textbf{(2-22)}$$

For the battery cell, the cost of the battery in $US per energy capacity in kWh is presented as follows: where $\left({}^{P}/_{E}\right)$ is the power to energy ratio of each battery cell. In this simulation, a value of 4 is assumed for the model of a lithium battery [47]. The cost of the battery pack is calculated by

$$\mathrm{Cost}_{\mathrm{Pack,Battery},\$} = \left(\mathrm{Cost}_{\mathrm{cell,Battery},\$/\mathrm{kWh}} + 13\right) \times \mathrm{Capacity}_{\mathrm{cell,Battery,kWh}} + 680 \quad \textbf{(2-23)}$$

and is based on information using a long-term assumption from [46].

Total powertrain cost can be calculated by the cost of both the motor and battery, as presented by

$$\mathrm{Cost}_{\mathrm{Powertrain},\$} = \mathrm{Cost}_{\mathrm{Motor},\$} + \mathrm{Cost}_{\mathrm{Pack,Battery},\$} \quad \textbf{(2-24)}$$

2.3.4 Regenerative braking control rules for BEV

Without the braking system, a 1500kg vehicle with a speed of 70 km/h requires approximately 2 km to bring itself to rest, while with a braking system only a few tens of meters are required [48]. The main concern of the braking system is to stop the vehicle in the shortest possible distance with safety and comfort [48]. In the BEV, the braking system can be either solely regenerative or friction brake, or both. The main objective of regenerative braking is to maximise the recoverability of kinetic energy associated with vehicle inertia at a given speed. The control algorithm is required to switch between friction and regenerative braking to make the most of energy efficiency and maintain vehicle safety and comfort [49].

This section explains the model of a regenerative braking system and its control strategy. The regenerative braking model includes a control strategy to switch between the use of a regenerative brake and a friction brake. The main concern of this regenerative braking model is to calculate the amount of recoverable kinetic energy of the vehicle while the vehicle is in the deceleration period.

Energy consumption is the priority factor for this simulation, while the vehicle dynamics and effects of vehicle stability are beyond the scope of this study. The friction brake system normally consists of a hydraulic system. The process of switching between regenerative braking and friction braking is estimated by reducing the friction brake force (similarly to reducing the hydraulic brake pressure in a physical brake system) and compensating the braking torque by the use of the electric machine. In this study the detailed process of pressure reduction is negligible. Only the recoverable kinetic energy from the regenerative braking is being considered.

- **Regenerative braking control strategy**

Control rules are presented to estimate the energy recovered of vehicle braking situations. These rules are implemented for vehicle stability and safety purposes.

1) Maximum regenerative braking torque was limited at the available negative torque of the motor at that particular motor speed as

$$T_{\text{Regen}} = \max(T_{\text{Regen,Require}}, T_{\text{Motor,Regen,max}}) \quad \textbf{(2-25)}$$

   If the required negative torque is greater than the available motor torque, a mechanical friction brake will be operated with the regenerative braking to maintain the amount of sufficient brake demanded [50].

2) If the vehicle speed is lower than 10 km/h, the regenerative braking will be disabled [51]. This is because the amount of energy recovered below this speed is very small and the disabled regenerative braking below this speed also keeps passengers comfortable [52].

3) For emergency braking (acceleration > 0.7g [48]) all brake forces are provided by the friction brake to maintain vehicle safety [53]. It was presented in [48] that at a deceleration greater than 0.7g, with a vehicle mass of 1500 kg and vehicle speed faster than 70 km/h, a braking power of more than 250 kW will be created, which is greater than the maximum available power of the motor.

4) The regenerative braking will be disabled if a battery's SOC is greater than 90%. If a charging current is greater than 2C (two times the battery capacity in amp-hour) of the battery capacity, then the regenerative braking is also limited. This control aims to protect the battery from over-charging.

2.4 Powertrain performance and drivability (acceleration time)

Vehicle acceleration time is considered as a powertrain drivability and performance. This factor affects the BEV in terms of 'how the vehicle is fun to drive' [54] and it will also affect the marketing aspect. The equation to estimate this performance is to calculate time to accelerate BEV from 0 m/s to 27.78 m/s (0-100 km/h) presented by

$$\mathrm{Time}_{\text{Acceleration 0-100 km/h}} = \int_{0}^{27.78} \frac{m}{F_w}\, dv(t) \qquad \textbf{(2-26)}$$

2.5 Chapter conclusion

This chapter described general idea methods of the estimation of energy consumption, weight and cost of the BEV powertrain. The quasi-static backward simulation is a main methodology used in this simulation where this technique was modified from the quasi-static toolbox. Examples of control algorithms were presented, such as the regenerative braking control rules. Finally, these techniques will be used for optimising the SM-SA BEV powertrain in the next chapter.

3 Battery electric vehicle optimisation with single motor

3.1 Introduction

This chapter implements the BEV powertrain model from the Chapter 2 to optimise their components sizing. The quasi-static backward simulation technique which modified from the quasi-static toolbox were used for this simulation. This chapter will limit the powertrain topology to the SM-SA type and used the Nissan Leaf (2011/2012 model) as a vehicle case study. Two driving cycle, the NEDC and Artemis, will be considered and the optimisation technique will be applied to indicate the optimum powertrain sizing. Finally, the results from this chapter will be used as a benchmark to optimise different BEV powertrain topologies.

3.2 Vehicle case study, the Nissan Leaf

The Nissan Leaf, one of the pure production BEV, has been introduced since 2010. The name of the vehicle, LEAF, stands for *Leading Environmentally-friendly, Affordable, Family car* [55] and this indicates that the Nissan Leaf is designed as an everyday use, family car, rather than a very high performance sports car. For this reason, the Nissan Leaf will be the vehicle case study used for our study as we will be looking to optimise a compact pure EV that can be used on a daily basis. At the time that this thesis is being written, the Nissan Leaf model 2016 is now available; however, this simulation uses the vehicle information of the previous version (the 2011/2012 model) as theses information are used at this study started.

3.3 System model

The model of the vehicle case study is based on the Nissan Leaf. The front wheel drive with a single motor and fixed ratio gearbox is developed as presented in Figure 3-1. This type of vehicle topology is called a “Single Motor Single Axle”. The main components of this vehicle type include;

1) The vehicle body, this vehicle information is used to calculate all resistances from the external environment.

2) The transmission, which is the connection between the wheels and motor. It also performs as the torque/speed transformer between them.

3) The electric machine, which is the sole source of the traction power for the BEV.

4) Lastly, the battery, which performs as a fuel tank for the BEV as it stores all the energy for traction of the vehicle.

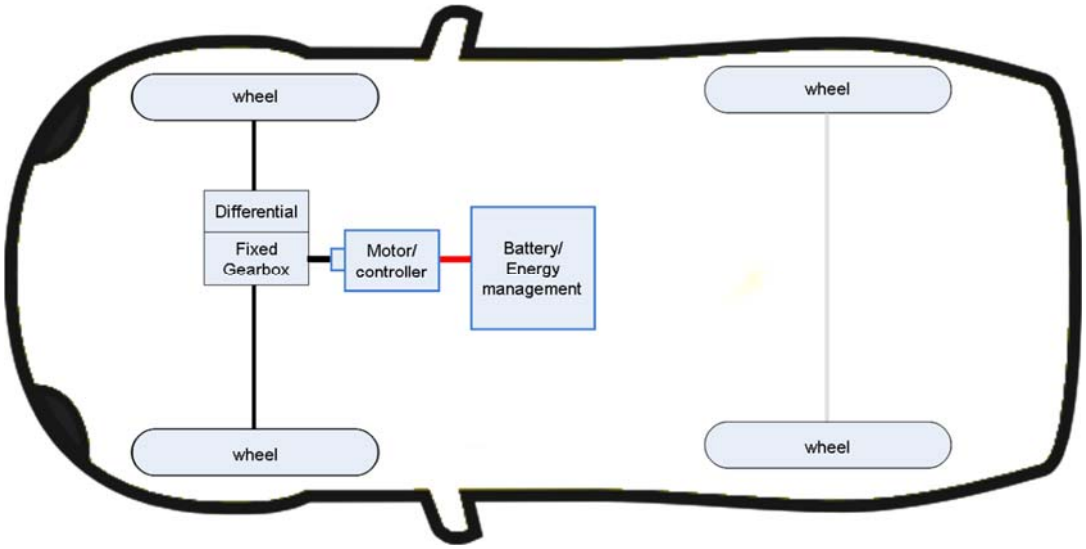

Figure 3-1 SM-SA Vehicle layout

3.3.1 Vehicle body specification

The aim of the quasi-static backward simulation is to calculate the transformation of power between components. Each of the components provide losses that make the total energy increase. For the vehicle body, the power required of the vehicle body will be calculated in order to move the vehicle along the driving cycle. Power required by the vehicle body is calculated from the product of total torque and speed of the vehicle. Forces that act on the vehicle body include aerodynamics drag forces, rolling resistance and vehicle inertial forces. The assumption made for this simulation is that the vehicle is travelling on a flat road only and any force due to the hill climbing of the vehicle is ignored. Vehicle speed is calculated from the speed that vehicle body perfectly follows the driving cycle and the speed is transferred to the rotational speed of the shaft gearbox and motor. The Nissan Leaf details of vehicle body specification are presented in *Appendix 1.*

3.3.2 Transmission and speed ratio

The Nissan Leaf is equipped with a fixed ratio transmission of 7.94:1. A standard tyre of P205/55R16 is provided that has an effective diameter of 0.632 m. As a result, this configuration makes the motor spin almost eight time faster than the wheels and this makes the motor operate in the high speed and high efficiency areas.

The fixed ratio transmission provides a higher efficiency compared to those with multi-ratio or continuously variable transmission (CVT) transmission [25]. The assumption made in this simulation is that the average efficiency of this fixed ratio gearbox is 97%. As the objective of this study is to estimate the vehicle energy consumption, then the dimension, package size and its volume of transmission is safely ignored. For this optimisation purposes, it is assumed that changing the transmission ratio will not affect the weight change of the whole vehicle. All transmission properties and their coupling devices, except the gear ratio, will remain unchanged.

In this chapter, a two-speed transmission is provided in order to investigate the amount of energy saved compared with the original Nissan Leaf with single transmission. The assumption will be made that transmission efficiency will be decreased by 2% due to losses in the multi-ratio gearbox and clutch. The weight of the additional gear set will be added to the original powertrain weight and the details are presented in the next section.

3.3.3 Torque map used in this simulation

For a quasi-static backward simulation, it is possible to calculate the energy consumption of the electric machine by using a static map as presented in [56]. The use of a motor map for this energy estimation has been described in section 2.2.3. In this section motor simulation using a static motor map will be explained in more detail.

A motor map is a 2D lookup table that contains the motor efficiency information. The motor efficiency is a function of motor torque and speed as described in equation (2-8). Figure 3-2 [57] shows the motor efficiency map of the Nissan Leaf. The vertical axis presents the torque of the motor and the horizontal axis is the motor speed. The different contour colours show the different efficiencies of the motor at a particular torque and speed. The motor map presents only a steady stage of the motor efficiency and this information is usually collected

by measuring the power when motors are tested with a dynamometer [25]. It can be seen from the efficiency map in Figure 3-2 [57] that a range of 85% to 95% energy efficiency is produced by the motor which shows that the electric motor is a better efficiency power source for the traction of a vehicle compared to those with the average 30% energy efficiency of a conventional internal combustion engine vehicle [25].

For the simulation this Nissan Leaf motor map has been converted into a lookup table in Simulink, as presented in Figure 3-3. A motor map image data was converted into a lookup table into a MATLAB's file with a data interpolation. Once this map has been converted into a lookup table, for using with the optimisation process, this modification assumes that the speed of the motor is limited at 10,500 rpm in every size of the motor. A peak torque and efficiency map was developed according to the standard size of the motor of the Nissan Leaf. A unit scale factor for motor power is 80 kW and unit peak torque is 280 Nm. The motor can be scaled up or down by multiplying factors to the unit scale of the motor, as presented in Figure 2-9. Due to a limit of motor information on the original motor from the Nissan Leaf, the assumption was made that an ability to operate in the regenerative braking has an identical efficiency to the operation in the traction mode.

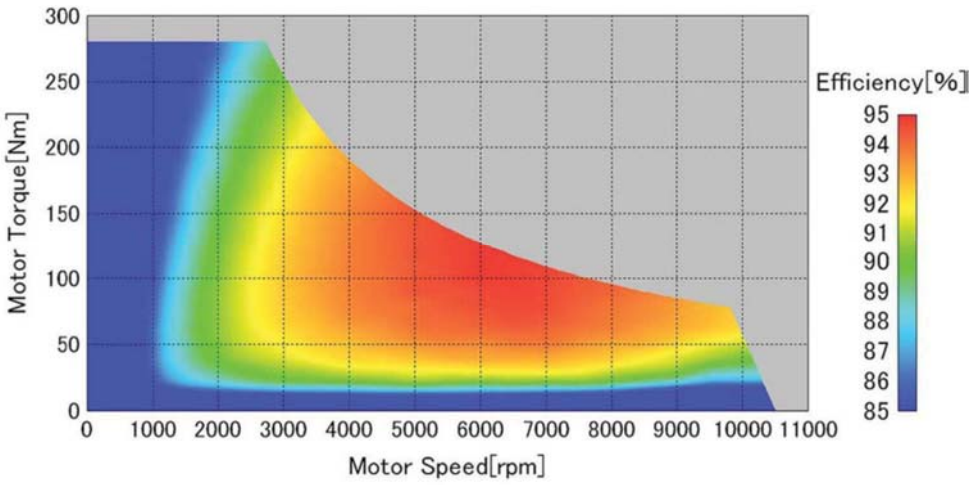

Figure 3-2 Motor efficiency map of the Nissan Leaf

In Figure 3-3, it can be seen that this lookup table provides motor efficiency data in both the traction (positive torque) and regenerative braking side (negative torque). The value in the z-axis is the efficiency of the electric machine. In the lookup table, it can be seen that these

values are greater than 1 and for regenerative braking, are less than 1. The meaning of these numbers in this backward facing simulation is that in the traction mode, power is required from the battery for traction and motor losses. On the other hand, when the vehicle is in the regenerative braking mode, the motor provides a power (negative power in this case) that is conserved from the vehicle inertia and can be stored to the battery. A number less than one means less power from kinetic energy can be conserved to charge the battery. For example, the power required from the motor for traction at 100 Nm and 200 rad/s can be calculated by $100\ \mathrm{Nm} \times 200 \frac{\mathrm{rad}}{\mathrm{s}} \times 1.05 = 21\mathrm{kW}$. The extra 1 kW is due to the motor losses. Moreover, for regenerative braking at -100 Nm (generator mode) and 200 rad/s, the power which stored to the battery can be calculated by $-100\ \mathrm{Nm} \times 200 \frac{\mathrm{rad}}{\mathrm{s}} \times 0.95 = 19.04\ \mathrm{kW}$.

3.3.4 Battery pack

Battery terminal voltage and battery capacity are calculated from the series-parallel combination of battery cells, as shown in Figure 2-10. The open circuit voltage of the battery is calculated from the open circuit voltage cell and the number of cells in series, as shown in equation (2-15). The Nissan Leaf uses laminate type Li-ion cells with a rated capacity of 33.1 Ah, detail described in [45]. However, due to the limited information on the battery of the Nissan Leaf, the cell open circuit voltage and internal cell resistance are approximated from the model of the 20 Ah Li-ion cell, as presented in Figure 3-4 and Figure 3-5. This simulation assumes that the temperature of battery remains constant at 25°C. Equations (2-9) to (2-15) describe the cell open circuit voltage and cell internal resistance while the battery is charging and discharging.

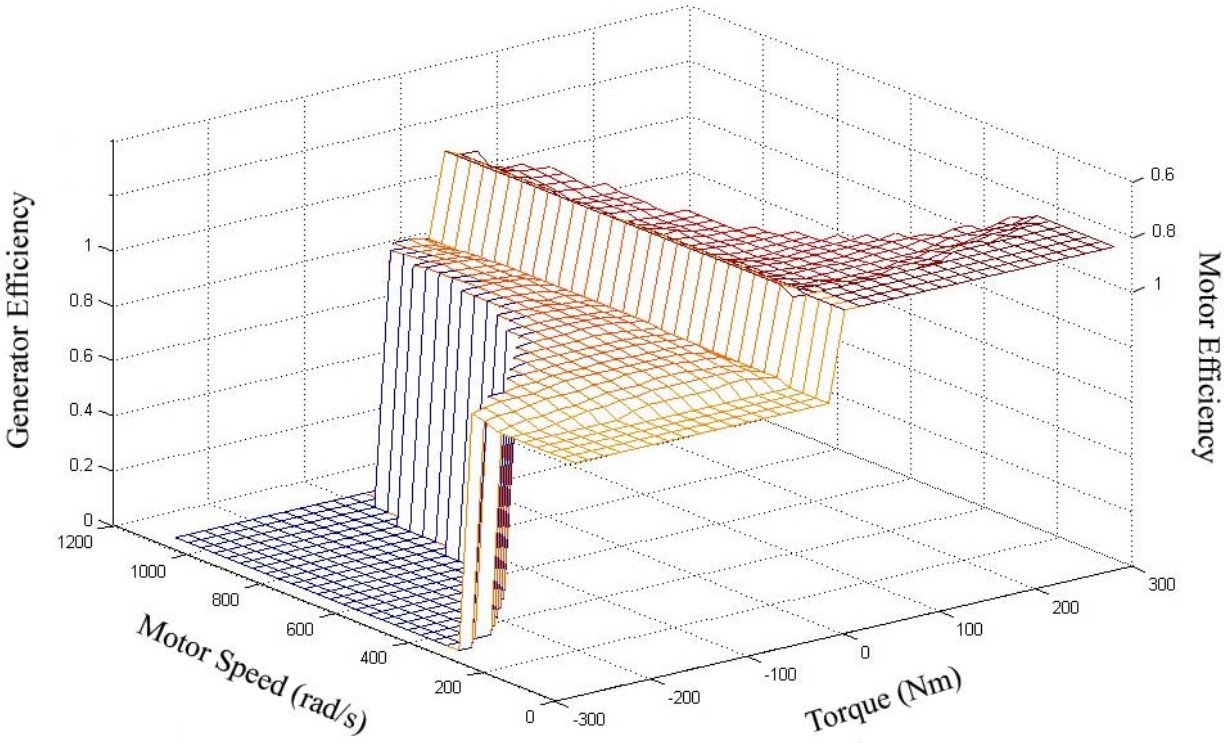

Figure 3-3 Motor Efficiency Map in the Lookup Table

3.3.5 **Vehicle weight**

Equations to calculate the powertrain weight are described in section 2.3.2. the details of how the vehicle mass can be estimated is presented in this chapter. It can be seen that the weight of the vehicle is importantly effect energy consumption as this issue will be described mathematically by sensitivity analysis method in the Chapter 5. The following section separates the calculation of vehicle mass into three main components: electric machine with transmission, battery, and vehicle body with chassis.

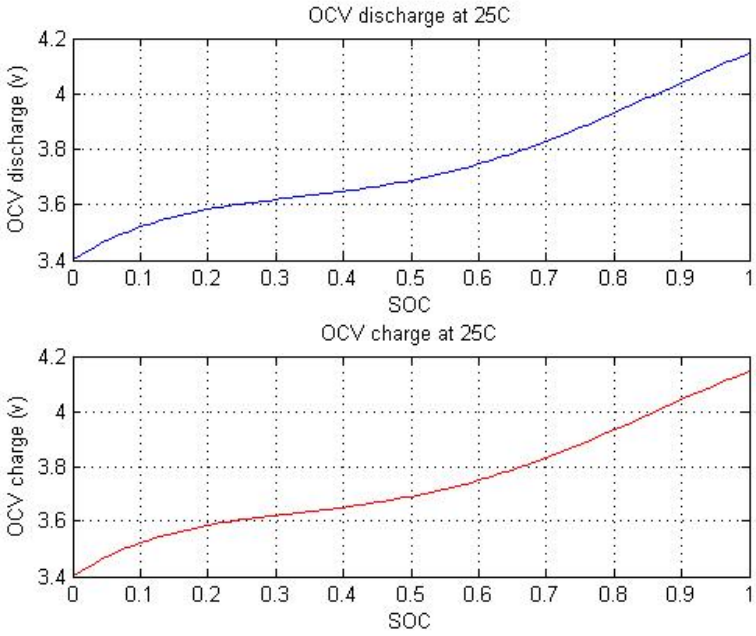

Figure 3-4 Battery discharge and charge open circuit voltage at 25ºC

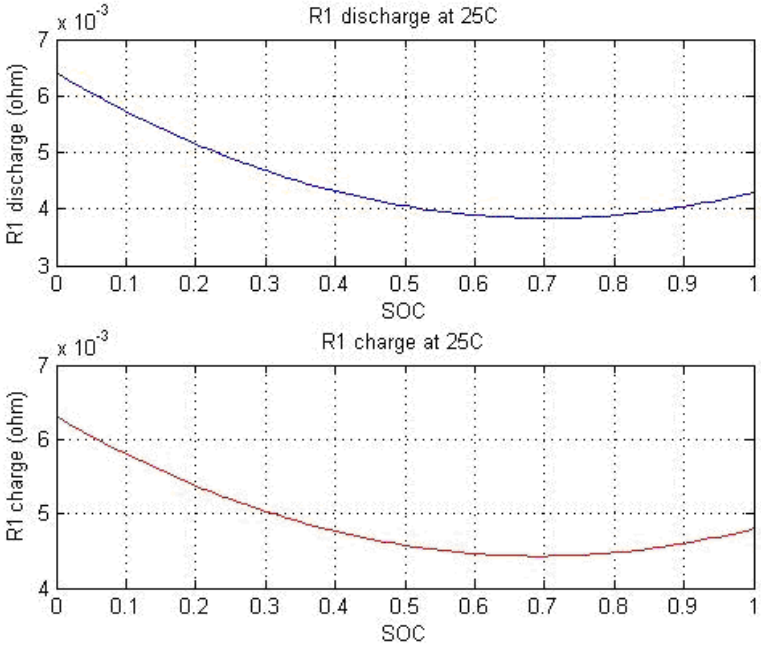

Figure 3-5 Battery internal resistance at 25ºC

- **Transmission and electric machine weight**

The weight of the electric motor and transmission in the SM-SA simulation are assumed to be integrated into a single unit. Fixed ratio transmission is selected in this optimisation, and it is also assumed that the gear ratio will not affect the weight of the motor and transmission. In other words, during the optimisation process, only the weight of the motor is changing and the weight of transmission remains constant.

The precise weight of the Nissan Leaf motor and transmission are not publicly available; however, the weight of the motor is estimated by using equations in the Section 2.3.2.

- **Battery weight**

The weight of the battery pack is calculated by the integration of battery cells, as presented in Figure 2-10. The precise weight of each battery cell for the Nissan Leaf was published by the battery manufacturer in [45]. The cell weight is 787 g and there are four cells in one module and 48 modules in a battery pack. There are $0.787 \text{ x } 4 \text{ x } 48 = 151.1$ kg for the Nissan Leaf 24 kWh battery pack. The assumption of 0.06 kg/kW for mass of thermal management system and 0.14 kg/kW for mass of harness and bus bar [46] were made. The total estimated cell weight will be 0.975 kg per battery cell; the total estimated weight of the battery pack will be 187.4 kg.

- **Calculate the vehicle curb weight**

Vehicle kerb weight based on the original Nissan Leaf is 1521 kg (i.e. based on the 2011/2012 model). The weight of the powertrain as mentioned previously is estimated. In case of a powertrain size change, the difference in powertrain weight is calculated and multiplied by a mass compounding factor of 1.6 to compensate for the weight of the vehicle chassis. For example, the standard powertrain and battery of the original Nissan Leaf is calculated based on equations (2-18) and (2-19). Table 3-1 shows a comparison of vehicle weight between the case study vehicle and an example vehicle equipped with 100 kW motor.

Table 3-1 Comparison of vehicle weight.		
	Case Study Vehicle	Vehicle with 100kW motor
Motor (Power, Weight)	80 kW, 64.16 kg	100 kW, 74.8
Battery $(\text{Capacity, Weight})$	24 kWh, 187.4	24 kWh, 187.4
Total Vehicle Weight	1521 kg	1689 kg

The motor weight will be $0.532 \times 80 + 21.6 = 64.16\ \text{kg}$ and the weight of the battery will be $96 \times 2 \times 0.975 = 187.4\ \text{kg}$. The total powertrain weight of the 80 kW motor and 24 kWh battery will be $64.16 + 187.4 = 251.5\ \text{kg}$. However, if the motor size is increased to be, for example, 100 kW, the calculation will be $0.532 \times 100 + 21.6 = 74.8\ \text{kg}$ and the overall vehicle weight will be $(1521\text{-}64.16\text{-}187.4) + (74.8 + 187.4) \times 1.6 = 1689$ kg.

3.4 BEV powertrain control strategies

The model used in this study was created by a quasi-static backward simulation technique, thus, driver model and powertrain control were not required. However, there are some local control rules that have been applied in this SM-SA vehicle simulation.

3.4.1 Regenerative braking control

The detail of the regenerative braking control algorithm was described in section 2.3.4. This control strategy will help the simulation to obtain results as close to reality as possible and also prevent the effect of vehicle dynamics while using this regenerative braking.

3.4.2 Two-speed transmission ratio control

The vehicle with two-speed transmission and using the gear change algorithm has been simulated, as presented in section 2.2.2.

3.5 Optimisation

3.5.1 Optimisation methodologies

The purpose of this work is to design an energy efficient powertrain for the BEV. It can be seen that the main components of a BEV include an electric motor, transmission and battery,

as described earlier. By combining these components and changing their size, the energy consumption will change. The question then is ‘What is the optimum configuration and size of the BEV that will result in using minimum energy consumption while providing sufficiently good vehicle drivability?’

This section aims to introduce an optimisation technique to search for the best possible parameters of the BEV that provides a minimum energy consumption and satisfies the constraints. Figure 3-6 shows the interconnection diagram of the BEV powertrain components. This vehicle simulation divides the BEV powertrain into four individual groups: vehicle, transmission, motor and battery. Each group has a function to solve specific equations before sending the results to the other relevant groups, e.g. the vehicle energy consumption is the result of the operating points of the motor that are affected by motor size and transmission ratio.

The Genetic Algorithm is an optimisation method selected for this study because of its robustness and it does not require gradient information. Other gradient based and non-gradient based optimisation technique may possible to use in this application but this chapter is scoped to the Genetic Algorithm optimisation only.

- **Genetic algorithm**

The Genetic Algorithm is a computational method to search for the best solution from within a search space. This method was inspired by the natural selection of biological evolution and was introduced by Holland in the 1970s. The algorithms of this optimisation tool are simple, robust and use a derivative-free method that provides a power to search on both continuous and discontinuous functions.

The beginning of the optimisation process is to create a population of optimisation variables randomly throughout the search space. Then the variables are coding into a binary string. The selection, crossover and mutation methods are mimicked by natural selection. The selection process tries to select a fitter individual which is better than the average population to be promoted into the next generation. Crossover is a process to exchange information between selected individuals. This process is similar to sexual reproduction in nature. In terms of the Genetic Algorithm method, crossover is a random process to create two new

strings by exchanging an equivalent length of selected strings. Finally, the mutation is a process to randomly flip binary bits in an individual chromosome. After these processes have been applied to the initial population, the next generation will be created and this process is repeated until it exceeds a limited number of generations or meets the convergence criteria. Details of Genetic Algorithm can be found in [35].

3.5.2 Objective function

This optimisation uses the single objective as the optimisation technique. The objective function in this optimisation is the energy consumption that is calculated for the battery model, as described in (2-16). Optimisation equations and the objective function are expressed as the optimisation problem:

$$\text{minimise } J(X_D) \tag{3-1}$$

where

$$J(X_D) = E(X_D) = \int_{t_0}^{t} V_{T,Batt}(t) \cdot I_{T,Batt}(t)\, dt \tag{3-2}$$

and where the optimisation parameters (X_D) are motor size, transmission ratio and battery size of the vehicle.

3.5.3 Constraints

Constraints make the optimiser to search within a feasible solution space. Limitation of the powertrain will be applied to the constraints as they will be described in this following section.

- **Limitation of motor torque and motor speed**

While the size of the motor was selected by the optimiser, the motor torque has to be large enough to complete the driving cycle. The size of the motor can be increased or decreased for the motor peak torque, as described in section 2.2.3. The maximum motor speed was limited, as described before. While motor size and gear ratio were selected, this constraint was applied to reject infeasible solutions when the motor torque and speed exceeded the motor limitations.

- **Limitation on battery current**

The size of battery was also selected by the optimiser. The selection is based on varying the number of battery cells in both parallel and series, as described in section 2.2.4. This constraint aims to limit the battery charge and discharge current to prevent battery damage. Battery discharge and charge currents were limited at 5C and 2C of the total capacities of the battery, respectively, where C is the battery capacity in Ah. This limitation prevents the optimiser from choosing too few numbers of batteries in parallel.

- **Vehicle range on NEDC**

The range of a BEV defined in this simulation is the minimum distance that can be completed within a single charge. It is dependent on many factors such as driver behaviour, speed of vehicle, traffic or weather. However, one of the important factors is driving style. The US Environmental Protection Agency (EPA) has rated the Nissan Leaf model 2011/2012 based on a five cycle testing at 34 kWh per 100 miles (21.25 kWh per 100 km). The range of the Nissan Leaf for the 2012/2013 model on the NEDC was published as in the 175 km range[44]. Due to the limited information on this test regulation, the decision was made to start the initial SOC at 100% and repeat the NEDC driving cycle until the SOC dropped below 5%. Then the simulation was terminated and the range of the vehicle on the NEDC read out. This vehicle range constraint will be beneficial in selecting a battery pack size. Without this constraint, a possible result after the optimisation will give a small sized battery with a limited range. This is because the smaller battery size will give a minimum vehicle energy consumption.

- **Acceleration time**

One aspect of vehicle performance that might affect the vehicle demand and its life-cycle is how the vehicle responds to a rapid acceleration. This constraint aims to limit the lower boundary of an electric motor size which affects a vehicle's acceleration time, as described later in Section 2.4. Acceleration time was defined in this simulation as the time required for the vehicle to accelerate from rest to reach a speed of 100 km/h as presented in equation (2-26).

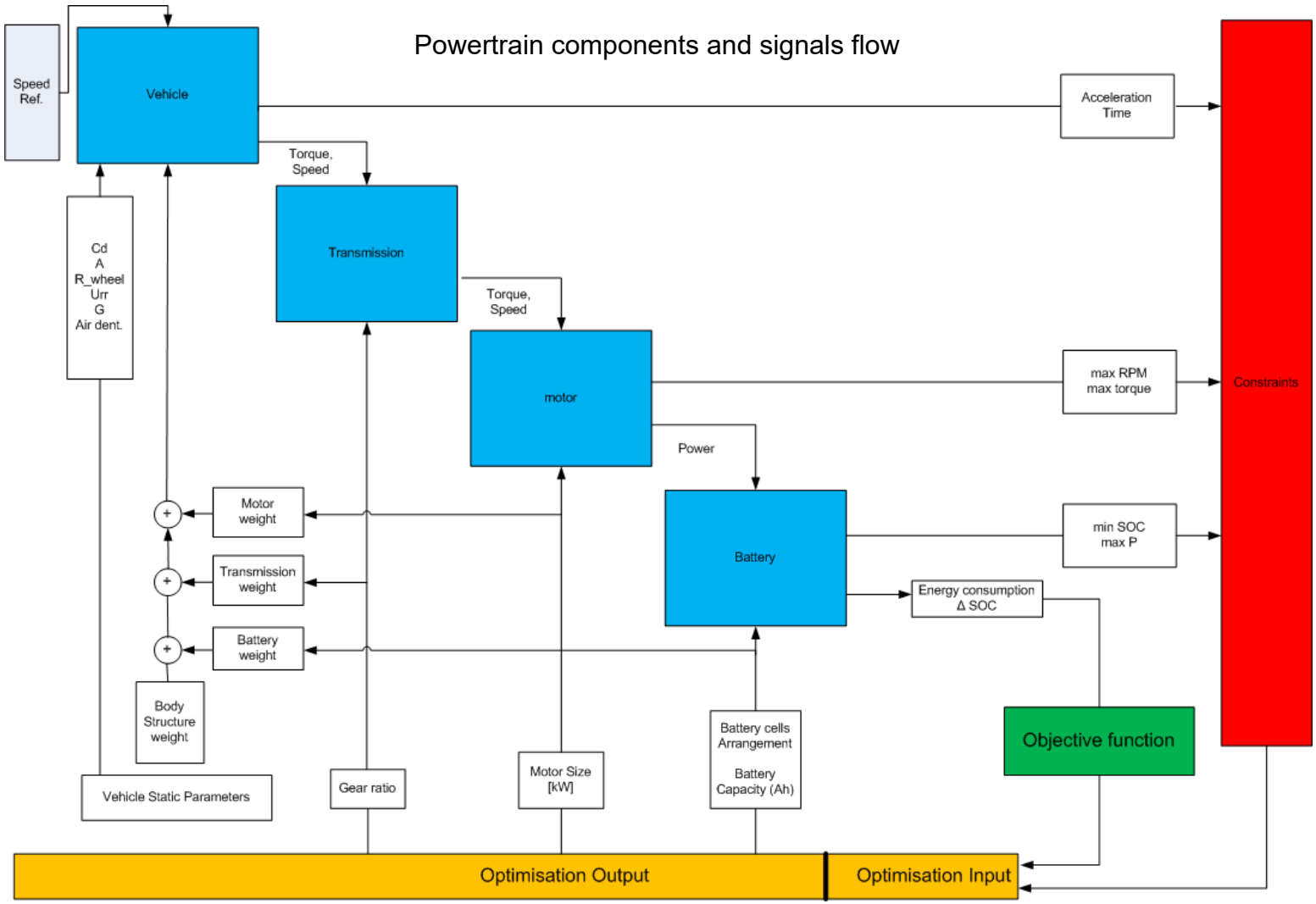

Figure 3-6 BEV powertrain components and model signals flow

3.6 Optimisation results

Table 3-2 Optimisation results

Result No.		Motor [kW]	Battery [kWh]	Gear1	Gear2	Shift point [km/h]	0-97 km/h [s]	Range NEDC [km]	Artemis consumption [kWh] combine	urban	rural	motor
1	Nissan Leaf	80	24	7.9	-	-	9.5	>175	11.3	0.56	2.2	5.7
2	Optimise Artemis 1 gear	78.5	23	7.9	-	-	9.5	>175	11.18	0.55	2.17	5.6
3	Optimise Artemis 2 gears	71.2	22.3	13.2	4.7	68.1	9.42	>175	11.16	0.53	2.19	5.6
4	2 gears w/o weight added	71.2	21.8	13.2	4.7	68.1	9.38	>175	10.91	0.52	2.14	5.48
5	Optimise Urban 2 gear	72.8	23	11.2	9.5	102.2	9.5	>175	N/A	0.54	2.22	N/A
6	Optimise Urban 1 gear	74	22.5	10	-	-	9.5	>175	N/A	0.53	2.16	N/A
7	Optimise Rural 2 gear	73	22.5	12.29	6.64	55.7	9.45	>175	11.28	0.54	2.21	5.66
8	Optimise Rural 1 gear	78.5	22.3	8	-	-	9.47	>175	11.18	0.54	2.17	5.63
9	Optimise Motorway 2 gear	71.2	22.5	12	4.6	74.3	9.5	>175	11.17	0.53	2.19	5.6
10	Optimise Motorway 1 gear	84	22.5	6.7	-	-	9.4	>175	11.2	0.56	2.19	5.6

Table 3-3 Optimisation results in percentage change

Result No.		Motor [% kW]	Battery [% kWh]	Gear1 [-]	Gear2 [-]	Shift point [-]	0-97 km/h [% sec]	Range NEDC [-]	Artemis consumption [% in kWh] combine	urban	rural	motor
1	Nissan Leaf	0	0				0		0.00	0.00	0.00	0.00
2	Optimise Artemis 1 gear	-1.88	-4.17				0.00		1.06	1.79	1.36	1.75
3	Optimise Artemis 2 gear	-11.00	-7.08				0.84		1.24	5.36	0.45	1.75
4	2 gear w/o weight added	-11.00	-9.17				1.26		3.45	7.14	2.73	3.86
5	Optimise Urban 2 gear	-9.00	-4.17				0.00		N/A	3.57	-0.91	N/A
6	Optimise Urban 1 gear	-7.50	-6.25				0.00		N/A	5.36	1.82	N/A
7	Optimise Rural 2 gear	-8.75	-6.25				0.53		0.18	3.57	-0.45	0.70
8	Optimise Rural 1 gear	-1.88	-7.08				0.32		1.06	3.57	1.36	1.23
9	Optimise Motorway 2 gear	-11.00	-6.25				0.00		1.15	5.36	0.45	1.75
10	Optimise Motorway 1 gear	5.00	-6.25				1.05		0.88	0.00	0.45	1.75

Table 3-2 presents the simulation and optimisation results of the Nissan Leaf against various types of the Artemis driving cycle. The optimisation results are presented in two groups, the first group was optimised against the combined Artemis cycle (results numbers two to four) and another group was optimised against individual driving cycles such as urban, rural and motorway (results numbers five to ten). In each of these driving cycles the optimisation results are presented both with a single gear ratio and two-speed gear ratio. Result number one presents the simulation of the original Nissan Leaf that is used as a reference for other results. Table 3-3 shows the same results as Table 3-2 but in terms of percentage difference to the original Nissan Leaf.

Parameters of the Nissan Leaf that were optimised include motor size in kW, battery size in kWh, gear ratio and shift point (when using a two-speed gear). The objective function is the total energy consumption when the vehicle completes one driving cycle in kWh. Constraints were constructed on the range of the vehicle against the NEDC, which had to be greater than 175 km and the acceleration time had to be less than 9.5 s.

In the optimisation against the urban Artemis driving cycle (results numbers five and six), it can be seen that the size of the motor can be reduced by 9% and 7% when using a two-speed gear and increased gear ratio of around 10:1 respectively, while the acceleration time stays the same as the original Nissan Leaf. The consumption of the Artemis urban reduces by up to 5% when using the fixed gear ratio. However, these optimised parameters cannot be used when the vehicle is driven on the motorway due to the too high gear ratio that causes the motor to operate over the speed limit.

On the rural driving cycle, this cycle contains the speed profiles that are in the middle, between urban and motorway. It can be seen that if a vehicle is designed to use a single gear ratio, this driving cycle will give a possible solution for every range of speed. The optimisation results show that the best possible gear ratio for a fixed gear is 8:1 which is close to the original one of the Nissan Leaf and the gear ratio from the optimisation of the combined Artemis cycle with a single gear.

For a two-speed gearbox, the consumption on the Artemis rural was similar to the original gear ratio of the Nissan Leaf. However, the two-speed gearbox was able to reduce the size of the motor by 8% while the acceleration time was improved.

The optimisation against the motorway driving cycle shows close results between the two-speed and single gears. For the two-speed gear, the traction motor can be reduced in size by 11% while the acceleration time stays the same and consumption improves. For a single gear, the motor has to increase in size by 5% to keep the acceleration less than 9.5 s.

For the combined Artemis driving cycle, it is clear to see that the vehicle consumption reduces in both a single gear and a two-speed gear. Moreover, the acceleration performance also increases when using a two-speed gear. It can be seen from the results of the optimised gear ratio that if a single gear were to be selected, the ratio of 7.9 gives the best result and this parameter is the same as the original result for the Nissan Leaf. However, if a two-speed gear is selected, the higher gear ratio will benefit the acceleration time and vehicle driving in urban areas because the motor will operate at higher speeds and in more efficient areas. Alternatively, a lower gear ratio will be an advantage while the vehicle is travelling at high speeds by reducing the motor speed to the most efficient area.

One additional to be noted that, if the weight of a two-speed gear box is decreased and the efficiency is increased by the new technology. It is clear to see in result number four that a two-speed gear will improve consumption in the combined Artemis driving cycle by more than 3% and also improve consumption while the vehicle is operated in individual urban, rural and motorways conditions.

3.7 Chapter conclusion

In this chapter, a Genetic Algorithm optimisation solver was implemented with a cost function of minimum energy consumption. These optimisation results present the possible powertrain parameters that have minimum energy consumption and satisfy vehicle constraints. Constraints used in this optimisation include vehicle range, acceleration time, limit of battery current and limit of motor torque and speed. Simulation results of regenerative braking control rules were presented and implemented within the optimisation. Some findings are discovered in this optimisation result include:

- The battery size should be balanced between required range and required vehicle performances. A larger size of battery gave a better result in vehicle range but provided some negative effects of acceleration time and energy consumption.
- There are some range of gear ratio which is suitable for each of road condition. For example, lower gear ratio of 6.5:1 gave the most efficient energy consumption in the motorway condition while a higher gear ratio of 12.6:1 presents the best consumption efficiency of urban traffic. However, to design a powertrain which is capable for every road condition, gear ratio range between 8:1 may suitable for this single ration transmission BEV.
- For the two-speed gearbox, almost 2% of the energy consumption and 1% of the acceleration time were improved. These results based on assumption of 20 kg weight was added and the transmission efficiency was reduced by 2%.
- In the case of the two-speed gearbox, if the additional weight and inefficiency is negligible due to the advanced transmission technology; the improvement will be almost 4% of energy consumption and 1.3% of acceleration time.
- Two-speed transmission might be a possible option for the BEV manufacturers to increase the powertrain efficiency and vehicle performance for BEVs used in a wide range of speed profiles

4 A Multi-objective comparison of four BEV topologies

4.1 Introduction

In the previous chapter the properties of a conventional SM-SA type of the BEV were considered. In this chapter, the investigation is extended to the three different types of BEV powertrain. A comparison study will be performed in this chapter to find the benefits and costs of each topology. This chapter will begin by describing the BEV topologies considered. The changes and extensions to previous modelling methods, equation used and assumptions will be described. The results will show a trade-off between three objective functions to the selected powertrain topologies. Results and discussions will be described in the later section in this chapter.

4.1.1 Possibility of using multiple electric machines for BEV

Due to simplicity of electric powertrain and the advantage of a precise control of the electric motor, it is possible to add more traction motors to wheels or to another axle of the BEV. These are some possible BEV topologies of the research and prototype vehicles.

- **Double electric machine with double axles drive**

Instead of using only a traction motor at either front or rear axle, both axle can be driven by their separate motor and gearbox. When two traction sources are combined in a single vehicle, with an appropriate controlling method, there are more degree of freedom to operate these power sources in the efficiency and effective ways. This powertrain topology is already developed in the production BEV. The Tesla Model X [14] is equipped with motors and single ratio gearboxes in both front and rear axle. This vehicle become a four-wheel-drive BEV which is currently available in the market. The manufacturer claimed the acceleration performance of 0 to 100 km/s in less than 3 sec.

- **Multiple machine with independent wheel driven**

To further reduce the mechanical devices, wheel can be individually driven by an electric machine. Two traction motors can be used to drive each side of the wheel. The speed and torque of left and right wheels can be equalised electronically. The mechanical differential is eliminated which results in an improvement in efficiency and a reduction in weight [23]. In addition, low speed, high torque motors are needed. Fixed gearing, belt drive or planetary gearbox can be connected between motor and wheel to reduce the speed of the motor and increase torque. Thus, more space becomes available. One of the key advantages of this powertrain architecture is that small (power) motors, which are working together, increase the chance of optimising the efficiency operating points of motors which leads to a reduction in energy consumption [22]. Electronics stability control can be performed by applying vehicle dynamics control directly to the motor [58].

This type of machine is widely used in the electric wheelchair. Using two motors with a gearbox at each of their wheels. By control these motors, the wheelchair can be driven and turned easily. For using with a wheelchair which operated in low speed, this concept is possible however, to use with a BEV there are some challenges in terms of vehicle dynamics to be considered. It is required to control the torque balance between left and right wheels by using an electronic differential. This method may increase the complexity of the non-linear control. Fail to operate will causing problems in vehicle stability and safety [58]. Furthermore, by increasing the number of traction motors, two small motors are working together instead of one large motor. Therefore, the cost of motor per kilowatt is more expensive than a single motor [43]. The number of motor control units and power electronic devices also increase. These affect the overall cost of the system [58].

- **In-wheel motor drive**

In-wheel motors are one of the current research topics to improve driving methods for BEVs [59], [22]. However, the numbers using in-wheel motors in

passenger cars are limited number and most of them are still at the research and development stage. The use of in-wheel motor drives are also available in different areas of research, such as in robotics, as presented in [22]. As in-wheel motor wheels are independent from the drive shaft, this motor is also used in research on an Omni-direction Kart (OK-1) vehicle which is equipped with a four-wheel, in-wheel motor which has its ability to turn at 0 radius [60]. These researches indicate the possibility of using in-wheel motors in a different type of vehicle and discuss the advantages of their high mobility. However, these are applied only at low speeds and mainly focus on the motion of the vehicle rather than the energy consumption.

In terms of energy efficiency, the in-wheel motor is integrated into the vehicle wheel which then eliminates all the mechanical gears and results in no losses in transmission [43]. The in-wheel motor makes a vehicle lighter, more compact, and reduces losses by friction losses and heat losses in transmission. All the power is transferred by wire which benefits space saving and the flexibility of components arrangement and also lowers the centre of gravity [21],[61],[62]. Literature in [63] shows the use of a wheel motor on a motor cycle; the results show that with a wheel motor and using regenerative braking, it can be increased their range by 20%.

However, there are several negative aspects that might affect vehicle performance. The in-wheel motor requires an electronic differential. This is important while the vehicle is driving into the curve path. Consequently, this results in complex torque and speed control between motors. Moreover, an integrated motor in the wheel increases the wheel mass and inertia which causes the effect of un-sprung mass, thus affecting stability, safety and comfort [64],[58], [61],[65].

There are some positive aspects of using in-wheel and independent motors in terms of vehicle dynamics and control. The paper in [66] presents the advantages of using an electric motor as a direct drive in terms of vehicle stability and control. Because the electric motor has some benefits in quick torque generation, possibly

torque estimation. The results in most vehicle stability controls, such as anti-lock braking system (ABS), direct yaw moment control and integrated vehicle dynamic control systems, can be performed more easily than with conventional engine vehicles by using the benefits of electric motors. More details on vehicle dynamics are also available in [58],[66],[67],[68]. The paper in [69] discusses an assisted steering system and global torque control for a four-wheel-independent-drive EV. And the paper in [70] implemented torque-vectoring to control vehicle yaw rate by controlling left and right motors individually.

In-wheel motors require high torque/low speed and this may result in more losses due to higher current required than with a traditional electric motor. The development of an axial flux permanent magnetic machine is considered in [58], [61] and this will help to design and select a suitable in-wheel motor to be used in the BEV [58],[21].

4.1.2 Comparison between different powertrain topologies

Qian et al. [22] present a comparison of energy consumption between a four-wheel independent drive and a centre drive EV. This research uses the reference vehicle model from the Smartcar EV and rescales the motor efficiency map by decreasing motor speed and increasing motor torque by a factor of 0.1 and 2.5 respectively. By using this scale factor, the motor power remains equivalent to the original Smartcar EV. For the four-wheel independent drive, the gearbox was eliminated. It was assumed that torque distributed between the left and right wheels, wheels are in non-slippery condition and regenerative braking is neglected. The results show a more than 13% energy saving compared to the traditional centre drive. Research in [71] also presents the concept design of pure EV by comparing between a centre drive and a gearless drive. This research used the Volkswagen Golf as a reference vehicle. The results show that due to the losses from the gearbox, the centre drive consumed 1-2% more energy than the gearless drive.

4.2 Selected powertrain topologies

In this section, three additional topologies are selected to be simulated and optimised in this chapter. These topologies are the DM-DA, IWM-SA and IWM-DA. The details of each of these topologies will be explained in the following sections.

4.2.1 Double motor, double axles (DM-DA)

This type of powertrain is extended from the SM-SA type of powertrain. A second motor is added at the rear axle and a fixed gearbox was still used for both axles. The vehicle then becomes a 4WD vehicle as presented in Figure 4-1. The two front and rear vehicle axles become independent because of their own electric machine and both are equipped with and independent a single transmission ratio. One reason behind this selection is that it was found that the transmission efficiency has the most sensitive parameters in the BEV powertrain, more details will be discussed in the Chapter 5.

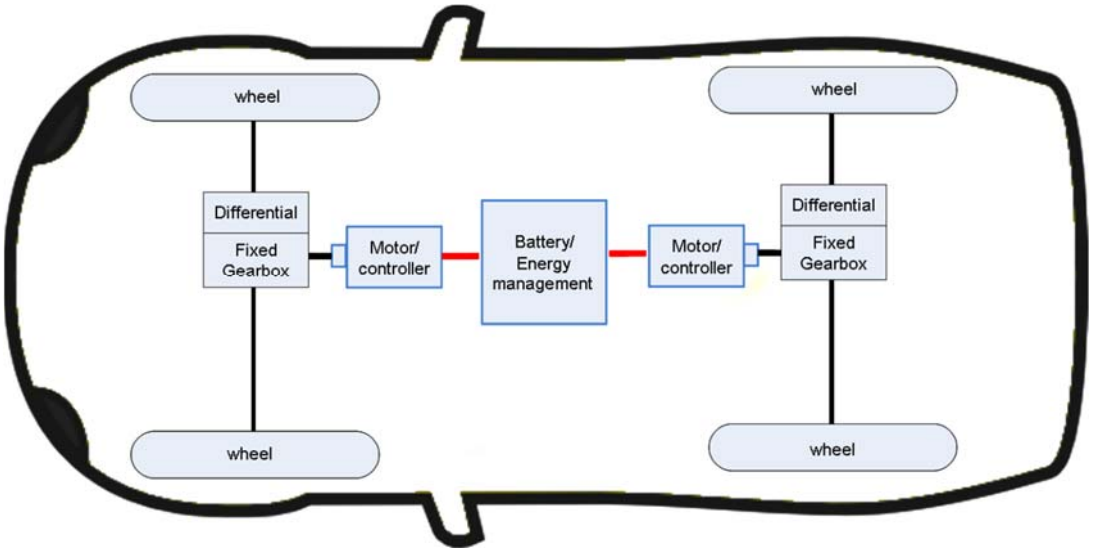

Figure 4-1 Double motor double axles (DM-DA)

It can be seen from the SM-SA type that, unlike a conventional vehicle, the electric machine has enough torque to start traction a BEV and a single ratio transmission is sufficient for the BEV application. However, motor efficiency is not uniform over the torque and speed range. The most efficient operating points are

in a small range of torque and speed as presented as a red area in Figure 3-2. Moreover, if the BEV is to be used in every traffic condition (different driving cycle), two electric machines at different operating points could give a designer greater to match components to requirements. Any given torque demand will be met from either axle, so this topology will be equipped with a torque-split algorithm that will allocate torque between the two axles.

4.2.2 In-wheel motor, single axle (IWM-SA)

In-wheel motors have been considered for use with EV for many years and they can be found as a traction motor for vehicles in many conceptual vehicles. In addition, in the academic and research areas, there are literatures contain number of sources describing these motors' use in vehicle traction as presented earlier section in this chapter. However, only a small number of in-wheel motor production BEVs are available in the market today, probably due to difficulties with some of the problems of vehicle handling and complex control algorithm on vehicle dynamics.

If the limitations can be overcome, in-wheel motors have potential for next-generation BEVs as they offer many benefits. Because of their compact package, lighter weight and direct drive, less space is required, and they provide greater efficiency because they experience no transmission losses. With a more efficient powertrain and lighter vehicle, we might expect better performance and lower energy consumption. In this study, it can see if this is true and will seek to understand the trade-offs between energy efficiency, acceleration performance in relation to other topologies.

This IWM-SA BEV is similar to the SM-SA, apart from the use of in-wheel motors as presented in Figure 4-2. By comparing this vehicle to SM-SA BEV in Figure 3-1, it can be seen that most of the mechanical linkages (black line) have been replaced by electrical linkages (red line). In effect, the gearbox and shaft are replaced by electric cables. All traction forces are produced at the wheels and use direct drive.

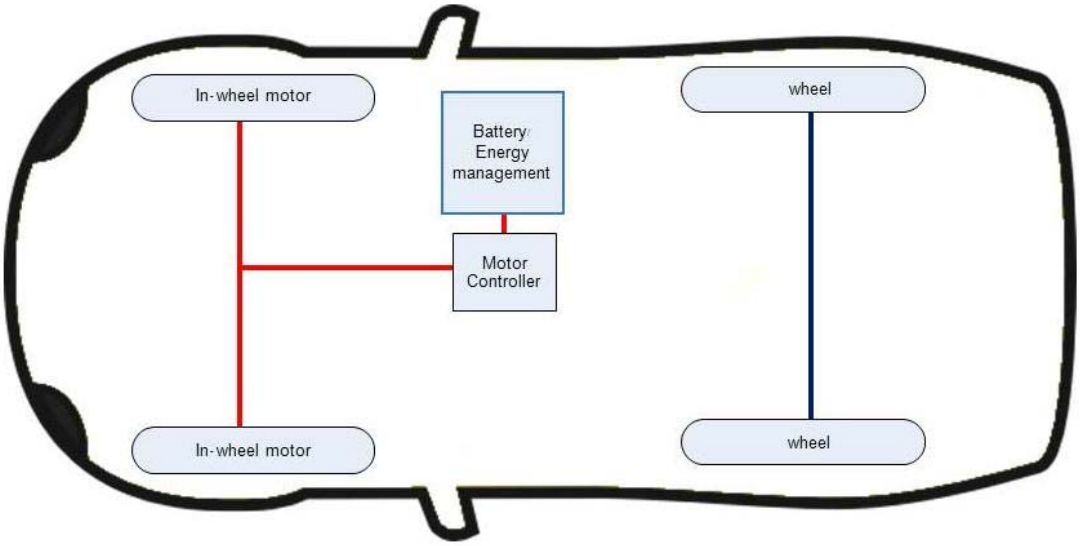

Figure 4-2 In-wheel motor single axle (IWM-SA)

In this topology, the two front in-wheel motors have to be the same size, since differing sizes would present challenges for vehicle stability.

4.2.3 In-wheel motor, double axle (IWM-DA)

This topology is similar to the IWM-SA type, but provides four-wheel drive by adding another two in-wheel motors at each wheel in the rear axle. This is illustrated in Figure 4-3. The advantage is that each wheel can share the load which means that smaller sized motors can be attached in each wheel for the same total amount of power compared to others topologies. As in the DM-DA type, a torque-split algorithm can be applied to maximise the motor efficiency for any given torque demand. An added benefit of this topology is that the vehicle becomes a 4WD, which tends to result in favourable vehicle dynamics.

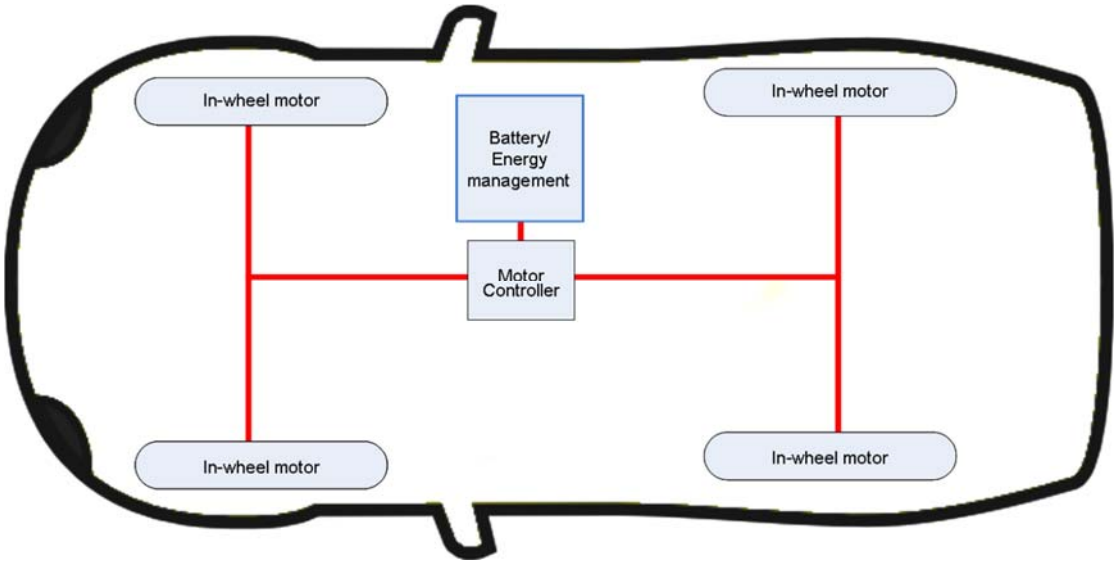

Figure 4-3 In-wheel motor double axles (IWM-DA)

4.3 System model

4.3.1 Modified motor efficiency map for In-wheel motors

In the first two cases (SM-SA, DM-DA), a scalable version of the permanent magnet synchronous machine motor from the Nissan Leaf is used, as mentioned in section 3.3.3. However, for the in-wheel motor, the torque and speed characteristics are different, as mentioned in section 4.1.1 For a reasonable comparison between a conventional and an in-wheel motor, the motor efficiency map is based on the original Nissan Leaf map with torque and speed axis modification. The torque and speed scale were modified to match the normal in-wheel motor available in the market. The original motor map provides a peak torque at 280 Nm, based on a speed of 280 rad/s and a max speed of around 1100 rad/s. This motor delivers up to 80 kW of power. For the in-wheel motor, the torque scale is extended by a factor of 2.5 at the torque axis to get the max torque to 700 Nm and based on a speed of 53 rad/s and a max speed of around 210 rad/s. The peak power becomes 38.5 kW as presented in Figure 4-4.

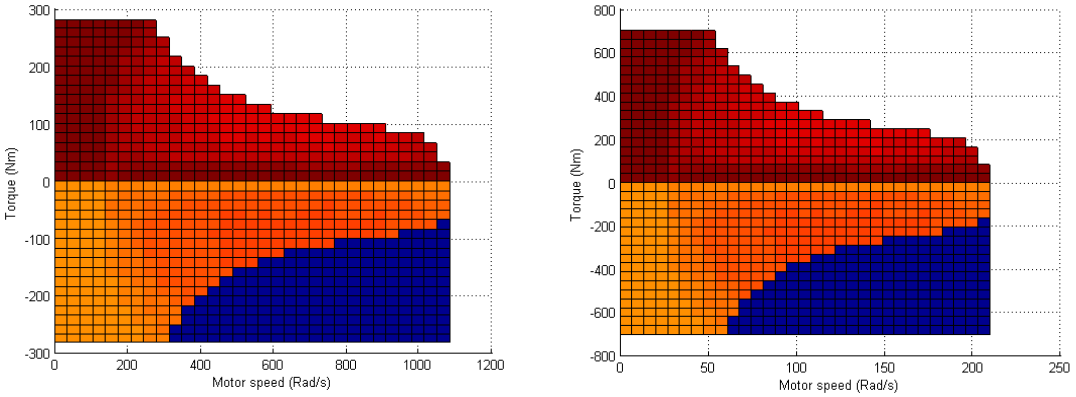

(a) (b)

Figure 4-4 Modified motor map for in-wheel vehicle

(a) Original motor map with 80 kW peak power.

(b) Modified motor map with 38.5 kW peak power

4.3.2 Weight of vehicle

The equations to calculate the powertrain weight are described in section 2.3.2. In this chapter, a method of vehicle mass estimation will be presented in details. As can be seen, the weight of the vehicle affects both acceleration performance and energy consumption. As it can be seen from the result in the Chapter 5 that vehicle mass is a parameter that sensitive to energy consumption. The following section separates the calculation of vehicle mass into three components: electric machine and transmission, battery and vehicle body.

- **Weight of transmission and electric machine**

This section aims to integrate the weight of the electric machine and its transmission into a single unit. It is assumed in this study that the SM-SA and DM-DA, each motor is equipped with a single ratio transmission only. And it is also assumed that all transmission ratios are uniform in weight calculation.

The exact weight of the Nissan Leaf motor is not published by Nissan; however, the weight of the motor is estimated by using the average weight of the permanent magnet motor at the same peak power as the Nissan Leaf. The estimation of

motor weight is based on the data available. This table shows assumptions of transmission weights in different powertrain topologies.

Table 4-1 Weight of transmission in different topologies	
Type	**Transmission weight**
SM-SA	Unchanged for every powertrain size
DM-DA	Unchanged for the front axle and 30 kg added for rear axle
IWM-SA	The reduction of 25% applied for overall powertrain weight
IWM-DA	The reduction of 25% applied for overall powertrain weight

Table 4-1 and Table 4-2 show details of assumptions and the equations on the weight of motors and transmission. In this DM-DA type, 30 kg of additional transmission is added to the total vehicle weight. And 25% of weight reduction will be applied to in-wheel vehicles as they do not require transmission.

Table 4-2 Weight of motors and transmission in different topologies			
	Front motor	**Rear motor**	**Transmission**
SM-SA	$0.532 \times P_{motor,kW} + 21.6$	No motor	Unchanged
DM-DA	$0.532 \times P_{motor,kW} + 21.6$	$0.532 \times P_{motor,kW} + 21.6$	30 kg added
IWM-SA	$(0.532 \times P_{motor,kW} + 21.6) \times 2$	No motor	25% removed
IWM-DA	$(0.532 \times P_{motor,kW} + 21.6) \times 2$	$(0.532 \times P_{motor,kW} + 21.6) \times 2$	25% removed

From these tables, it can be found that if the vehicle is subjected to the equal combination of total electric machine power (80 kW SM-SA and 40 + 40 kW DM-DA) the DM-DA type is always heavier than the SM-SA. These results will be shown in the Table 4-4

- **Weight of battery**

The weight of the battery pack is calculated by the integration of battery cells. The weight of the battery cell for the Nissan Leaf was published in [45]. The cell

weight is 787 g and there are four cells in one module and 48 modules in a battery pack. There are 0.787 x 4 x 48 = 151.1 kg. Therefore an assumption can be made of 0.06 kg/kW for the mass of thermal management system and 0.14 kg/kW for the mass of harness and bus bar [46]. The total weight of cell weight will be 0.975 kg of battery cell as described by

$$W_{Battery} = N_{\text{cells,seies,Battery}} \times N_{\text{cells,parellel,Battery}} \times 0.975 \quad \textbf{(4-1)}$$

The total estimated weight of the 24 kWh battery will be 187.2 kg. The mass of the battery estimation in every topology remains the same as the SM-SA type because they use a similar type of battery pack.

- **weight of vehicle body and chassis**

Vehicle body and chassis weight are estimated from the original Nissan Leaf total kerb weight which is 1521 kg (the 2011/2012 model) and the weight of the powertrain which is described previously. In case the powertrain size changes, the difference in powertrain weight is calculated and multiplied by a mass compounding factor of 1.6 to compensate for the weight increase of the vehicle chassis.

4.3.3 Cost of powertrain

Table 4-3 shows details of equations and the assumptions made for calculating the powertrain cost.

Table 4-3 Cost of Motors and Transmission in different topologies

	Front	Rear	Transmission
SM-SA	$16 \times P_{motor,kW} + 385$	No motor	As SM-SA
DM-DA	$16 \times P_{motor,kW} + 385$	$16 \times P_{motor,kW} + 385$	$2\text{nd gearbox} + 5\%$
IWM-SA	$(16 \times P_{motor,kW} + 385) \times 2$	No motor	As SM-SA
IWM-DA	$(16 \times P_{motor,kW} + 385) \times 2$	$(16 \times P_{motor,kW} + 385) \times 2$	As SM-SA

Battery cost for every powertrain topology is calculated by the same method as presented in this section.

$$\text{Cost}_{\text{cell,Battery,\$/kWh}} = 11.1\times\left({}^{P}/_{E}\right) + 221.1 \quad \textbf{(4-2)}$$

$$\text{Cost}_{\text{Pack,Battery,\$}} = \left(\text{Cost}_{\text{cell,Battery,\$/kWh}} + 13\right)\times\text{Capacity}_{\text{pack,Batt,kWh}} + 680 \quad \textbf{(4-3)}$$

Total powertrain weight and cost are calculated based on the weight and cost of the motor, transmission and battery as presented by

$$\text{Cost}_{\text{Powertrain,\$}} = \text{Cost}_{\text{Motor,\$}} + \text{Cost}_{\text{Pack,Battery,\$}} \quad \textbf{(4-4)}$$

4.3.4 Drivability (acceleration time)

The equation to calculate the acceleration test time is a simple integration of traction force, vehicle total mass and velocity. The integration takes a limit between 0 m/s to 27.78 m/s (0 – 100 km/h) as presented by

$$\text{Time}_{\text{Acceleration 0-100 km/h}} = \int_{0}^{27.78} \frac{m}{F_w(v)}\, dv \quad (4\text{-}5)$$

4.4 Multi-objective optimisation on different BEV topologies

The multi-objective optimisation for the BEV topologies are considered to minimise three objectives. The first objective is energy consumption on the combined Artemis driving cycle, the second objective is accelerative time from 0-100 km/h and the last objective is the powertrain cost. The constraint of this optimisation is the range of NEDC that require to be greater than 175 km. This multi-objective optimisation using Genetic Algorithm solvers from the MATLAB Global Optimisation Toolbox, the detail of this software is available from [72]. Equation of the cost functions and constraints of this multi-objective optimisation are presented by

$$\text{Minimise } J_1(X_D), J_2(X_D), J_3(X_D) \quad (4\text{-}6)$$

$$J_1(X_D) = E(X_D) = \text{cycle energy consumption} \quad (4\text{-}7)$$

$$J_2(X_D) = (\text{acceleration time})_{0-100\ km/h} \quad (4\text{-}8)$$

$$J_3 = \text{Cost}_{\text{Powertrain,\$}} \quad (4\text{-}9)$$

subject to $\text{Range}(\text{NEDC}) \geq 175\ \text{km}$ (4-10)

4.5 Results

4.5.1 Vehicle simulations without optimisation

Table 4-4 shows the vehicle weight estimation on the different BEV topologies when a total 80 kW motor such as the Nissan Leaf was applied to every topology and some assumptions are applied to the transmission weight. The first topology, SM-SA, a single 80 kW motor at a front axle is applied. In this type the parameters are set as a benchmark for the comparison. For the DM-DA, it is applied two 40 kW motors at the front and rear axle, for the IWM-SA a two 40 kW in-wheel motor at each left and right wheel on the front axle and for the IWM-DA is applied a four 20 kW in-wheel motor at each of their wheels. This comparison presents a vehicle weight assumption for different powertrain topologies if the same motor size (80 kw) and battery size (24 kWh) as the Nissan Leaf is applied.

The results show that the DM-DA will gain the most extra weight because of using an additional motor and gearbox on the rear axle. For in-wheel topologies, a smaller sized with four motors are applied; however, due to the beneficial gearless drive, an assumption of 25% of powertrain weight reduction was made and this made the whole powertrain just a little different from the original case study vehicle.

Table 4-4 Vehicle weight estimation equivalent to 80kW motor				
	Front motor (power, weight, number)	Rear motor (power, weight, number)	Transmission **weight**	Different from Nissan Leaf (kg)
SM-SA	80 kW, 64.16 kg, 1	No motor	Front only	0
DM-DA	40 kW, 42.88 kg,1	40 kW, 42.88 kg, 1	Front and Rear, 30kg added	+51.6
IWM-SA	40kW, 42.88 kg, 2	No motor	25% reduce	+0.16
IWM-DA	20kW, 32.24 kg, 2	20kW, 32.24, 2	25% reduce	+32.56

Table 4-5 shows the simulation results for all objective functions (energy consumption, acceleration time and powertrain cost) from the vehicle parameters of the Table 4-4 on the combined Artemis cycle. The simulation results show that the in-wheel topologies consume less energy consumption than the original vehicle case study. The interesting results show that the DM-DA type had around 50 kg extra added due to the rear axle motor and transmission; however, the vehicle consumed around 1% extra energy than the original vehicle. This is because of the effect of the motor torque split that divides the vehicle torque into front and rear motors efficiently. The next section will show a consumption result improved if all motors and transmission ratios are optimised.

Table 4-5 Estimation of objective functions				
	Total Weight (kg)	Acceleration Time (s)	Cost (US$)	Energy (kWh/100km)
SM-SA	1521	9.9	8,920.3	16.47
DM-DA	1572.6	10.5	9,305.3	16.64
IWM-SA	1521	11.18	9,325.7	15.99
IWM-DA	1553.6	11.47	10,108	16.05

4.5.2 Results of multi-objective optimization for different topologies

Figure 4-5 shows the results of the multi-objective optimisation between the energy consumption and acceleration time of different BEV topologies. A solid line shows the benchmark of the acceleration of the Nissan Leaf. It is clear to see that all optimised results in every topology give a better result than the original Nissan Leaf. Energy consumption and acceleration performance are traded off against each other. Better acceleration requires a large motor with more weight that consumes more energy. The Pareto-front in this Figure shows the best optimisation results and trade-off between these objectives.

Table 4-6 shows the detailed results of each topology at the Nissan Leaf benchmark (9.9 sec acceleration time). To get this acceleration performance, it is required at least an 80 kW motor for every topology. The results show that IWM-DA gives the best energy consumption among other topologies with an improvement of more than 3% energy from the case study vehicle. The optimum result of SM-SA which is similar to the Nissan Leaf shows a small improvement from the case study vehicle. To obtain this improvement, the gear ratio of the SM-SA will be selected a little higher than the case study and requires a smaller sized battery. This make the vehicle consume a little better on the combined Artemis driving cycle with the same acceleration performance and range.

Figure 4-6 shows the powertrain cost for each of the BEV topologies. As can be seen from Figure 4-5, the IWM-DA gives the best results in both energy efficiency and acceleration. However, the disadvantage of this powertrain is the most expensive powertrain cost. To compare the energy consumption results with the benchmark result from the vehicle case study, a solid line in Figure 4-6 and information in Table 4-7 show the benchmark optimisation results between powertrain cost and energy consumption. The results show that for the optimised SM-SA, a slightly larger motor and gear ratio (84kW, 8.9:1) was selected and the battery size was reduced by 1 kWh. This optimisation result was around 2.3% cheaper. For other topologies, they are more expensive than the original vehicle. There are some interesting points to note, i.e. by using an in-wheel motor, the

IWM-SA is about 1% more on cost while the IWM-DA is about 26% more expensive. However, an expensive powertrain cost of the IWM-DA type is trade-off with a better energy consumption and drivability.

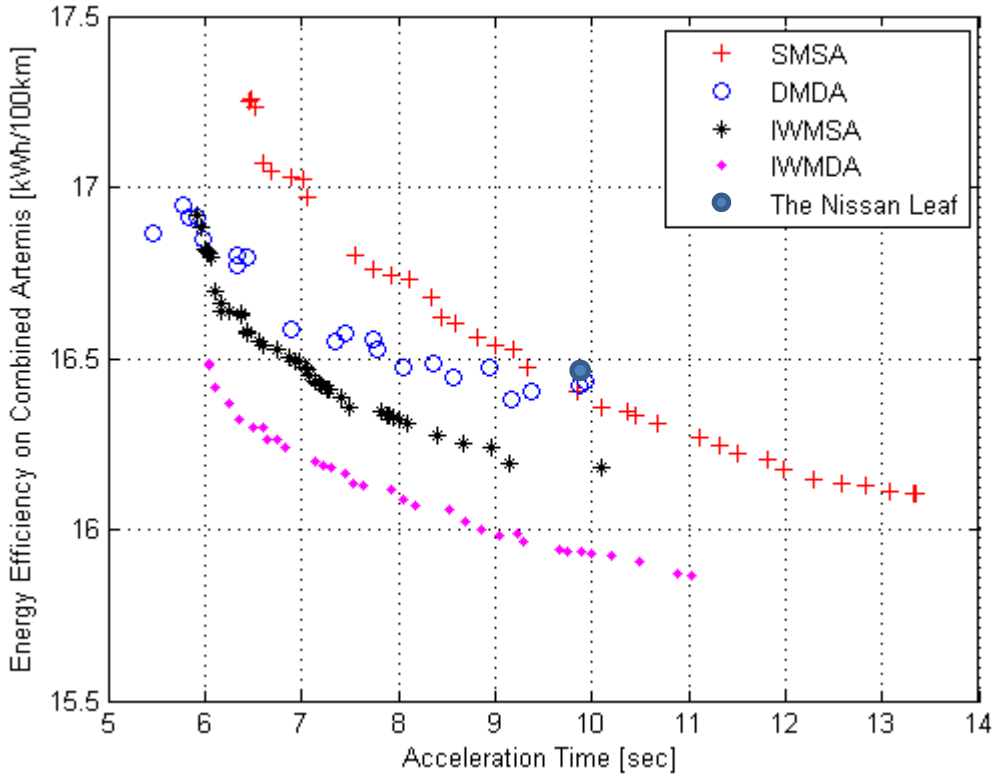

Figure 4-5 Pareto front of acceleration time and energy consumption

Table 4-6 Energy Consumption for Acceleration benchmark (9.9s)

	Motor Size in kW (Front, Rear)	Transmission Ratio	Battery Size (kWh)	Energy Consumption (kWh/100km), (%)
Case Study	80 kW, not present	7.9, -	24	16.47, (0%)
SM-SA	80 kW, not present	8.1, -	23	16.4, (-0.5%)
DM-DA	42 kW, 46 kW	6.56, 6.29	24	16.4, (-0.3%)
IWM-SA	43kW + 43kW, not present	Direct Drive	21.1	16.2, (-1.8%)
IWM-DA	29kW + 29kW, 17kW + 17kW	Direct Drive	22.3	16.0, (-3.3%)

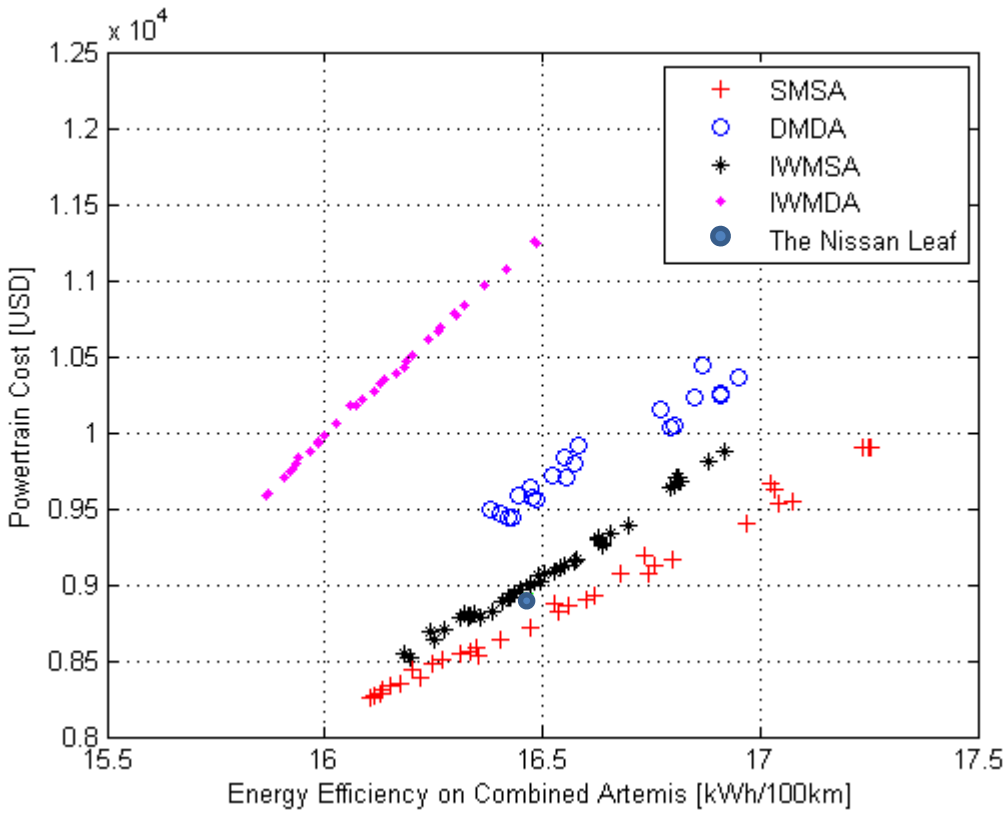

Figure 4-6 Pareto front of energy consumption and powertrain cost

Table 4-7 Powertrain cost for energy consumption benchmark (16.47kWh/100km)

	Motor Size in kW (Front, Rear)	Transmission Ratio	Battery Size (kWh)	Powertrain Cost (US$), (% change)
Case Study	80 kW, not present	7.9,-	24	8,920.3, (0%)
SM-SA	84 kW, not present	8.99, -	23.07	8710.75, (-2.35%)
DM-DA	60 kW, 40 kW	7.96, 8.01	24	9631, (+7.96%)
IWM-SA	61.7kW + 61.7kW , not present	Direct Drive	20.57	9002, (+0.91%)
IWM-DA	65kW + 65kW , 20kW + 20kW	Direct Drive	23.3	11258, (+25.98%)

4.6 Discussion of results by topology

4.6.1 SM-SA

The SM-SA is the simplest BEV powertrain that uses the most mechanical connection between components, thus, the powertrain cost is low and require less complex electronics control system. The result shows that 60 kW is the smallest motor size to complete the driving cycle. This solution provides the most minimum energy consumption but it has a poor acceleration performance.

This topology provides a greatest benefit in low-cost powertrain but it does not give a good trade-off between energy consumption and driveability performance.

4.6.2 DM-DA

This BEV topology has two separate motors in the front and rear axles. Providing two motors options and two set of single ratio gearbox, this topology has a benefit in improving consumption and performance to the SM-SA as there are more options to optimise the powertrain components.

This topology provided a better power for acceleration with minimum consumption than SM-SA. However, the disadvantages are that the powertrain cost is still higher than an SM-SA type and it may need a powertrain controller with torque split algorithm between front and rear axle. This topology is possibly suitable for an off-road BEV that requires power and 4WD ability.

4.6.3 IWM-SA

IWM-SA required a small additional powertrain cost compared to the SM-SA but it provided a better energy consumption and acceleration performance. However, the IWM-SA is not as good as the IWM-DA in term of energy efficiency and drivability performance but for the budget issue. The use of in-wheel motors may require a consideration of electronic differential algorithm and the un-sprung mass issues.

In the author's point of views, this topology will be suitable for the future small city BEV which is not require a high-performance powertrain but sufficient energy efficiency and lower price than the IWM-DA.

4.6.4 IWM-DA

IWM-DA is the topology that provided a very good acceleration time with minimum energy consumption. The drawback of this topology is their number of motors that make it become more expensive. Moreover, without using mechanical links between motors, it will be a complex task for the motor control algorithm. Vehicle dynamics are still a large issue for this topology. More limitation on the motor size will be considered if the vehicle's dynamic performance is investigated. This issue will be interesting to investigate in the future work.

4.7 Chapter conclusions

In this chapter the model, assumptions and optimisation results of the selected BEV powertrain topologies have been presented. The first two BEV powertrain topology, SM-SA and DM-DA, are already available as a production vehicle. However, the last two BEV topologies, the in-wheel types, are mostly available as a conceptual vehicle and research prototype. The findings in this chapter will give comparative details for those selected BEV topologies as far as the limitations of powertrain data is available.

- The first topology, SM-SA, benefit from its simple powertrain. This results in a lower powertrain cost compared to the other topologies.
- The DM-DA topology's additional motor at the rear wheels gives an extra degree of freedom to operate motors in an efficient way. Compared to the SM-SA, it is more expensive but it provides a good acceleration with minimum consumption.
- The in-wheel BEV topology has high drivability performance and low energy consumption because of the elimination of weight and efficiency

losses in mechanical transmission components. It is, however, the most expensive.

Each topology is trade-off between energy saving, driving performance and cost. Table 4-8 and Figure 4-7 summarise the keys strengths and weaknesses for each topology which may be a guideline for vehicle manufacturers to produce more available and a variety of styles of future BEVs.

Table 4-8 Trade-off between different topologies and objective functions

	Energy efficiency	Driving performance	Powertrain cost
Energy efficiency	IWM-DA	IWM-DA	SM-SA
Driving performance		DM-DA	IWM-SA
Powertrain cost			SM-SA

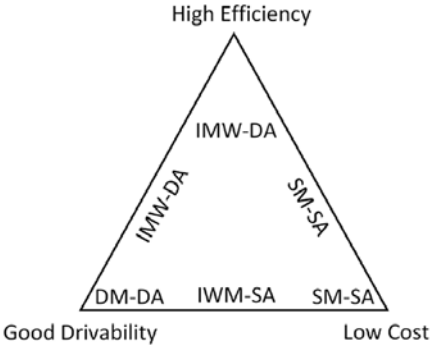

Figure 4-7 Trade- off between different topologies and objective functions

5 Sensitivity analysis for battery electric vehicle

5.1 Introduction

Key important components of a BEV powertrain are the electric machine, transmission and battery which are required to be designed simultaneously because parameters of these components also affect the interaction between them. For example, BEV range will be directly affected by the size of battery while the vehicle acceleration performance is strongly link to the size of motor. To be precise, battery size is not the only parameter that affects the vehicle range but motor size and gear ratio are parameter that used for estimating the vehicle range.

In general, BEV powertrain components and their sizing are usually designed simultaneously using optimisation technique as described earlier in the previous chapters. There is much literature that presents optimisation technique for vehicle powertrain in both single objective (e.g. [27],[73],[74]) and multi-objective (e.g. [75], [76]). Usually these optimisation techniques just to find the cost function and constraints without exploring insight the interaction between components and the energy consumption.

To investigate the effect of parameters on the objective function, a sensitivity analysis can be performed on the parameters of the BEV powertrain. Sensitivity analysis is a technique to answer the question of which input parameters and assumption parameters are the most important to determine the objective function. Sensitivity analysis is also used to study the accuracy and robustness of mathematical models [77]. It is used in a wide area of research such as financials, ecology, nuclear physics and environmental science [78]. In engineering, sensitivity analysis has been used in aerospace vehicle design [79], in combustion modelling [80] and automotive [81],[82],[83],[84].

This chapter aims to obtain an insight into the BEV powertrain parameters by determining which of those parameters affect the energy consumption the most. The sensitivity analysis technique is implemented by starting with first order

sensitivity analysis, in Section 5.2.1, to determine the most sensitive parameter in the BEV powertrain. Then, the second order sensitivity analysis, in Section 5.2.2, is implemented to explore the cross-coupling effect between a pair of powertrain parameters. Finally, these techniques are applied to the SM-SA BEV and use the Nissan Leaf as a vehicle case study as presented in Section 5.3.

5.2 Mathematical techniques for sensitivity analysis

The BEV powertrain model can be generalised as an algebraic equation for a fixed driving cycle as presented by Guzzella and Sciarretta in [25]**.** Energy consumption can be expressed as an algebraic function of several parameters;

$$\bar{E} = f(p_1, p_2, \dots, p_n) \quad \textbf{(5-1)}$$

This technique in the literature [25] shows methods of calculating first order sensitivity analysis for a limited number parameters of road vehicle. In this thesis, a formal technique is developed that explores the effect of the energy consumption sensitivity on the BEV by extending EV powertrain parameters from the normal road vehicle such as motor efficiency, gear efficiency and regenerative breaking efficiency. Moreover, the effect of cross-coupling between different powertrain parameters using the second order sensitivity analysis is also introduced in this study. The mathematical technique for sensitivity analysis and their application with a case study of the C-segment BEV is explained in the Sections 5.3.

5.2.1 First order sensitivity analyses from the literature

In [25], for a fixed-driving cycle, energy consumption can be formulated as a quasi-static model of the vehicle parameters:

$$\bar{E} = f(\Phi) \quad \textbf{(5-2)}$$

where $\bar{E} = f(p_1, p_2, \dots, p_n)$ represents the vehicle key's parameters. In optimization terms, $\bar{E}$ is the objective function. Sensitivity to parameter p_i can be defined in terms of the partial derivatives:

$$S_{\mathrm{p_i}} \overset{\mathrm{def}}{=} \lim_{\delta \mathrm{p_i - nom} \to 0} \frac{[\bar{E}(p_{\mathrm{i-nom}} + \delta p_{\mathrm{i-nom}}) - \bar{E}(p_{\mathrm{i-nom}})]/\bar{E}(p_{\mathrm{i-nom}})}{\delta p_{\mathrm{i-nom}}/p_{\mathrm{i-nom}}} \quad \textbf{(5-3)}$$

Thus

$$S_{\mathrm{p_i}} = \frac{\partial \bar{E}}{\partial p_{\mathrm{i}}}(p_{\mathrm{i-nom}}) \cdot \frac{p_{\mathrm{i-nom}}}{\bar{E}(p_{\mathrm{i-nom}})} \quad \textbf{(5-4)}$$

This formula describes the change in energy consumed in response to small changes in vehicle parameters.

Equation (5-4) defines the first-order sensitivity analysis common in the literature. This analysis shows which parameters most affect the energy consumption at the nominal parameter values. For the designer, the result will shows which parameters should be considered to improve as a priority and to value them accurately.

In the literature [25], three vehicle parameters, aerodynamics drag area, vehicle mass and rolling resistance coefficient are compared. The standard NEDC has been used in this literature to investigate the sensitivity of the energy consumption. The results show that the mass of the vehicle is the most sensitive parameter for the energy consumption.

The literature [25] presents a very good method and results from the sensitivity analysis however, the results themselves were limited to the parameters of the vehicle body (drag mass and rolling resistant) only and not investigate into the vehicle powertrain such as transmission and electric machine efficiency. Moreover, the interaction between parameters has not been investigated. In practice, if the gearbox efficiency is improved it is likely that the efficiency of electric machine that connected to the gearbox will become more significant. In this thesis, the second order sensitivity analysis will present the coupling between parameters and help designers to focus on the improvement of the most sensitive parameters on the optimisation process.

5.2.2 Expression of second-order sensitivities

The second order sensitivity analysis is described by

$$\boldsymbol{S}'_{\Phi} = \begin{bmatrix} \frac{\partial^2 f(\Phi)}{\partial p_1^2} \cdot \frac{p_1^2}{\bar{E}} & \frac{\partial^2 f(\Phi)}{\partial p_1 \, \partial p_2} \cdot \frac{p_1 p_2}{\bar{E}} & \cdots & \frac{\partial^2 f(\Phi)}{\partial p_1 \, \partial p_{\mathrm{n}}} \cdot \frac{p_1 p_{\mathrm{n}}}{\bar{E}} \\ \frac{\partial^2 f(\Phi)}{\partial p_2 \, \partial p_1} \cdot \frac{p_2 p_1}{\bar{E}} & \frac{\partial^2 f(\Phi)}{\partial p_2^2} \cdot \frac{p_2^2}{\bar{E}} & \cdots & \frac{\partial^2 f(\Phi)}{\partial p_2 \, \partial p_{\mathrm{n}}} \cdot \frac{p_2 p_{\mathrm{n}}}{\bar{E}} \\ \vdots & \vdots & \ddots & \vdots \\ \frac{\partial^2 f(\Phi)}{\partial p_{\mathrm{n}} \, \partial p_1} \cdot \frac{p_{\mathrm{n}} p_1}{\bar{E}} & \frac{\partial^2 f(\Phi)}{\partial p_{\mathrm{n}} \, \partial p_1} \cdot \frac{p_{\mathrm{n}} p_2}{\bar{E}} & \cdots & \frac{\partial^2 f(\Phi)}{\partial p_{\mathrm{n}}^2} \cdot \frac{p_{\mathrm{n}}^2}{\bar{E}} \end{bmatrix}_{\Phi_{\mathrm{nom}}} \quad \textbf{(5-5)}$$

This second-order sensitivity analysis indicates the cross-coupling parameters in the powertrain equations. The equations (5-6) to (5-11) will present the examples of using first and second order sensitivity analysis to examine the sensitivity and cross-coupling of parameters.

To understand the equation (5-5) this following example will give a fundamental idea of cross-coupling effect between parameters. Consider a problem:

$$\hat{E} = 0.5\hat{p}_1 + 0.5\hat{p}_2 \quad \textbf{(5-6)}$$

where $\hat{E}$ is our objective function and $\hat{p}_1$ and $\hat{p}_2$ are the considered parameters.

The sensitivity of parameters is presented by the first-order partial derivative as presented by

$$\boldsymbol{S}_{\Phi} = [0.5 \quad 0.5] \quad \textbf{(5-7)}$$

It can see that $\hat{E}$ is equally sensitive to each parameter $\hat{p}_1$ and $\hat{p}_2$. Furthermore, it can see the second-order sensitivity are

$$\boldsymbol{S}'_{\Phi} = \begin{bmatrix} 0 & 0 \\ 0 & 0 \end{bmatrix} \quad \textbf{(5-8)}$$

which shows that the sensitivities are not cross-coupled: if a small change is made in p_1, then the sensitivity to p_2 will not change.

Consider another problem

$$\widehat{E} = \frac{\hat{p}_1}{\hat{p}_2} \tag{5-9}$$

The first-order sensitivity analysis is:

$$\boldsymbol{S}_{\Phi} = \left[\frac{1}{\hat{p}_2} \quad -\frac{\hat{p}_1}{\hat{p}_2^2}\right]_{\hat{\Phi}_{nom}} = [1 \quad -1] \tag{5-10}$$

and it can see from the equation (5-10) that $\overline{E}$ will increase in response to a small relative change in p_1 but p_2 will decrease in a similar quantity. And the second-order sensitivity analysis is

$$\boldsymbol{S}'_{\Phi} = \begin{bmatrix} 0 & -\frac{1}{\hat{p}_2^2} \\ -\frac{1}{\hat{p}_2^2} & \frac{2\hat{p}_1}{\hat{p}_2^3} \end{bmatrix}_{\hat{\Phi}_{nom}} = \begin{bmatrix} 0 & -1 \\ -1 & 2 \end{bmatrix} \tag{5-11}$$

From the equation (5-11) shows that p_1 is sensitive to p_2 and vice versa. But if p_2 is increased, the problem becomes more sensitive to p_2 itself; however, there is not a corresponding relationship for p_1. It can see that if p_1 is a vehicle's powertrain efficiency and p_2 is vehicle mass. It would say that if a vehicle mass is reduced, a powertrain efficiency will become an important factor to consider in this design.

In the next section, the techniques of applying formal second-order sensitivity analyses are developed and this technique is used for the quasi-static vehicle models. The following section shows the parameters of the BEV and the use of this sensitivity analysis to help the designer determine the interdependencies of the vehicle parameters.

5.3 Case study in powertrain optimization

In the previous section, the mathematics for the sensitivity analysis technique was introduced; in this section the technique is applied to a case study based on a popular real-world vehicle. BEVs have now entered the mass consumer market.

The Nissan LEAF a production C-segment vehicle is perhaps the best known. This section aims to present a simplified analytical BEV model and perform the first and second order sensitivity analysis. Vehicle parameters and powertrain components are based on publically available data [44] and are otherwise based on the authors' assumptions: which are based on the range performance data provided by the vehicle manufacturer [12]. In particular, this study has aimed to reproduce the stated "combined" range of 175 km on the NEDC with a 24 kWh battery.

Figure 5-1 shows a schematic diagram of the BEV powertrain of the Nissan LEAF. The vehicle is driven by a single 80 kW motor with a 7.9:1 constant ratio transmission at the front wheels. It is similar to the quasi-static backward simulation as in the previous chapter, to compute energy consumption, the calculations are started at the wheels. Driving cycle gives information of vehicle speed and losses due to environment are computed as functions of speed and acceleration then the required power at transmission, electric machine and battery is determined. Finally, all losses are combined and the energy consumption of the vehicle is calculated.

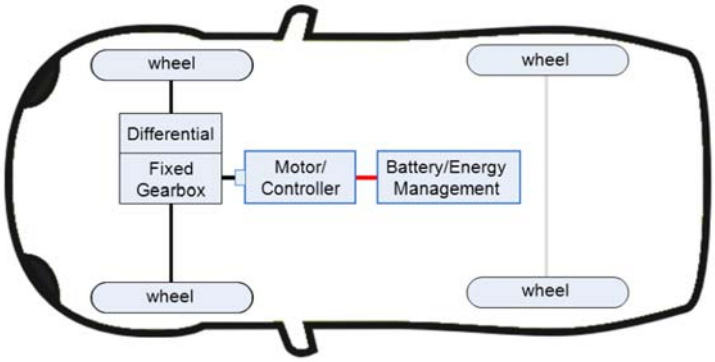

Figure 5-1 Schematic diagram of case study vehicle powertrain.

The assumption for this chapter are

i) The nominal average fixed ratio transmission efficiency is 97%.
ii) The nominal average combine motor and inverter efficiency is 85%.

iii) The battery average voltage (modelled as constant) is assumed to be 345V.
iv) The charge and discharge battery resistances are taken to be 216 × 10^{-3} ohm and 192 × 10^{-3} ohm.

The vehicle is also assumed to be driving on a level surface, so gradient effects are ignored. Two driving cycles are considered: the NEDC as specified in international testing standards [33], and a combined "real-world" cycle made from combinations of the well-known ARTEMIS cycles [34]. The "combined" ARTEMIS cycle which is used in this chapter consists of two cycles of the "urban" segment followed by two cycles of the "road" segment and then one cycle of the "motorway" segment as presented in the Section 2.1.1. In the following subsections, algebraic equations will be presented for describing the vehicle's energy consumption. The sensitivity analysis is then applied to them.

5.3.1 Vehicle model and energy calculation

In this chapter, the energy balance is considered to be associated with the following elements: aerodynamic drag force, rolling friction force, inertial forces, transmission losses, losses in the motor, and losses in the battery.

Energy balance can be classified from the integral of summing force acting onto the vehicle and average speed on each of the driving cycle:

$$E = \int_0^{\mathrm{T}} \sum \mathrm{F}(t) \cdot \overline{v}\,(t)\mathrm{dt} \tag{5-12}$$

Note that for practical reasons, energy, E, will be scaled so that it is expressed per unit distance rather than per unit time (this is consistent with the way standards are presented and enables a better understanding of the results). In the following equations, x_{total} is the driving distance (m). The consumption due to aerodynamic losses, E_{Aero}, is given by:

$$\begin{aligned} E_{\mathrm{Aero}} &= \frac{1}{X_{\mathrm{total}}} \cdot \frac{1}{2}(1.25) \cdot A_{\mathrm{f}} \cdot C_{\mathrm{d}} \cdot \sum_0^{\mathrm{T}} \overline{v}^3 \cdot t \cdot 100 \\ &= \frac{62.5}{x_{\mathrm{total}}} \cdot A_{\mathrm{f}} \cdot C_{\mathrm{d}} \cdot \overline{v}^3 \cdot T \end{aligned} \tag{5-13}$$

The energy consumption from rolling resistance is given by:

$$E_{\text{Rolling}} = \frac{1}{X_{\text{total}}} \cdot (9.81) \cdot m_{\text{v}} \cdot C_{\text{r}} \cdot \sum_{0}^{\text{T}} \overline{v} \cdot t \cdot 100 = \frac{981}{x_{\text{total}}} \cdot m_{\text{f}} \cdot C_{\text{r}} \cdot \overline{v} \cdot T \quad \textbf{(5-14)}$$

The energy consumption from inertia is given by:

$$E_{\text{Inertia}} = \frac{1}{X_{\text{total}}} \cdot m_{\text{v}} \cdot \sum_{0}^{\text{T}} (a_{\text{traction}} \cdot v \cdot t) \cdot 100 = \frac{100}{x_{\text{total}}} \cdot \overline{(a_{\text{traction}} \cdot v)} \cdot T \quad \textbf{(5-15)}$$

The energy recovered through regenerative braking is a function of inertia energy and percentage of regenerative braking:

$$E_{\text{ReGen}} = E_{\text{Inertia}} \cdot \eta_{\text{ReGen}} \quad \textbf{(5-16)}$$

where E_{ReGen} is the energy recovery by regenerative braking and η_{ReGen} is regenerative braking efficiency. Gear losses include losses due to the energy transfer between environmental losses and electric machine:

$$E_{\text{GearLoss}} = (E_{\text{Aero}} + E_{\text{Rolling}} + E_{\text{Inertia}} + E_{\text{ReGen}}) \cdot (1 - \eta_{\text{Gear}}) \quad \textbf{(5-17)}$$

where E_{GearLoss} is the energy loss in transmission in both traction and regenerative braking, and η_{Gear} is the transmission efficiency.

Motor losses are computed as:

$$E_{\text{MotorLoss}} = (E_{\text{Aero}} + E_{\text{Rolling}} + E_{\text{Inertia}} + E_{\text{ReGen}} + E_{\text{GearLoss}}) \cdot (1 - \eta_{\text{Motor}}) \quad \textbf{(5-18)}$$

where E_{MotoLoss} is the energy loss in motor in both traction and regenerative braking and η_{Moto} is the motor efficiency.

Battery energy dissipation is calculated on both discharge and charge current:

$$E_{\text{BattDischarge}} = \overline{P}_{\text{Traction}} \cdot T = I_{\text{RMS,Batt}}^2 \cdot R_{\text{d}} \cdot T = \left(\frac{\overline{E}}{T \cdot V_{\text{Batt}}}\right)^2 \cdot R_{\text{d}} \cdot T \quad \textbf{(5-19)}$$

$$E_{\text{BattCharge}} = [\frac{E_{\text{ReGen}}}{TV_{\text{Batt}}}]^2 \cdot R_{\text{c}} \cdot T \quad \textbf{(5-20)}$$

where $E_{\text{BattDisCharge}}$ and $E_{\text{BattCharge}}$ are losses in the battery due to discharge and charge the battery. The terms $I_{\text{RMS,Batt}}$, V_{Batt}, R_{d}, R_{c} and T are average battery current, battery voltage, battery discharge/charge resistant and simulation time, respectively. This leads us to the result we have been working towards: the total energy equation for the vehicle is:

$$E_{\text{Total}} = E_{\text{Aero}} + E_{\text{Rolling}} + E_{\text{Inertia}} - E_{\text{ReGen}} + E_{\text{GearLoss}} + E_{\text{MotorLoss}} + E_{\text{BattDischarge}} + E_{\text{Battcahrge}} \quad \textbf{(5-21)}$$

where the terms are given by the expressions above.

5.3.2 Energy consumption

Before a sensitivity analysis is performed, the predictions of energy consumption are firstly considered for the models and checked to make sure that they are reasonable. Table 5-1 shows the energy consumption on each of the vehicle and powertrain components on both NEDC and combined Artemis driving cycles. Energy consumption presented in this table is in kWh per 100 km range based on Equation (5-21) and with component sizes for the Nissan Leaf powertrain. The nominal regenerative braking efficiency is assumed to be 40%, but in this table the percentage of regenerative braking efficiency is selected differently to see the variation in energy consumption on each powertrain component. It is clear to see that the highest consumed energy in both NEDC and combined Artemis are associated with the vehicle inertia. The other biggest losses are due to aerodynamic drag force, followed by rolling resistant losses. The regenerative energy recovery is simply calculated from the percentage of the energy from vehicle inertia. Battery losses are also included in this calculation as presented in the Equations (5-19) and (5-20). However, battery energy losses are very small and it is therefore safe to ignore these losses.

5.3.3 First-order sensitivity analysis

The techniques of Section 5.2 have been applied to the model and the results are shown in Figure 5-2. It can be seen that for both the NEDC and ARTEMIS cycles, the most sensitive parameter sensitivities is weight. As the regenerative braking efficiency improves, gear and motor efficiency become even more sensitive (note that changing the regenerative braking fraction from 40% to 100% results in a large relative change). Vehicle inertia sensitivity is reduced when the regenerative braking efficiency is improved; however, the relative change is much smaller compared with the sensitivity changes of gear and motor efficiencies. The aerodynamic and rolling resistance sensitivities are also increased as the regenerative braking energy efficiency is improved, but with a smaller relative change

When comparing these two driving cycles, it can be seen that there is a large difference in energy consumption, as illustrated in Table 5-1, but the relative change in sensitivities are comparable. Some trends have been observed in the sensitivities for a single parameter, and they will be presented by several plots. In the following section, it will be seen that a second-order analysis could have predicted this as well, and also that it can achieve similar results far more quickly and easily.

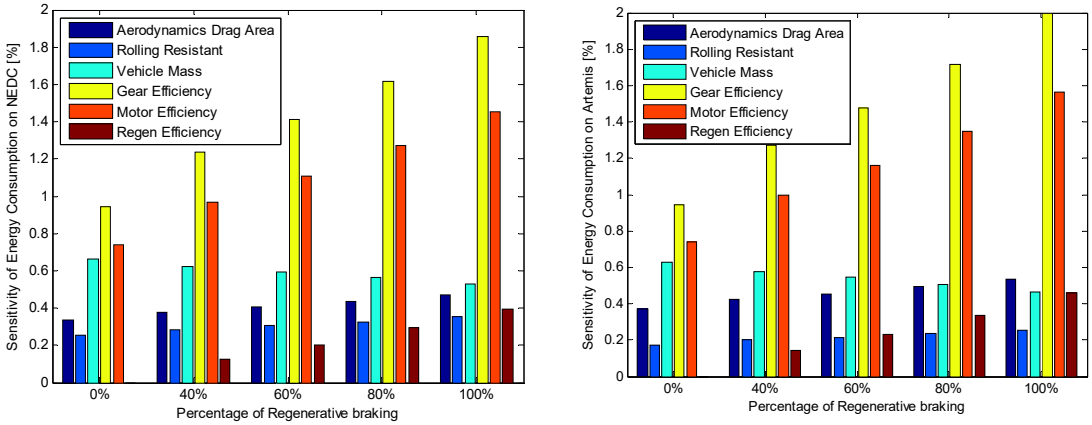

Figure 5-2 First-order sensitivity analysis of the nominal vehicle parameters. (a) NEDC and (b) Artemis Cycle

Table 5-1 Energy consumption on the Nissan Leaf in different percentage of regenerative braking.

Energy (kWh·100 km^{-1})	NEDC 0% regen	NEDC 40% regen	NEDC 50% regen	NEDC 80% regen	NEDC 100% regen
Aerodynamics	4.03	4.03	4.03	4.03	4.03
Rolling Resistance	3.05	3.05	3.05	3.05	3.05
Vehicle Mass	4.95	4.95	4.95	4.95	4.95
Regenerative Recovery	0.00	−1.98	−2.47	−3.96	−4.95
Transmission Loss	0.36	0.42	0.44	0.48	0.51
Motor Loss	1.86	2.16	2.24	2.47	2.62
Battery Discharge Loss			Negligible		
Battery Charge Loss			Negligible		
Total Energy (kWh·100 km^{-1})	14.25	12.63	12.23	11.02	10.21
Energy (kWh·100 km^{-1})	**Artemis 0% regen**	**Artemis 40% regen**	**Artemis 50% regen**	**Artemis 80% regen**	**Artemis 100% regen**
Aerodynamics	6.42	6.42	6.42	6.42	6.42
Rolling Resistance	3.05	3.05	3.05	3.05	3.05
Vehicle Mass	7.91	7.91	7.91	7.91	7.91
Regenerative Recovery	0.00	−2.37	−3.95	−6.33	−7.91
Transmission Loss	0.52	0.59	0.64	0.71	0.76
Motor Loss	2.68	3.05	3.30	3.66	3.91
Battery Discharge Loss			Negligible		
Battery Charge Loss			Negligible		
Total Energy (kWh·100 km^{-1})	20.58	18.64	17.35	15.42	14.13

5.3.4 Second-order sensitivity analysis

Figure 5-3 illustrates the results of second-order sensitivity analysis at the vehicle nominal points for NEDC and Artemis. Figure 5-3a shows the results for the NEDC in number values and text explanations and the same for Artemis cycle, as shown in Figure 5-3b.

It can be seen that the cross-coupling between the gear efficiency and the motor efficiency is very strong, as is the cross-coupling between gear efficiency and vehicle mass: the numerical values are close in magnitude to one. There is also strong cross-coupling between vehicle mass and motor efficiency. In fact, the gear and motor efficiency are also cross-coupled to every parameter. Cross-coupling between other parameters is smaller, and there are some cases where the cross-coupling is so small that it could be ignored. The same results are broadly true for both driving cycles. This relates well to the results shown in Figure 5-2: where it can be seen that there is significant coupling between the sensitivities to regenerative braking efficiency, vehicle mass, gear efficiency and motor efficiency, but not much with the aerodynamic drag area and the rolling resistance.

Figure 5-4 shows second order sensitivity results from selected parameters. In Figure 5-4a, energy consumption on NEDC of two parameters between aerodynamics and vehicle mass are presented. The black solid line illustrates change in vehicle mass only; the blue dash-dot line shows change in aerodynamic area only. The red dash line shows changes in energy consumption while both parameters are changed simultaneously. It can be seen that there is no coupling between aerodynamic drag area and vehicle mass. As a result, when varying both parameters simultaneously, the impact on the energy consumption is linear due to the parameters being decoupled.

Figure 5-4b shows the coupling sensitivities for mass and rolling resistance and Figure 5-4c illustrates these sensitivities for mass and gear efficiency. The coupling between mass rolling resistance and mass gear efficiency are respectively medium and very strong as presented in Figure 5-3. When two parameters are varying simultaneously, the impact on the energy consumption changes non-linearly as shown in red-dash line. This is due to the coupling effect between the aforementioned parameters as presented in Section 5.3.4.

$$S'_{\phi} = \begin{bmatrix} \sim 0 & \sim 0 & \sim 0 & -0.36 & -0.28 & 0 \\ \sim 0 & \sim 0 & 0.28 & -0.27 & -0.21 & 0 \\ \sim 0 & 0.28 & \sim 0 & -0.88 & -0.69 & -0.13 \\ -0.36 & -0.27 & -0.88 & \sim 0 & 0.91 & -0.18 \\ -0.28 & -0.21 & -0.69 & 0.91 & \sim 0 & -0.14 \\ 0 & 0 & -0.13 & -0.18 & -0.14 & \sim 0 \end{bmatrix}$$

	Aerodynamic Drag Area	Rolliing Resistant	Vehicle Mass	Gear Efficiency	Motor Efficiency	Re-Gen Efficiency
Aerodynamic Drag Area	NC	NC	NC	MC	MC	NC
Rolliing Resistant		NC	MC	MC	MC	NC
Vehicle Mass			NC	VSC	SC	MC
Gear Efficiency				NC	VSC	MC
Motor Efficiency					NC	MC
Re-Gen Efficiency						NC

(**a**)

$$S'_{\phi} = \begin{bmatrix} \sim 0 & \sim 0 & \sim 0 & -0.39 & -0.31 & 0 \\ \sim 0 & \sim 0 & 0.20 & -0.19 & -0.15 & 0 \\ \sim 0 & 0.20 & \sim 0 & -0.87 & -0.69 & -0.14 \\ -0.39 & -0.19 & -0.87 & \sim 0 & 0.94 & -0.2 \\ -0.31 & -0.15 & -0.69 & 0.94 & \sim 0 & -0.15 \\ 0 & 0 & -0.14 & -0.2 & -0.15 & \sim 0 \end{bmatrix}$$

	Aerodynamic Drag Area	Rolliing Resistant	Vehicle Mass	Gear Efficiency	Motor Efficiency	Re-Gen Efficiency
Aerodynamic Drag Area	NC	NC	NC	MC	MC	NC
Rolliing Resistant		NC	MC	MC	MC	NC
Vehicle Mass			NC	VSC	SC	MC
Gear Efficiency				NC	VSC	MC
Motor Efficiency					NC	MC
Re-Gen Efficiency						NC

(**b**)

Figure 5-3 Second-order sensitivity analysis for the nominal vehicle parameters.

(a) NEDC and (b) Artemis.

where the symbols are:

NC	No Coupling	MC	Medium Coupling	SC	Strong Coupling	VSC	Very Strong Coupling

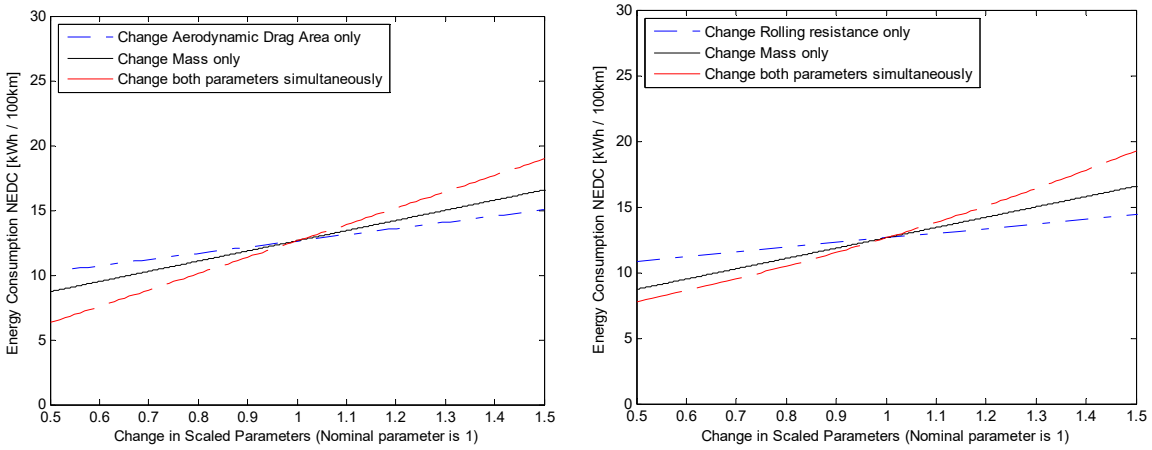

(**a**) (**b**)

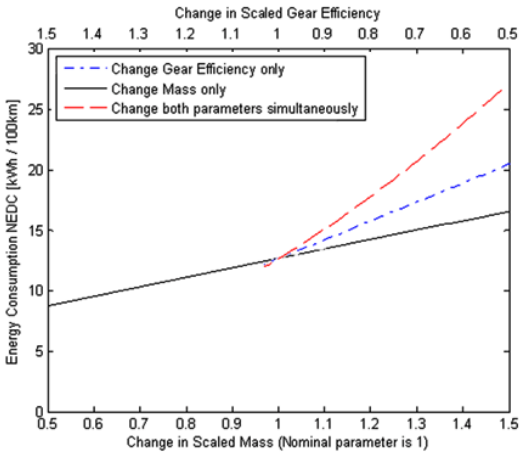

(**c**)

Figure 5-4 Second-order sensitivity analysis results.

(a) Coupling between mass and aerodynamic drag area (no coupling);

(b) Coupling between mass and rolling resistance (medium coupling);

(c) Coupling between mass and gear efficiency (very strong coupling).

5.4 Chapter discussion

The case study above has presented both first- and second-order sensitivity analyses. Compared to the literature, this study has considered a large parameter set including “traditional parameters” such as drag area and mass, but also adding detailed characteristics of the powertrain such as the gearbox efficiency and the motor efficiency. For the legally-mandated NEDC and the more realistic ARTEMIS driving cycle, it is shown that the greatest sensitivity is to the efficiency of the gearbox. This is particularly interesting because there are examples in the literature of attempts to reduce BEV energy consumption through the use of multiple transmission ratios to improve motor efficiency [85],[86]. Typically, the use of multiple transmission ratios makes the gearbox efficiency worse. The sensitivity results of this chapter suggest that in this particular case energy consumption is actually more sensitive to gearbox efficiency than motor efficiency, so it may sound reasonable to keep the more-efficient single-speed transmission for the selected vehicle.

The first-order analysis has shown which parameters have the greatest sensitivities, but the second-order analysis has shown how the parameters interact with each other. For example, it can be seen that there is very strong cross-coupling between the gearbox efficiency and the motor efficiency: this result shows that if the motor is made to be more efficient, the gearbox becomes (relatively) even more of a problem. If the optimal designs are considered, these results show that it need to be mindful of changes that will affect these parameters. Small changes of these parameters together is the optimum solution.

Conversely, some other parameters show that they are not strongly-coupled together. For those parameters, it does not need to take cross-coupling into account. As well as informing the design process, these sensitivities present about the accuracy of the results: if the model is very sensitive to a certain parameter, it need to be sure that the models are accurate, because a small change would result in significantly misleading results.

For the vehicle manufacturer, insight into cross-coupling is useful since it can act as a guide as to which aspects of a vehicle configuration are particularly interconnected. A vehicle manufacturer will often use multi-objective optimization to address the trade-offs between design parameters. A second-order sensitivity analysis would aid in selecting the correct set of parameters for this type of optimization. A first-order analysis tells the manufacturer which components to improve first, but a second-order analysis gives an idea which components will be of significance next. In the case study, for example, results show that drag area was only lightly coupled to drag gearbox efficiency, so it can work on one or the other in confidence, knowing that any gains will not be swamped by a new limiting factor. Conversely, it is certainly true that as it makes the gearbox more efficient, the efficiency of the motor will become more of a relative problem. It would be interesting though probably not tractable to weight sensitivities with development costs as a tool to directing research investment.

The model used in this example is illustrative and some assumptions were made: the assumption is that the electric machine efficiency is a constant 85% efficiency both when motoring and generating; in practice, it varies. The model of regenerative braking is also simplified: some sources in the literature estimate an efficiency of around 50% [25], though this can depend greatly on the driving cycle and limitations imposed in the interest of good vehicle dynamics. Another assumption considers a nominal transmission efficiency of 97%, which author feels is reasonable, but may not be perfect. Despite these limitations, author feels that the model is adequate for the purposes of this paper: sensitivity analysis shows which parameters will have the greatest effect on the results, if inaccuracies in the model are significant, sensitivity analysis will highlight this.

5.5 Chapter conclusions

This chapter has presented an extended technique for analysing parameter sensitivities in modern road vehicles. The new techniques consider first-order and second-order effects, showing both the effects on individual parameters and also the cross-coupling between different parameter sensitivities. This method is quick

and intuitive, and will help a vehicle designer quickly gain extra insights and identify cross-coupled parameters. The techniques have been demonstrated on an energy-minimisation problem for a C-segment BEV. The parameter set considered was larger than that typically encountered in the literature, and highlighted the sensitivity of the result to the powertrain efficiency.

The work to date has considered only a single topology in a theoretical context, and it would be interesting to conduct further work determining how useful second-order analyses are in practice. Second-order analysis could potentially inform research and development work, aiding engineers to understand how “limiting factors” interact and giving insight into the technical challenges that will arise once today’s problems have been addressed. However, to be certain of benefits, it would be worth evaluating the techniques in the context of a development project and determining whether the theory translates into useful practice.

6 Modelling EV powertrain as a differentially flat system

6.1 Introduction

This chapter presents some possibilities of exploiting the differential flatness property of the model to simulate an EV powertrain. The powertrain model in this study is limited to a longitudinal vehicle dynamic and electrical energy consumption is a main attribute to consider. The well-known methods of modelling the longitudinal dynamics of a road vehicle, i.e. the forward-facing simulation and quasi-static backward simulation, will be presented and compared to the differentially flat property. Differential flatness is a property of the system dynamics which mean that if an output is flat, the system dynamics can be inverted so that the system input can be calculated from the flat output and its derivatives without iteration. Thus if a system output is flat, it becomes very easy to simulate the system for a known flat output and unknown inputs. This study will link the similar properties of the flatness technique to the well-known simulation methods and combine the merit issues from these two.

Longitudinal vehicle dynamics have been modelled and simulated in earlier times, before the electric powertrain became as commonly used as it has recently. The purpose of the simulation is to study the gas emissions as it used in the conventional internal combustion engine. Since the BEV has zero emission at the tail pipe, the energy consumption of the electric powertrain will be a main consideration for this simulation. To design HEV, longitudinal vehicle simulation is an important tool for designing a powertrain configuration. It is very clear to see that, to achieve the optimum energy consumption, a number of literatures show that the electric powertrain allows designers to arrange the powertrain components in a number of different ways. For example, the recent HEV can have its powertrain arranged in at least three ways, i.e. series, parallel and series-parallel. In addition, as a purely EV, the complexities of the internal combustion engine are detached, and there are a considerable numbers of possible powertrain topologies, as presented previously in Chapter 4.

The chapter starts by introducing the differentially flat property of the BEV powertrain model. This property is exploited for estimating energy consumption by inverting the dynamics. The merit and limitation of this technique on the BEV application is then discussed. The details explanation of forward-facing and quasi-static backward methods which are commonly used in powertrain simulation will also be addressed in the Section 6.4 to introduce a better understanding of these techniques.

6.2 Modelling and simulation of the EV powertrain

Computational modelling and simulation are methods of testing the system, e.g. the vehicle powertrain, in the preliminary stage without involving physical instruments or powertrain test rigs, by using computer programming and mathematical equations. These computational tools can save the designer both time and cost when designing and evaluating the prototype of the powertrain. There are two well-known simulation methods that are used in powertrain design: forward-facing simulation and quasi-static backward simulation as will be described in detail in Section 6.4. The name ‘forward’ and ‘backward’ indicate the energy and power flow in the simulation (engine to wheels as forward, or wheels to engine as backward); details of these two will be addressed and explained in the following section.

There are two methods to obtain the results from models of a dynamic system as stated by Bosgra in [87] and mentioned again by Hofman in [88].

- *Experimental modelling:* this technique aims to find the systematic relationship of the real system variables by measuring them during experiments
- *Theoretical or physical modelling:* this technique uses mathematical model and scientific theory to describe the system behaviour.

This study will focus on the theoretical and physical modelling only. In order to obtain the most benefits from the model there are some valuable suggestions made by Gao et al. in [27], that the model is representative of the system in all or

some aspects depending on the intention of the study. In addition, to create a model, there is some trade-off between the amount of assumptions (uncertainties), amount of simulation time, and the effort required to set up the model to obtain a sufficient level of model accuracy.

6.2.1 Dynamical modelling and simulation

The behaviour of a system is usually described by the dynamical model in a format of mathematical equations. One of the classical examples of a dynamical model in a mechanical engineering study can be represented by a mass-spring and damper system; the resistance and capacitors circuit is also a fundamental system for the electrical engineer. Other complex systems such as cruise control of the road vehicle, radar tracker and the space-shutter control can be initially described by this fundamental dynamical equation. The models of these systems can be found in many excellent text books, for example [89],[90]

Fundamentally, the dynamical system is usually described by this state equation format as presented by

$$\frac{d\boldsymbol{x}}{dt} = \boldsymbol{f}(\boldsymbol{x}(t), \boldsymbol{u}(t)), \boldsymbol{x}(t)\epsilon R^n, \boldsymbol{u}(t)\epsilon R^m$$
$$\boldsymbol{y}(t) = \boldsymbol{h}(\boldsymbol{x}(t), \boldsymbol{u}(t)) \quad \textbf{(6-1)}$$

where $\boldsymbol{x}(t)$ is a vector of state variables, $\boldsymbol{u}(t)$ is a vector of input signals and $\boldsymbol{y}(t)$ is a vector of output variables. The term $\frac{dx}{dt}$ represents the change of $\boldsymbol{x}(t)$ with respect to time. Then f and h are the mapping of their arguments to the vectors of the appropriate dimension. In other words, this state of the system is a collection of variables that summarise the past of the system and are used for predicting the future [91].

The dynamical modelling and simulation is used for longitudinal vehicle study by simulating the vehicle to follow the causality of the powertrain system. For example, the vehicle dynamic simulation starts at the desired velocity and the vehicle is controlled by the driver model to follow that velocity which is what

normally happens in a real-life situation. The driver model controls the vehicle speed by either controlling the traction force (engine of motor torque), as is usually implemented in a road vehicle, or controlling the traction speed as presented in Figure 6-13. Thus the power plant (engine or motor) powers the vehicle through the transmission and wheels which causes the vehicle to accelerate. This simulation technique is also called forward facing simulation and details are described in the Section 6.4.1.

6.2.2 Quasi-static backward simulation

On the other hand, the backward model means inverting the physical causality of the powertrain system by using the predefined velocity references as a starting simulation process. The velocity reference is also called a driving cycle and is usually similar to the term desired velocity in the forward-facing simulation. However, the difference between these two simulation techniques is that the driving cycle used in the forward-facing simulation requires a driver model (control methods) to differentiate between the desired velocity and actual velocity before controlling vehicle. In contrast, the quasi-static backward simulation does not require the driving model to control the vehicle but makes the assumption that the vehicle is perfectly following the velocity references vector, $\boldsymbol{v}$. The velocity reference, v_i, indicates vehicle in each time step, t_i, in every interval, h, as described by

$$v(t_i) = v_i$$
$$t_i = i \cdot h, i = 0, \dots, n \quad \textbf{(6-2)}$$

Details of this quasi-static backward simulation is described in the Section 6.4.2 of this chapter.

There are two techniques for estimating energy consumption, the forward-facing simulation which requires the driver model to control vehicle speed tracking and quasi-static backward simulation which is assumed the perfect tracking performance. In fact, the issue of tracking performance may cause a different result between these simulations. The study in [92] indicates that in the emission

legislation, the driving cycle has to be tracked within a certain limit by the human. Thus, it was found that two different velocity trajectories (within prescribed limits) may result in different fuel consumptions. This leads to the fact that velocity tracking performance will affect fuel consumption.

6.2.3 Inversion of the dynamical model simulation

The forward-facing simulation and quasi-static backward simulation are two common longitudinal analysis tools for powertrain design the details of these two method will be discussed in the Section 6.4. There are some advantageous features between both of them which are described in Figure 6-1 by [92]. The quasi-static backward simulation was recommended as a tool for the optimisation of powertrain design space, powertrain configuration and some system-level powertrain control strategies as these applications require a great number of simulations during their process. The quasi-static backward simulation provides the key advantage of a fast simulation time within an acceptable range of accuracy. The forward-facing simulation, on the other hand, provides a greater detail of simulation accuracy and the system dynamic behaviour but with some drawbacks of a longer time simulation.

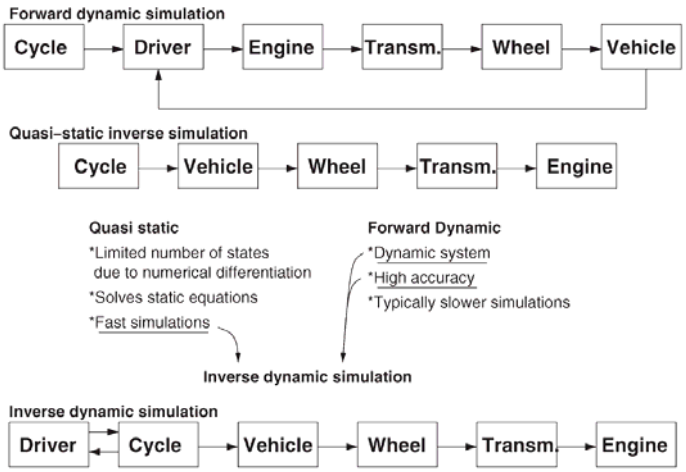

Figure 6-1 The combined merits of inverse dynamic simulation

Froberg et al. presented a simulation method which is fast simulation without losing transient dynamical performance in their inversion of the dynamical model simulation in 2008. This simulation approach was adapted from the theory of the

stable inversion of nonlinear systems. Their development extended the quasi-static method by including dynamical properties of powertrain, such as transient behaviour.

The difference between quasi-static backward simulation and inversion of the dynamical model simulation was stated in [92] as; the quasi-static method uses only one state variable i.e., vehicle speed $v(t)$

$$u(t) = f(v(t), \dot{v}(t)) \tag{6-3}$$

While the inversion of the dynamical model simulation may include more states z in their simulation. As a result, higher derivatives, such as

$$u(t) = F\big(v(t), \dot{v}(t), z(t), \dot{z}(t)\big) = \mathcal{F}\big(v(t), \dot{v}(t), \ddot{v}(t)\big) \tag{6-4}$$

of the speed profile or driving cycle are required. Froberg et al. also extended their applications of inverse dynamic powertrain simulation to control the gas flow dynamic in a diesel engine presented in [92]

Petit and Sciarretta presented a solution to the energy management problems of an EV by using an inversion-based approach simulation in [93]. They presented the EV model as a two-states single-input dynamical system. An electric machine modelling was simplified by a DC-type motor. The objective of their study was to introduce a simulation tool for an optimum control of EV application. Finally, they also claimed that the inversion of the dynamical system provides an effective and accurate means of powertrain simulation [93].

6.3 Differentially flat system

The inverse simulation of a dynamical system is claimed to be a technique that provides better accuracy than the quasi-static backward simulation method and requires less computation time than the forward-facing simulation one [92]. In an application of the EV powertrain modelling, some literature was presented in the earlier section to confirm these advantages. However, number of research papers using this technique in EV powertrain simulation applications are still small in number.

This section aims to introduce a differentially flat system model of the EV powertrain. The model is focused on the application of powertrain sizing and optimisation. The rest of this section includes an introduction to the background and concept of differential flatness; then the application of an EV powertrain energy estimation will be demonstrated and implemented by a case study of modelling an electric powertrain.

6.3.1 Background

Differential flatness, also referred to as flatness, is a property of the system dynamics in which the control and state vectors of the dynamical system can be expressed as a function of the output and its derivatives [94]. Flatness was firstly introduced by Flies in 1992 and has been applied in a variety of different applications where a predefined trajectory is provided [95]. These applications include multi-rotor aerial vehicle [96], [97], [98] wheeled mobile robot [99], control strategies of the nonlinear system [94] and also automotive applications.

A differentially flat system can be expressed by these following equations. Firstly, starting with a general nonlinear dynamic system similar to that presented earlier in equation (6-1) and presented again in more detail as

$$\begin{gathered}\dot{\boldsymbol{x}} = \boldsymbol{f}(\boldsymbol{x}(t), \boldsymbol{u}(t)) \\ \boldsymbol{x} = [x_1, x_2, \dots, x_n]^{\boldsymbol{T}}, \boldsymbol{x} \epsilon R^n \\ \boldsymbol{u} = [u_1, u_2, \dots, u_m]^{\boldsymbol{T}}, \boldsymbol{u} \epsilon R^m \\ \boldsymbol{y}(t) = \boldsymbol{h}(\boldsymbol{x}(t), \boldsymbol{u}(t)) \\ \boldsymbol{y} = [y_1, y_2, \dots, y_p]^{\boldsymbol{T}}, \boldsymbol{y} \epsilon R^p\end{gathered} \quad \textbf{(6-5)}$$

where $\boldsymbol{x}$ is a vector of the state variables which is represented as an n-dimension, $\boldsymbol{u}$ is the input vector of m-dimension, $\boldsymbol{y}$ is an output vector of p-dimension, $\{n, m, p\}$ are numbers, $\{n, m, p\} \in N$ and $m \leq n$.

The system (equations) can be called a differentially flat system if, and only if, there exists a

$$\boldsymbol{y} = [y_1, y_2, \dots, y_n]^{\boldsymbol{T}}, \boldsymbol{y} \epsilon R^p, \ \ p = m \tag{6-6}$$

such that

$$\boldsymbol{y} = \ \emptyset(\ \boldsymbol{x}, u, \dot{u}, \dots, u^{\alpha}) \tag{6-7}$$

then $\boldsymbol{y}$ and its derivatives $\dot{\boldsymbol{y}}, \ddot{\boldsymbol{y}}, \dots.$, are independent.

Conversely $\boldsymbol{x}$, $\boldsymbol{u}$ can be expressed as:

$$\begin{aligned} \boldsymbol{x} &= \ \boldsymbol{\varphi}\left(y, \dot{y}, \dots, y^{\beta}\right) \\ \boldsymbol{u} &= \ \boldsymbol{\psi}(y, \dot{y}, \dots, y^{(\beta+1)}) \end{aligned} \tag{6-8}$$

with

$$\dot{\varphi} = \ \boldsymbol{f}(\varphi, \psi) \tag{6-9}$$

Vector $\boldsymbol{y}$ is called a flat output, and $\emptyset, \boldsymbol{\varphi}, \boldsymbol{\psi}$ are smooth functions.

This flat system can be also explained in a simple description, such that:

1) The nonlinear dynamical equations in (6-5) are those in which $\boldsymbol{x}$ and $\boldsymbol{u}$ are state variables and input variables respectively. Then if it is possible to invert this causality by finding a vector of $\boldsymbol{y}$ which is an output vector and its size is equal to the input vector $\boldsymbol{u}$, then this vector y is called a flat output.
2) There is a one-to-one relationship between the vector $\boldsymbol{y}$ and $\boldsymbol{u}$ [100],[94].
3) The output $\boldsymbol{y}$ is differentiable and its successive derivatives $\dot{\boldsymbol{y}}, \ddot{\boldsymbol{y}}, \dots.$, are independent.
4) The state vector $\boldsymbol{x}$ of this differentially flat system and its control input $\boldsymbol{u}$ can be expressed as a function of flat output $\boldsymbol{y}$ and their derivatives as presented in (6-8) [100],[101].
5) This differentially flat system represents its dynamical system without dynamics. In other words, time in the dynamical system is removed and replaced by a one-to-one mapping between outputs and inputs [102]. As

a result, the state variable and control input can be estimated by the trajectory of output $\boldsymbol{y}$ without performing integration [103],[102].

The system dynamics as presented in Figure 6-2 can be modelled in the form of equation (6-5) as

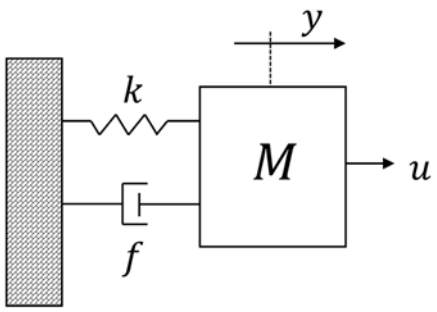

Figure 6-2 Mechanical mass-spring-damper system

The position, x, of the mass, M, can be defined by

$$\dot{x_1} = x_2$$
$$\dot{x_2} = \frac{1}{M}(-kx_1 - fx_2 + u) \quad \textbf{(6-10)}$$

where $x_1 = y$, $x_2 = \dot{y}$ and $u = F$ and where F is the external force, y is the position of the mass M, f is the friction coefficient and k is the spring coefficient constant.

Equation (6-10) can be rearranged into the form of equation (6-8) as

$$u = ky + f\dot{y} + M\ddot{y}$$
$$x_1 = y \quad \textbf{(6-11)}$$
$$x_2 = \dot{y}$$

Thus the mass-spring-damper system is a flat system.

6.3.2 Flatness in automotive applications

There are some examples in which the flatness system was also implemented and applied to automotive and electric powertrain applications. For example, the study in [104] presented the use of a flatness based control for anti-slip regulation

of a hybrid vehicle by controlling the torque from the electric motor to eliminate rear wheels slip. Three control laws were compared: PI control, a linearising feedback control and flatness based control. The flatness control in this study was presented as a feedforward controller which required a flat output to command system dynamics. As a result, an open loop control law can be implemented using flatness in this system.

The study in [105] presented the design of a feedforward controller of an HEV drivetrain by using a differential flatness approach. The two-degree of freedom of the electric drivetrain structure was presented. The electric machine torque and speed controller were implemented with a feedforward control design using the differential flatness. The study illustrates the simplicity and efficiency of the flatness based feedforward controller design of the HEV powertrain.

The study in [106] presented the control algorithm of multi-sources of energy for the electric traction of a road vehicle. The lithium-ion battery was considered to be the primary energy source and the supercapacitors provided an additional power source. The flatness principle was implemented to control the nonlinear energy flow between energy sources within the DC voltage bus (DC power lines). This control strategy generates reference trajectories of electrostatic energy contained in the capacitors to control the bus voltage without solving any differential equations.

The study in [102] presented the control approach of the hybrid power sources, which are fuel cell and supercapacitor, using a differential flatness-based controller. A control method for power source supplied distribution was implemented using a flatness approach. This study states that using a differential flatness property results in proposing simple solutions to manage and stabilise the hybrid energy sources.

6.3.3 BEV powertrain model as a differentially flat system

- **Powertrain equations**

It can be seen from the dynamics equation that the velocity can be calculated from equation (6-40). Recalling the fundamental equation of longitudinal dynamic of road vehicle as

$$\frac{dv(t)}{dt} = \frac{1}{M_v}(F_t(t) - F_r(t)) \tag{6-12}$$

If the traction force is mainly considered, the equation can be arranged as

$$F_t(t) = F_r(t) + M_v \cdot \frac{dv(t)}{dt} \tag{6-13}$$
$$F_t = F_r + M_v \cdot \dot{\boldsymbol{v}}$$

where F_t is the traction force, M_v the total vehicle mass and inertia, $\dot{\boldsymbol{v}}$ the vehicle acceleration, and the acceleration $\frac{dv(t)}{dt}$ can be rewritten as $\dot{\boldsymbol{v}}$ in this equation.

The F_r which are environmental forces and can be described as

$$F_r = F_{\text{Aerodynamic}} + F_{\text{Rolling resistant}} + F_{\text{Slope}} \tag{6-14}$$
$$\boldsymbol{F}_r = \frac{1}{2}\rho \cdot C_d \cdot A \cdot \boldsymbol{v}|\boldsymbol{v}| + M_b g C_r + M_b g \sin\alpha$$

where ρ is the air density, C_d the drag coefficient, A the vehicle frontal area, C_r the rolling resistant coefficient, α the slope angle, g the gravitational acceleration, M_b the body mass and $\boldsymbol{v}$, which is represented in bold, represents a **vector** of the vehicle velocity.

It can be described that

$$\boldsymbol{v} = [v_1, v_2, \dots, v_p] \tag{6-15}$$
$$\dot{\boldsymbol{v}} = [\dot{v}_1, \dot{v}_2, \dots, \dot{v}_p]$$

where $\boldsymbol{v}$ and its derivative, $\dot{\boldsymbol{v}}$, are vectors with dimension p.

Equation (6-13) can be rewritten as

$$\boldsymbol{F}_r = \frac{1}{2}\rho \cdot C_d \cdot A \cdot \boldsymbol{v}|\boldsymbol{v}| + M_b g C_r \cos\alpha + M_b g \sin\alpha \quad \textbf{(6-16)}$$

where $\boldsymbol{F}_t$ is a vector with dimension p similar to vectors $\boldsymbol{v}$ and $\dot{\boldsymbol{v}}$.

This force $\boldsymbol{F}_t$ is the traction force of the vehicle body. If the torque in the powertrain which is used to propel the vehicle is considered, the equation can be described as

$$\boldsymbol{T}_w = \boldsymbol{F}_t \cdot r_d \quad \textbf{(6-17)}$$

where $\boldsymbol{T}_w$ is a vector of the traction torque at the wheels and r_d is an effective tyre radius

Torque is transferred from wheels to motor via transmission. If the BEV is considered as a single gear ratio, torque between wheels and motor can be described as

$$\boldsymbol{T}_m = \frac{\boldsymbol{T}_w}{i_g \cdot \eta_g} + b\boldsymbol{\omega}_m = \boldsymbol{T}_L + b\boldsymbol{\omega}_m \quad \textbf{(6-18)}$$

where $\boldsymbol{T}_m$ is a vector of torque at the motor, $\boldsymbol{T}_L$ is a motor load torque (not including motor friction), i_g is a single speed gear ratio, η_g is a gearbox efficiency and b is a mechanical friction coefficient in the motor.

Similarly, the speed of the motor is modified from the speed of the vehicle and can be calculated through the gearbox and wheel radius by

$$\boldsymbol{\omega}_m = \boldsymbol{\omega}_w \cdot i_g = \frac{\boldsymbol{v}}{r_d} \cdot i_g \quad \textbf{(6-19)}$$

where $\boldsymbol{\omega}_m$ is a vector of motor speed, $\boldsymbol{\omega}_w$ is a vector of speed at wheels.

Mass of the vehicle can be defined as the mass of the body M_b and total mass of the vehicle including rotational inertia M_v as presented by

$$M_v = M_b + \left(J_m + J_{gDrive}\right) \cdot \frac{i_g^2}{r_d^2} + J_{gDriven} \cdot \frac{1}{r_d^2} \quad \textbf{(6-20)}$$

where J_m, J_{gDrive}, $J_{gDriven}$ are moments of inertia of the motor, drive and driven gear respectively.

If a DC motor is considered, motor current $\boldsymbol{I}_m$, can be described as function of torque at the motor and the motor constant, K_m

$$\boldsymbol{I}_m = \frac{\boldsymbol{T}_m}{K_m} \tag{6-21}$$

where $\boldsymbol{I}_m$ and $\boldsymbol{T}_m$ are vectors of dimension p.

To combine equations (6-17) to (6-21), the motor current $\boldsymbol{I}_m$ can be described as the speed input $\boldsymbol{v}$ and its derivatives, as in

$$\boldsymbol{I}_m = \frac{\boldsymbol{T}_m}{K_m} = \frac{\boldsymbol{T}_w}{i_g \cdot \eta_g \cdot K_m} + \frac{b\boldsymbol{\omega}_m}{K_m} = \frac{1}{K_m}\left(\frac{\boldsymbol{F}_t \cdot r_d}{i_g \cdot \eta_g} + b\frac{\boldsymbol{v}}{r_d} \cdot i_g\right) \tag{6-22}$$

$$\boldsymbol{I}_m = \frac{r_d}{i_g \cdot \eta_g \cdot K_m} \cdot \left(\frac{1}{2}\rho \cdot C_d \cdot A \cdot \boldsymbol{v}|\boldsymbol{v}| + M_v g C_r + M_v g \sin\alpha + M_v \dot{\boldsymbol{v}}\right) + \frac{b \cdot i_g}{r_d} \cdot \boldsymbol{v}$$

The motor current $\boldsymbol{I}_m$ can be differentiated and presented as;

$$\dot{\boldsymbol{I}}_m = \frac{r_d}{i_g \cdot \eta_g \cdot K_m} \cdot (\rho \cdot C_d \cdot A \cdot \boldsymbol{v} + M_v \ddot{\boldsymbol{v}}) + \frac{b \cdot i_g}{r_d} \cdot \dot{\boldsymbol{v}} \tag{6-23}$$

If the voltage supply to the DC motor is considered, the following equation presents a simple DC motor the voltage supply $\boldsymbol{V}$ of which can be described as a function of the vehicle velocity, $\boldsymbol{v}$

$$\boldsymbol{V_m} = L\dot{\boldsymbol{I}}_m + R\boldsymbol{I}_m + K_m \cdot \boldsymbol{\omega}_m$$

$$\boldsymbol{V_m} = L\left\{\frac{r_d}{i_g \cdot \eta_g \cdot K_m} \cdot (\rho \cdot C_d \cdot A \cdot \boldsymbol{v} + M_v \ddot{\boldsymbol{v}})\right\} + R\{\frac{r_d}{i_g \cdot \eta_g \cdot K_m} \cdot \left(\frac{1}{2}\rho \cdot C_d \cdot A \cdot \boldsymbol{v}|\boldsymbol{v}| + M_v g C_r + M_v g \sin\alpha + M_v \dot{\boldsymbol{v}}\right) + \frac{b \cdot i_g}{r_d} \cdot \boldsymbol{v}\} + K_m \cdot \frac{\boldsymbol{v}}{r_d} \cdot i_g \tag{6-24}$$

where $\boldsymbol{V}$ and $\boldsymbol{v}$ are vectors of similar dimension p.

- **Driving cycle modification**

The NEDC, which is used for the emission test, originally provided the data resolution in every one second (1Hz) [33]. In this section the driving cycle modification has two main objectives. Firstly, the driving cycle has to be differentiable in order to be used with the differential flatness simulation.

Secondly, a better data resolution will be beneficial in providing more information on transient behaviour.

The one hertz driving cycle is interpolated to the required frequency by using the Hermite piecewise cubic function [107] as presented in Figure 6-3. Piecewise cubic is a function defined for all time t (in Figure 6-3) which is a cubic polynomial will be interpolated between the original one hertz data. A piecewise cubic interpolant $v_c(t)$, is a piecewise cubic which interpolates the data.

As the interpolated data are required to be differentiable, the Hermite cubic interpolant, using a cubic spline which is provided with two continuous derivatives, is implemented. Basically, in each interval of original data $[t_i, t_{i+1}]$, the interpolated velocity $v_c(t)$ is represented by four coefficients of the cubic function. This cubic function represents interpolated data between intervals. The detail of this piecewise interpolation can be further consulted in [107].

MATLAB provides standard functions of piecewise interpolation with the commands of $'\mathrm{spline}'$ and $'\mathrm{pchip}'$ [108]. In this study, these two commands were implemented to interpolate the velocity data. In Figure 6-3, it is clear that both functions are passed through the data but they interpolate differently. The spline function gives a better smoothness and is closer to the original data but has more overshooting, while the pchip give a better tracking without overshooting the original data.

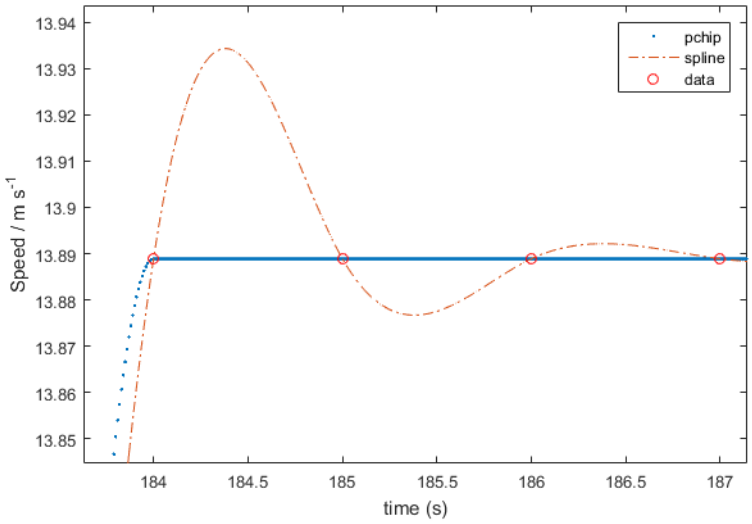

Figure 6-3 Pchip and spline piecewise interpolations

- **Electric machine parameterisation**

The differences between the modelling of electric machine in quasi-static backward simulation and the flatness simulation are that the quasi-static backward simulation presented by [30] models the motor efficiency map as a looking-up table, as presented in Figure 6-14, while the flatness simulation model electric machine from dynamical equations uses motor physical parameters. This section describes a method of parameterising the electric machine equations by using available data from the published motor specifications. This electric machine parameterisation starts from the dynamical equation as presented by

$$\begin{aligned} V_m &= L\dot{I}_m + RI_m + K_m \cdot \omega_m \\ T_m - T_L - B\omega_m &= J\dot{\omega}_m \\ KI_m - T_L - B\omega_m &= J\dot{\omega}_m \end{aligned} \quad \textbf{(6-25)}$$

If the steady state is considered, all transient parameters can be eliminated. Then equation (6-25) is replaced by

$$\begin{aligned} V_m &= RI_m + K_m \cdot \omega_m \\ T_m &= KI_m = T_L + B\omega_m \end{aligned} \quad \textbf{(6-26)}$$

Motor power can be obtained by a product of motor current and voltage and is represented by

$$P = V_m I_m = R I_m^2 + K_m \omega_m I_m \tag{6-27}$$

The efficiency of the motor can be defined by a fraction between outputs and inputs, as the output is the mechanical torque and the input is electric power. The motor efficiency can be presented by starting with the fundamental output/input equation as

$$\varepsilon_m(\boldsymbol{T_L}, \boldsymbol{\omega_m}) = \frac{T_m \omega_m}{V_m I_m} = \frac{(T_L + B\omega_m)\omega_m}{R I_m^2 + K_m \omega_m I_m} = \frac{T_L + B\omega_m^2}{\frac{(T_L + B\omega_m)}{K_m} \cdot (R \frac{(T_L + B\omega_m)}{K_m} + K_m \cdot \omega_m)} \tag{6-28}$$

Finally, the efficiency can be determined with a function of the torque load T_L and motor speed ω_m.

The steady-state efficiency data of the electric motor can be obtained by motor testing and is usually published as the motor technical datasheet. The motor's unknown parameters K_m, R and B can be estimated by comparing the motor efficiency in equation (6-28) with the published motor efficiency information. To compare these parameters, a minimisation technique could be implemented by using the cost function as

$$\min F(K_m, R, B, T_L, \omega_m) = \min \sum_{\boldsymbol{T_L=0, \omega_m=0}}^{\boldsymbol{T_L=T_{max},\ \omega_m=\omega_{max}}} [\varepsilon_0(T_L, \omega_m) - \varepsilon_m(K_m R, B, T_L, \omega_m)]^2 \tag{6-29}$$

to estimate the unknown parameters by comparing motor efficiency in equation (6-28) with available published motor efficiency, where ε_0 is efficiency from the motor's published data and ε_m is the motor efficiency model in equation (6-28).

- **Energy consumption estimation**

Total energy consumption (excluding losses in the battery) can calculated from data after the motor, as presented in Figure 6-14, as the fundamental equation of energy consumption is to integrate power with respect to time, as presented in equation (3-2). However, for discrete time data, the energy $\bar{E}$, can be calculated by a summation of power, as presented by

$$\bar{E} = \sum_{i=0}^{n} P_{m,i} \cdot h \quad \textbf{(6-30)}$$

where $P_{m,i}$ is the element of each motor power, which is a function of each velocity v_i, and h is a time interval between velocities.

The motor is powered by the DC electrical energy supplied by the battery; then the motor power consumption can be calculated by a product of motor voltage $V_{m,i}$ and motor current $I_{m,i}$ as indicated by

$$P_{m,i}(v, \dot{v}, \ddot{v}) = V_{m,i}(v, \dot{v}, \ddot{v}) \cdot I_{m,i}(v, \dot{v}) \quad \textbf{(6-31)}$$

Power losses in power electronic switching devices, such as an inverter, may not be included directly in this equation; however, their losses may already be included in an overall motor efficiency, as presented in Figure 6-4.

A positive power in equation (6-31) represents a traction power, while the negative power is the result of power captured by regenerative braking. In theory, all kinetic energy should be captured by the regenerative braking and the ideal motor power can be represented by

$$P_{m,100\%\ \text{Regen}} = P_{m,i} \quad \textbf{(6-32)}$$

However, not all kinetic energy can be captured and converted back into electrical energy. As a result, the electric powertrain can be modelled by estimating factors of regeneration (from 0% to 100%) to represent the ability of power conversion due to regenerative braking. If 0% regenerative braking is considered, the motor power can be presented by

$$P_{m,0\%\ \text{Regen}} = P_m \cdot P_{m,\, a_i>0} \quad \textbf{(6-33)}$$

where all the negative power (power at acceleration < 0) is being eliminated, and the factor of estimating regenerative braking r, can be presented as

$$P_{m,\ \ r\%\ \text{Regen}} = P_m - P_m \cdot P_{m,\, a_i<0} \cdot r/100 \quad \textbf{(6-34)}$$

- **Limitation of modelling batteries as a differentially flat system**

The differentially flat system was broadly applied to many systems from linear time-invariant single-input-single-output systems to multivariable nonlinear systems and optimal control applications, examples of which are presented clearly in [109]. However, not every system can be modelled as a differentially flat system. This section will present some limitations of the flat system when applied to the electric powertrain.

In the previous section, the model of a BEV powertrain was described and presented as a differentially flat system. The energy consumption was estimated by the power used from the motor. The battery is an important component in the BEV powertrain. In most cases, the battery affects the vehicle energy consumption by its mass, as different battery chemistries have their own specific energy density (in Wh/kg). Firstly, increased battery capacity means increasing the vehicle load. Secondly, losses in the battery due to its internal resistance can also be included as losses in the BEV powertrain; however, battery losses are considered to be a very small compared to the overall losses in the entire powertrain. This assumption is already presented in detail in the sensitivity analysis of the BEV powertrain, in Chapter 5. Thirdly, the concept of battery efficiency has already been mentioned in [25]. At least two definitions can be defined for battery efficiency, such as efficiency due to full charge/discharge cycle and power ratio between charge and discharge current. However, the battery efficiency topic is beyond the scope of this thesis. The assumption that battery losses are relatively small, compared to the overall powertrain losses, will be applied and battery losses will be safely ignored in this study.

The battery model which is used for a system level powertrain analysis usually provides information on how much electrical charge is stored in the battery and this is indicated by the battery SOC. Battery SOC is defined as how much the electric charge Q_i, is available in the battery related to the nominal battery capacity Q_0 as indicated by

$$SOC = \frac{Q_i}{Q_0} \tag{6-35}$$

Battery capacity is expressed in coulomb but in the BEV application, it is usually indicated in Ah (ampere-hours). A simplified battery model is usually created as an equivalent circuit of voltage source and battery internal resistance, as presented in Figure 2-10. The power required from the motor, as in equation (6-30), is converted to battery current $I_{BT,i}$ and is a function of motor power $P_{m,i}$ and battery terminal voltage V_{BT} as presented by

$$\dot{Q}_i = I_{BT,i} = \frac{P_{m,i}}{V_{BT}(Soc, I_{i-1})} \tag{6-36}$$

The current $I_{BT,i}$ represents current drawn from a battery and is equal to the rate of electrical charge $\dot{Q}_i$. The positive power is an energy removed from the battery and vice versa. Battery charge at a particular time t_i, is indicated by charge Q_i, in the battery and can be calculated by the charge removed from the initial, fully charged battery capacity Q_0.

$$Q_i = Q_0 - \sum_{i=0}^{i} \dot{Q}_i \cdot h \tag{6-37}$$

As a result, the battery terminal voltage, V_{BT}, can be calculated, as presented by

$$V_{BT}(SOC, I_{i-1}) = V_{ocv}(SOC) \cdot N_{cells} - I_{B,i} \cdot R_{B,i}(Soc) \tag{6-38}$$

and is a function of battery open-circuit voltage and battery resistance both of which are functions of battery SOC. The diagram in Figure 6-6 summarises the equations and signals flow in the battery model.

Sections 6.3.3 aim to verify that the differentially flat system is possible to be applied to BEV powertrain modelling. By starting from the vehicle referent speed $\boldsymbol{v}$, and its further derivatives $\dot{\boldsymbol{v}}, \ddot{\boldsymbol{v}}$, the motor power consumption in equation (6-31) can be described by voltage $V_{m,i}$ and current $I_{m,i}$ both of which are

functions of $v, \dot{v}, \ddot{v}$. Thus, if the battery is considered to be a flat system, the SOC has to be a function of $v, \dot{v}, \ddot{v}$ only.

Figure 6-6 shows that the SOC is calculated by the charge Q_i which is a result of the rate of charge $\dot{Q}_i$, (current $I_{BT,i}$), and the current $I_{BT,i}$ is a result of battery terminal voltage V_{BT}, which is a function of the battery open-circuit voltage and internal resistance which are functions of the SOC. At this stage, it can be concluded that the battery model, which is using an equivalent circuit of voltage source and internal resistance, both of which are functions of battery SOC, is not possible to be modelled as a differentially flat system.

6.3.4 Implementation of flatness in BEV model and simulation

The earlier sections in this chapter present some related methods for modelling and simulation of a BEV powertrain for the purpose of energy estimation and powertrain sizing. The differential flatness is the method emphasised in this chapter and it was verified that the BEV powertrain can be modelled as a flat system except for the battery losses and its SOC. However, the main objective of this chapter is to present the energy consumption estimation technique for the BEV powertrain, for which the energy consumption is calculated by motor power required, as presented in section 6.3.3; this modelling technique will then be used for powertrain sizing and optimisation in Chapter 7. This section aims to implement the idea of modelling the BEV powertrain as a flat system. The outline of this section is: results of motor parameterisation, modified driving cycle results and energy estimation of the BEV powertrain.

- **Motor parameters estimation from the motor map**

In many applications, where the electric machine is required as a power converter, manufacturers usually provide technical information for their products. In most cases, manufacturers usually publish the motor information (freely available on their website) as a motor efficiency map, similar to the one presented in Figure 6-4 [110], rather than the actual resistance or conductance values of their motor. This information can be useful to guide designers by giving an

overview of the motor efficiency but it is sometimes inadequate for a detailed design and precise model tuning.

The motor efficiency information is a function of the operating torque and speed, as presented in their vertical and horizontal axes. By using this parameterisation method, the motor parameters were estimated, and compared to the original motor map published by the motor manufacturer, Yasa [110], by the methods described in section 6.3.3. MATLAB's function 'fminsearch' was implemented to find the optimum solution of the motor parameter, as described in equation (6-29). The optimum solution is presented Table 6-1.

By comparing the original motor efficiency map in Figure 6-4 and using the parameterisation method, Table 6-1 shows the optimum values of the model motor parameters, and Figure 6-5 shows the efficiency difference of the optimum solution for DC motor parameters.

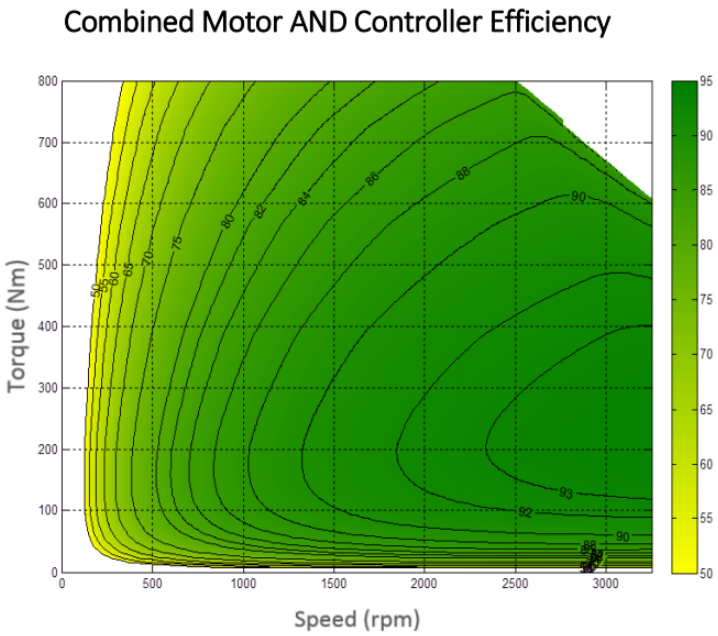

Figure 6-4 Motor efficiency map

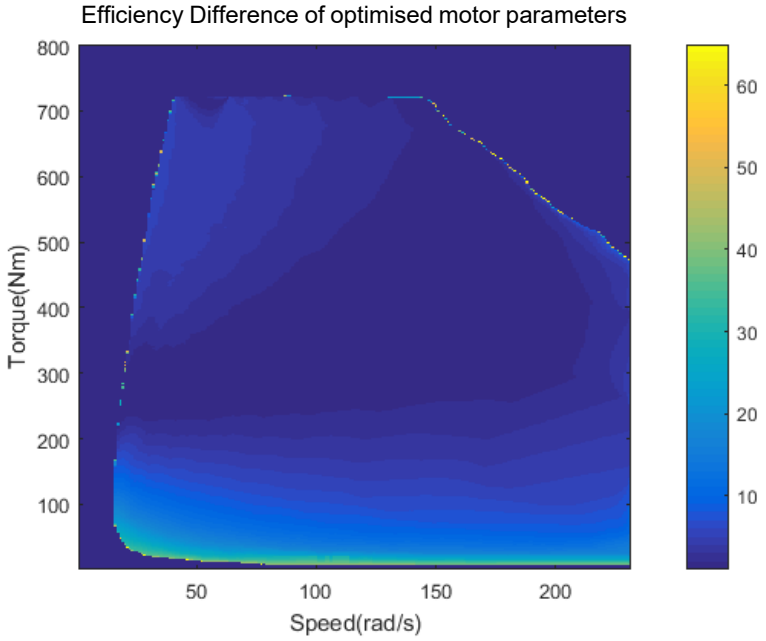

Figure 6-5 Difference in motor efficiency map

Table 6-1 Optimum results of DC motor parameterisation			
	Resistance, R	Friction coefficient, B	Motor constant, K_m
Optimum solution	5 x 10^{-4} Ω	2 x 10^{-4}	0.1

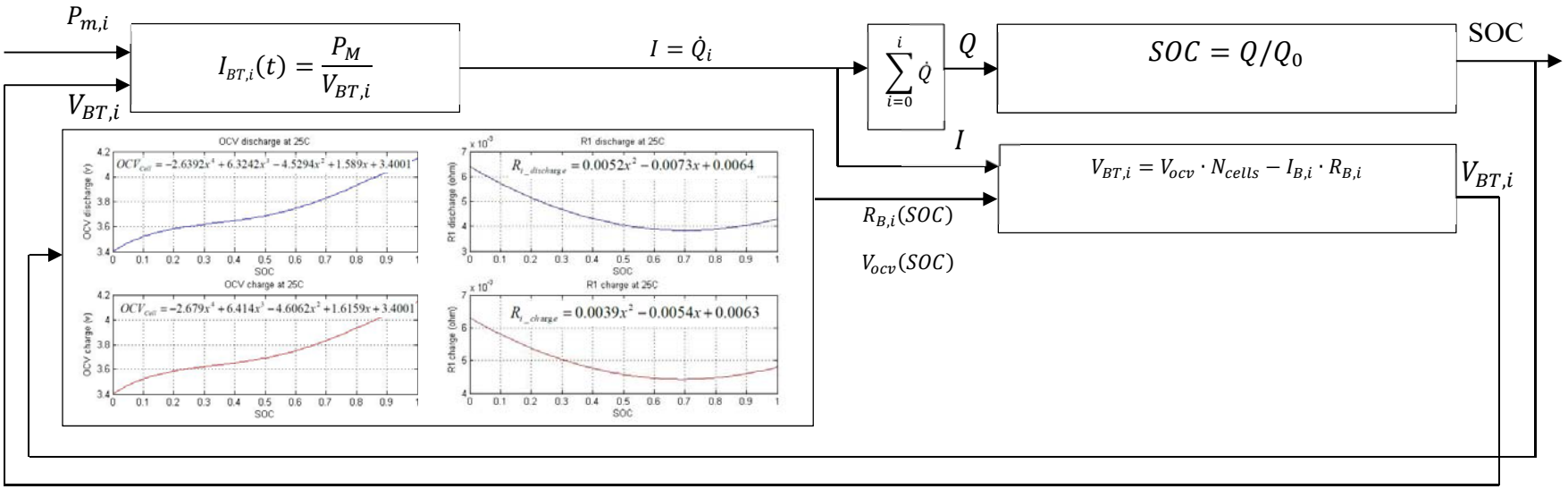

Figure 6-6 Model to estimate the battery SOC

- **Driving cycle modification results**

The original driving cycle is modified in this study for two main reasons: to make them differentiable and to increase their resolution, as described in detail in section 6.3.3. Figure 6-7 presents the derivative of acceleration, called ‘jerk’. As the resolution is 100Hz, the details of this signal can be seen in every 0.01-time step.

It can also be seen from Figure 6-8 that Figure 6-7 is a zoom window of the jerk information at around 136 sec. It is clear to see that the driving cycle achieves the objectives by make the driving cycle a smooth function (differentiable) and provides more detail information for a transient behaviour estimation.

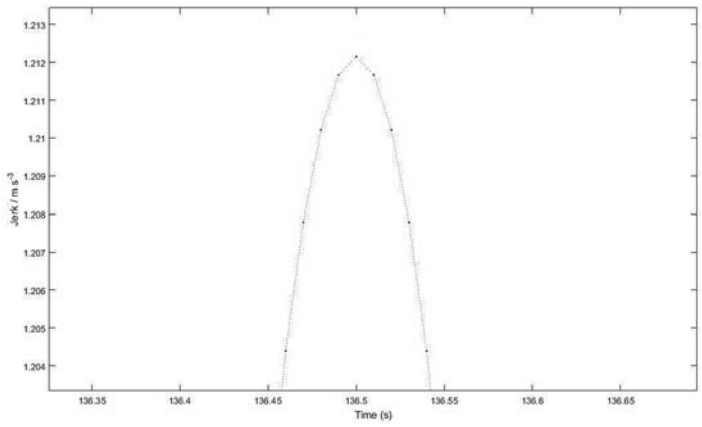

Figure 6-7 Derivative of acceleration (jerk) of the driving cycle

The rest of this section presents simulation results by starting at the results of the force and power required to drive a vehicle over the NEDC cycle, as presented in Figure 6-9(a) and (b). Figure 6-10 shows the required motor current and rate of motor current, then Figure 6-11 presents the energy consumption in both per time and per distance in a different regenerative braking scenario.

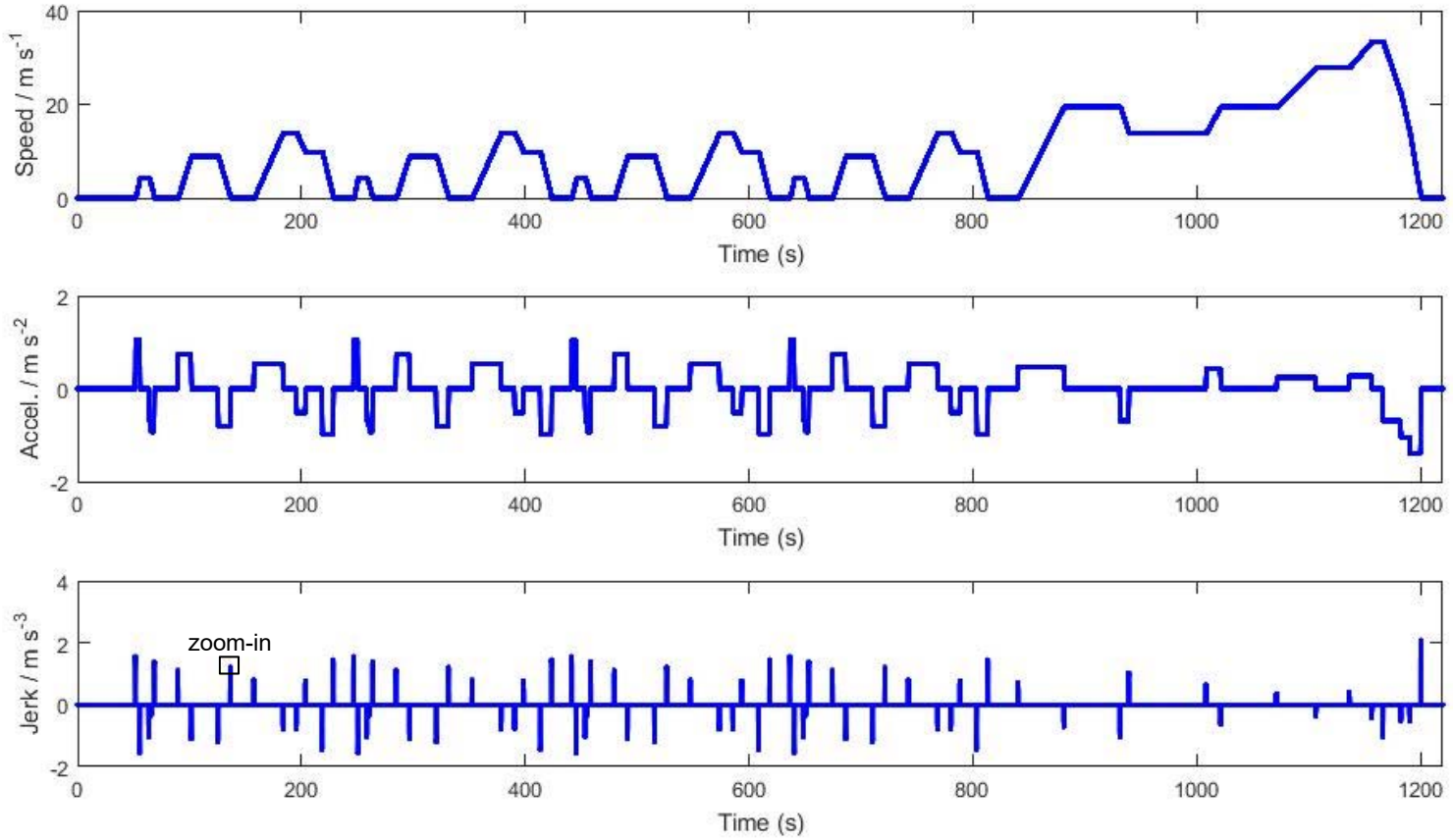

Figure 6-8 Modified NEDC

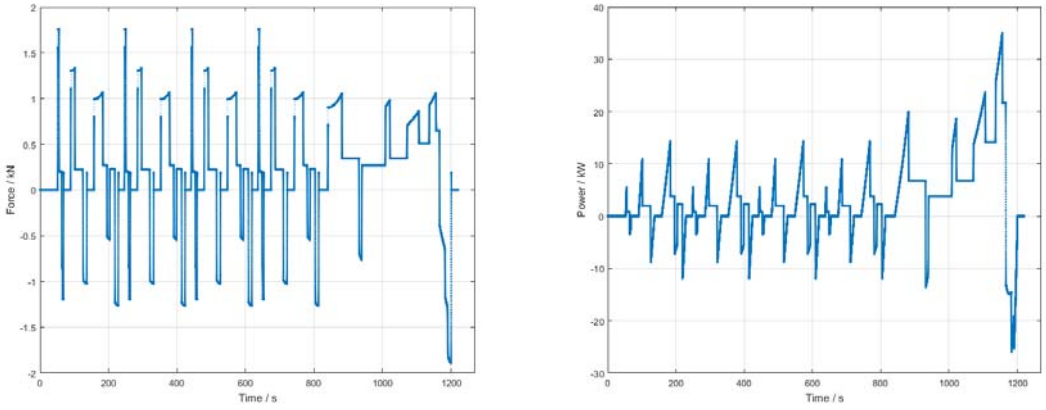

(a) (b)

Figure 6-9 Force and power by the powertrain

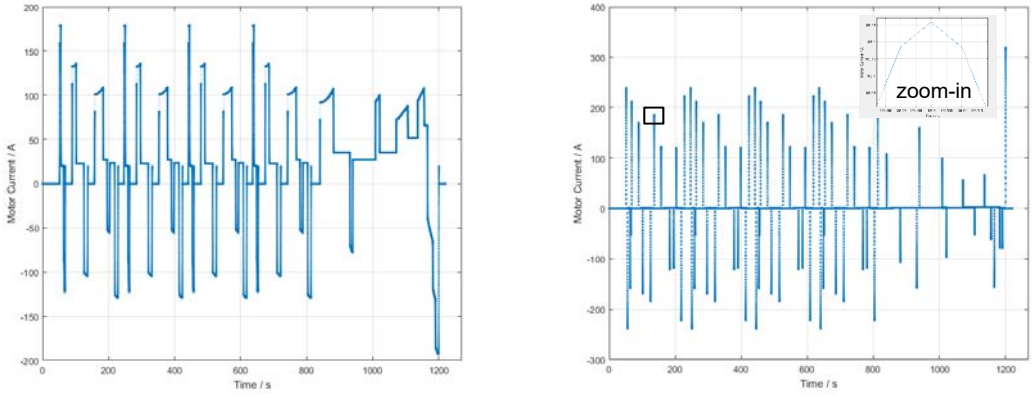

(a) (b)

Figure 6-10 Current and change in current of the motor

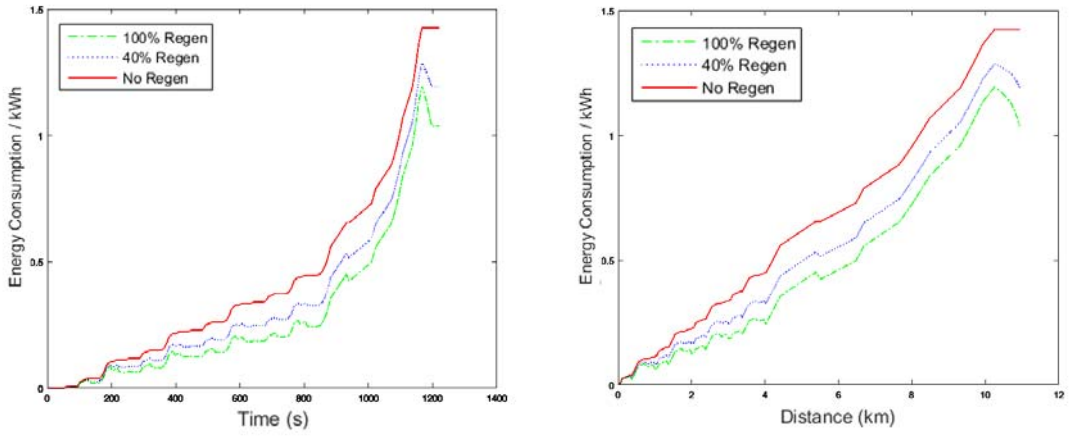

(a) (b)

Figure 6-11 Energy consumption versus time and distance

6.4 Simulation tools for BEV powertrain energy estimation

6.4.1 Forward-facing simulation using dynamical models

Mathematical models to describe the behaviour of a vehicle powertrain can be defined in as much in detail as the level of accuracy expected from them. In this study, the energy consumption is the key concern therefore all other vehicle dynamic aspects may be safely neglected. The conventional and EV model can be fundamentally described by Newton's 2nd law of motion as presented by

$$F_t(t) - F_r(t) = M_v \cdot \dot{v}(t) \tag{6-39}$$

The vehicle can be modelled as a lump of mass (modelled as a particle with mass), M_v, and the traction force, F_t, which is a function of time, and pushing the vehicle forward. The environmental forces, F_r, will pull the vehicle in an opposite direction to the traction force. As a result, the resultant force between F_t and F_r causes the vehicle of mass M_v to move with acceleration $\dot{v}$.

Equation (6-39) can be rearranged to a state space format as in equation (6-1) and replaced by

$$\dot{v}(t) = \frac{1}{M_v}(F_t(t) - F_r(t)) \tag{6-40}$$

The environmental forces, $F_r(t)$, can be described in detail as

$$\begin{aligned} F_r &= F_{\text{Aerodynamic}} + F_{\text{Rolling resistant}} + F_{\text{Slope}} \\ F_r(t) &= \frac{1}{2}\rho \cdot C_d \cdot A \cdot v(t)|v(t)| + M_b g C_r + M_b g \sin\alpha \end{aligned} \tag{6-41}$$

where ρ is the air density, C_d the drag coefficient, A the vehicle frontal area, C_r the rolling resistant coefficient, α the slope angle, g the gravitational acceleration, M_b the body mass and v the vehicle velocity. The velocity in the aerodynamic part is presented as $|v(t)|$ to make sure that the aerodynamic drag will only be opposite to the vehicle's moving direction.

In this study, traction force, F_t, is solely propelled by the electric motor which is described as the torque, T_m, and the relationship between traction force and motor torque is described by

$$F_t(t) = \frac{T_w(t)}{r_d} = \frac{T_m(t) \cdot i_g \cdot \eta_g}{r_d} = \frac{i_g \cdot \eta_g}{r_d} \cdot T_m(t) - T_b(t) \quad \textbf{(6-42)}$$

where T_w and T_m are torque at the wheels and motor respectively. The r_d, i_g and η_g are the effective tyre radius, gear ratio and average efficiency of the gearbox; T_b is the mechanical losses in the motor which are a function of the motor speed.

If a simple DC motor is considered, motor current, I_m, can be described as a function of motor torque and the motor constant, K_m

$$T_m(t) = K_m \cdot I_m(t) \quad \textbf{(6-43)}$$

Motor supply voltage V_m can be described as the Kirchhoff's law of voltage around the loop as presented by

$$V_m(t) = L\dot{I}_m(t) + RI_m(t) + K_m\omega_m(t) \quad \textbf{(6-44)}$$

where V_m is a DC supply voltage to the motor, L is the motor inductance, R is the motor resistance, $\dot{I}_m$ is a derivative of motor current I_m and ω_m is the motor rotational speed.

The wheel speed, ω_w, vehicle speed v and the motor speed ω_m are related to each other as described by

$$\frac{v(t)}{r_d} = \omega_w(t) = \frac{\omega_m(t)}{i_g} \quad \textbf{(6-45)}$$

Equation (6-44) can also be described as a state equation and can be rewritten by

$$\dot{I}_m(t) = \frac{1}{L}(V_m(t) - RI_m(t) - K_m\omega_m(t)) \quad \textbf{(6-46)}$$

These equations represent the simplified model of an electric road vehicle which is using a DC motor as the only source of traction force. There are two states in these equations; the first is the vehicle acceleration $\dot{v}(t)$ and the second is the rate of motor current $\dot{I}_m(t)$ as presented in equations (6-40) and (6-46). These differential equations can be solved by integration to obtain the output v and I_m by these following equations.

$$v(t) = \int_0^t \dot{v}(t)\, dt = \int_0^t \frac{1}{M_v}(F_t(t) - F_r(t))\, dt \quad \textbf{(6-47)}$$

$$I_m(t) = \int_0^t \dot{I}(t) dt = \int_0^t \frac{1}{L}(V_m(t) - RI_m(t) - K_m\omega_m(t))\, dt \quad \textbf{(6-48)}$$

Figure 6-13 shows the diagram that represents all these dynamical equations in a graphical signal flow diagram. This is somewhat similar to graphical programming tools, such as Simulink from MathWorks which is widely used in solving nonlinear differential equations [111].

- **Driver model**

The driver of a physical road vehicle is referred to as a person who controls the speed and direction of that car. However, the driver model in this vehicle simulation is represented as a controller to control speed of the vehicle model and is usually demonstrated as a PI or PID controller [112],[113]. The driver model which is described in [36] consists of two PI controllers to control both the vehicle accelerator and brake pedal. This driver model represents a similar situation to the internal combustion engine vehicle which is that the internal combustion engine is generally used for accelerating the vehicle and the brake torque is supplied from the mechanical friction brake. However, for the simplified EV model, as presented in Figure 6-13, the driver model can be represented by just a single PI controller to control the voltage of the motor. In the case of vehicle deceleration, the brake torque is solely supplied from the motor and this negative motor torque is produced from regenerative braking.

The forward-facing simulation is represented by multiple state equations and required numerical integration to obtain a vehicle speed trajectory. The driver model is an important part of vehicle tracking and to control vehicle speed as close as possible to the given speed references. Moreover, this situation is similar to other control applications in which the tracking behaviour is dependent on the quality of the controller. The tuning of the driver model is certainly required and one method of driver model tuning is represented by assigning controller parameters (P and I control gain) as optimisation design variables as presented in [36] and [92].

- **Use of a forward-facing model**

forward-facing simulation represents a precise view of vehicle model drivability because it was created by the dynamical equations and it is also present both in the transient and steady-state of the system. Moreover, the limitation of the physical system is possibly captured using this technique [36]. The development of a control algorithm and the implementation of hardware-in-the-loop (HIL) are usually required for this forward model technique. There is some literature that uses the forward model in controller design and HIL, as presented in [112].

There is a question about whether or not the forward-facing simulation is a useful technique, as mentioned earlier, and if it is possible to use this technique for powertrain component sizing. Mohan et al. (2013) presented a comparative study between the use of forward-facing and backward-facing in powertrain sizing. They concluded that the forward-facing simulation technique is possible to be used in this application as long as the driver model is co-optimised, along with the powertrain components. However, this technique may suffer from slower simulation time because the computation has to run at the smaller time step compared to the quasi-static backward simulation one.

6.4.2 Quasi-static backward facing simulation

In this quasi-static backward simulation, a driving cycle which is an n-dimension vector is defined as the reference velocity, as in

$$v(t_i) = v_i$$
$$t_i = i \cdot h, i = 0, \dots, n \quad \textbf{(6-49)}$$

where v is a velocity vector which is a function of time t_i, constant interval h and dimension n. The elevation profile and gear ratio profile are sometime indicated together with this velocity profile. These data will be presented versus time. Elements of the velocity profile in the velocity vector are usually indicated by a different of speed at a constant time interval which is normally in one second. However, different time intervals and varying time intervals are possible to implement depending on the objective of the simulation. The representative velocity, $\bar{v}_i$, which is used to calculate the traction force in the quasi-static backward simulation is an average velocity presented in

$$v(t) = \bar{v}_i = \frac{v_i + v_{i-1}}{2}, \forall\, t\epsilon[(i-1) \cdot h, i \cdot h] \quad \textbf{(6-50)}$$

and average acceleration can be described as

$$a(t) = \bar{a}_i = \frac{v_i - v_{i-1}}{h}, \forall\, t\epsilon[(i-1) \cdot h, i \cdot h] \quad \textbf{(6-51)}$$

then vehicle travelling distance, $\bar{x}_i$, can be defined as a summation of velocity over the driving cycle, as described in

$$\bar{x}_i = \sum_{i=1}^{n} h \cdot v_i \quad \textbf{(6-52)}$$

These reference data used for calculating the traction force of the quasi-static backward simulation are summarised and presented in Figure 6-12.

The energy estimation equations for quasi-static backward simulation were previously presented in Chapter 2. However, in this section, these equations will be summarised and briefly re-presented for a comparative view between various types of vehicle simulation. The traction force $\boldsymbol{F_{t,i}}$ consists of forces of environmental and vehicle inertia, as presented in

$$F_{t,i} = F_{a,i} + F_{r,i} + F_{g,i} + m_v \cdot a_i$$
$$F_{t,i} = \frac{1}{2} \cdot \rho \cdot A \cdot C_d \cdot \bar{v}_i{}^2 + C_r \cdot m_v \cdot g \cdot cos(\alpha_i) + m_v \cdot g \cdot sin(\alpha_i) + m_v \cdot \bar{a}_i \quad \textbf{(6-53)}$$

where $F_{a,i}$, $F_{r,i}$ and $F_{g,i}$ are the forces of aerodynamic, rolling resistance and grading respectively. Then the traction force $F_{t,i}$ is converted to torque at the wheels, $T_{w,i}$, and similarly, vehicle velocity is converted to the wheels' speed, $\omega_{w,i}$, as

$$T_{w,i} = F_{t,i} \cdot r_d$$
$$\omega_{w,i} = \frac{\bar{v}_i}{r_d} \quad \textbf{(6-54)}$$

where r_d is an effective tyre radius.

Torque at motor, $T_{m,i}$, and motor speed, $\omega_{m,i}$, can be converted from torque and speed at wheels as

$$T_{m,i} = \frac{T_{w,i}}{i_g \cdot \eta_g}$$
$$\omega_{m,i} = \omega_{w,i} \cdot i_g \quad \textbf{(6-55)}$$

where i_g is the gear ratio and η_g the average gear efficiency. Then, the motor power is calculated from the product of motor torque, speed and efficiency as

$$P_{m,i} = T_{m,i} \cdot \omega_{m,i} / \eta_{m,i}$$
$$\eta_{m,i} = f(T_{m,i}, \omega_{m,i}, \phi_M) \quad \textbf{(6-56)}$$

where $\eta_{m,i}$ is the motor efficiency which is a function of motor torque, motor speed and motor size, ϕ_M. This motor efficiency is usually represented as a motor map which is a looking-up table. The motor efficiency at a particular point is dependent on the torque and speed of the motor at that operating point. The details of this motor efficiency map have already been presented in Section 3.3.3.

Figure 6-14 presents a summarised version of equations (6-49) to (6-56) in a graphical format. It is interesting to see that the signal flow of this quasi-static

backward simulation is one-directional from the driving cycle to the power and energy required from the motor. This simulation technique can be computed as a series of algebraic equations, which allow a large computational time interval and do not require any feedback or controlling techniques as in the forward-facing simulation presented in Figure 6-13. As a result, this quasi-static backward simulation is presented as a method that offers a substantial benefit when used to optimise a long trip simulation [30].

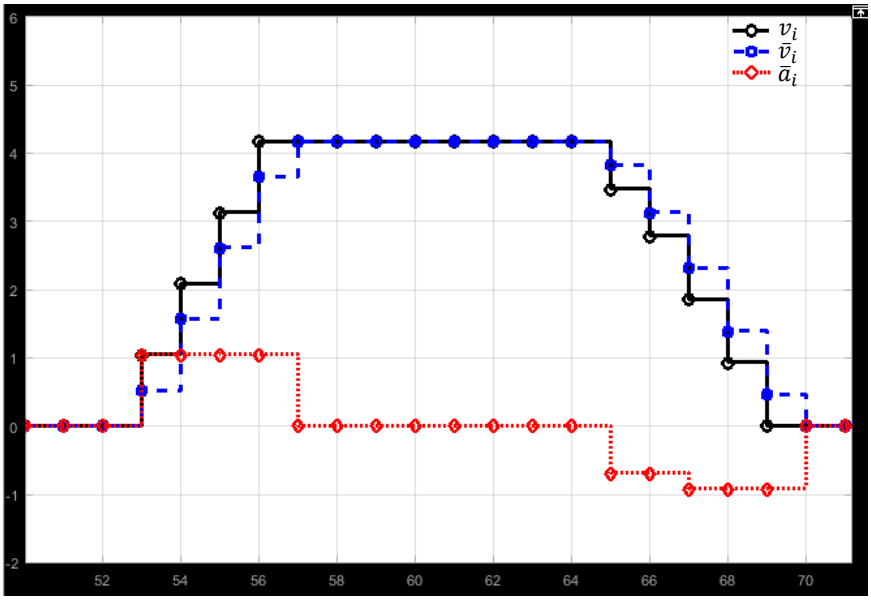

Figure 6-12 Velocity profiles for quasi-static backward simulation

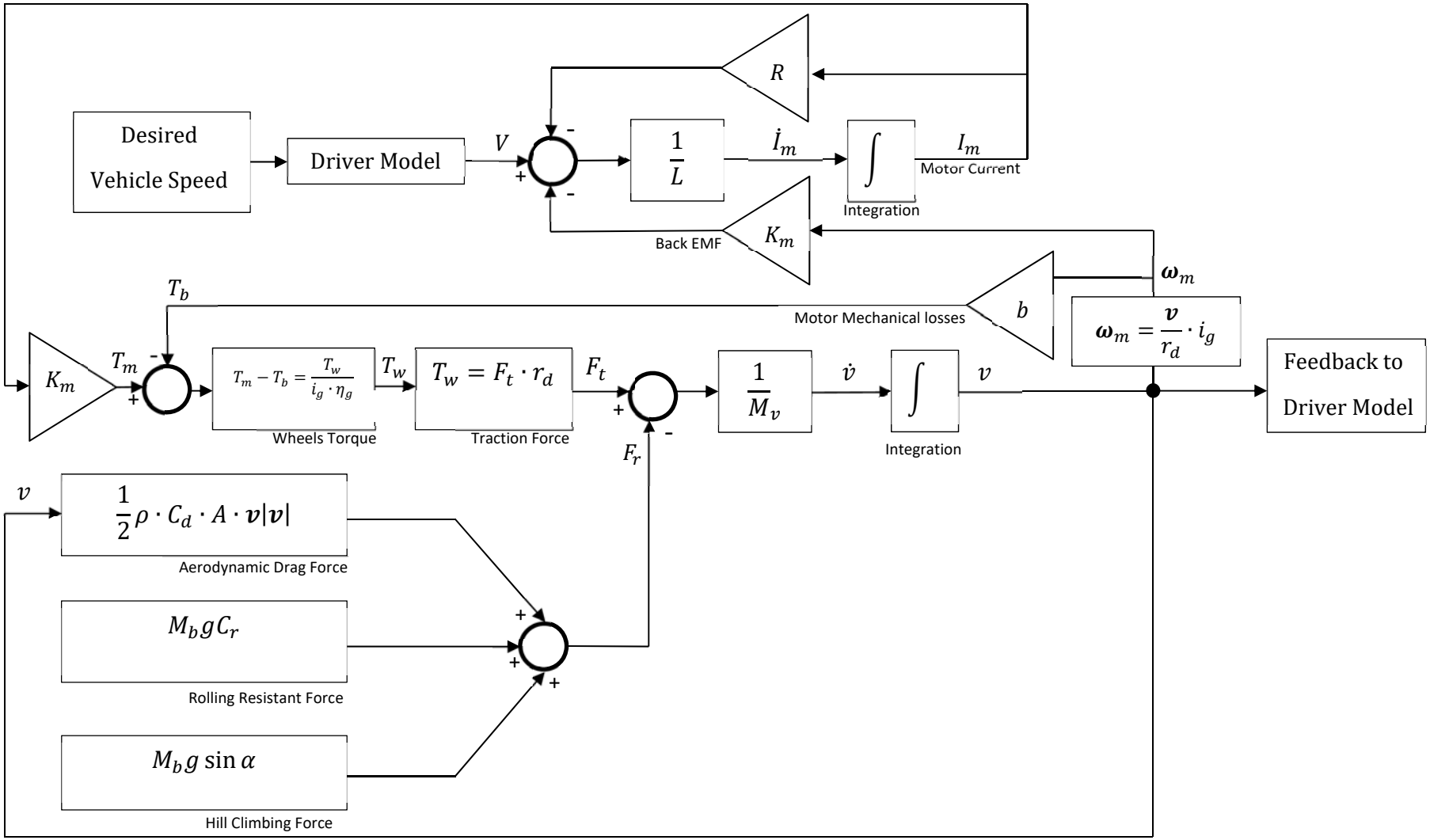

Figure 6-13 Model of a simplified electric vehicle presented in a graphical programming view

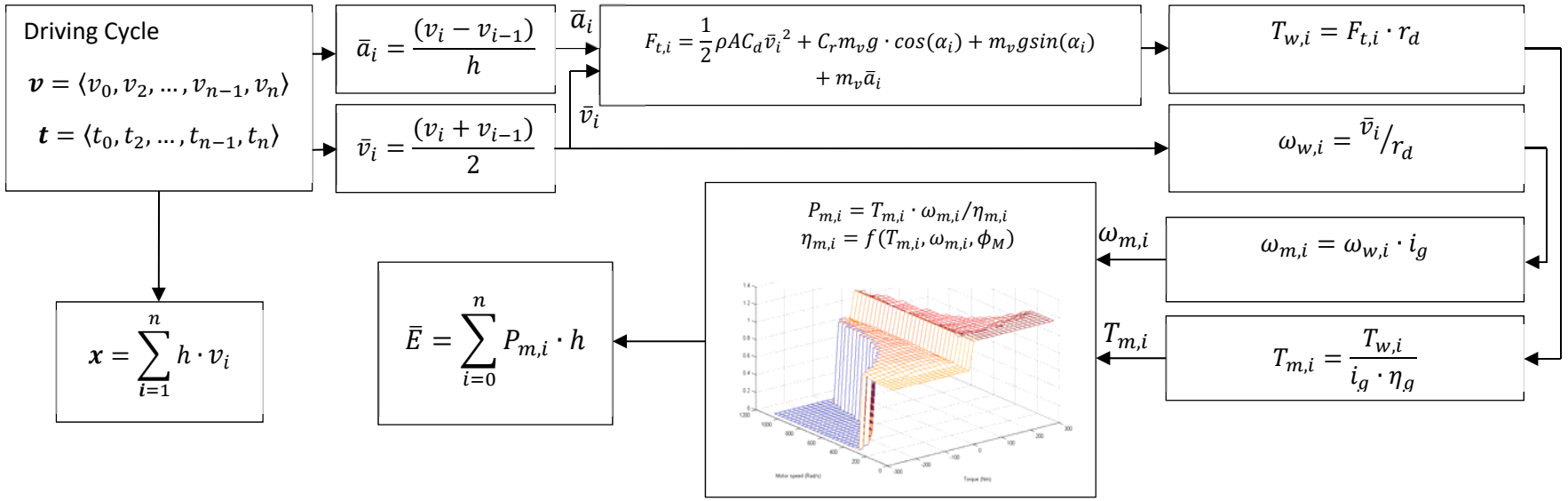

Figure 6-14 Model of the quasi-static backward simulation

6.5 Chapter discussions

Computational modelling and simulation is a tool to examine and design a system using mathematical equations to describe their behaviour. This technique is also applied and used in designing the powertrain for a road vehicle and especially in electric powertrain design where more possible topologies are available. There are many computational tools available in both freeware and commercial software; however, most of them can be classified broadly into two categories: forward and backward simulations. The terms forward and backward do not mean any particular technique but the author aims to justify them by the signal flow during the simulation. With the forward simulation, the current and past trajectories are known but the future trajectory is unknown. The forward simulation will seek the nearest future trajectory (for which time step Δt, is usually defined by a small increment either fixed or variable) as close as possible to the desired trajectories. As a result, a control method is required in this operation.

The backward simulation, on the other hand, is when the current, past and future trajectories are already defined beforehand. This issue makes the backward simulation follow defined trajectories. As a result, this technique allows a less complex simulation and the controlling process is also negligible. In fact, the legislative requirement for a road vehicle also uses a predefined speed profile for the vehicle test [33] which is somehow similar to the backward simulation. The backward simulation in the powertrain study was presented using two techniques; the first is the quasi-static backward simulation and the other is the inverse simulation, details of which were presented in the earlier section of this chapter. The differential flatness, which is a property of the system dynamics is emphasised and applied to the BEV powertrain simulation.

To justify, if the system is a differentially flat, the system should follow a differentially flat property, as presented in section 6.3.1; then the electric powertrain was modelled as a differentially flat system, as presented in section 6.3.3. To be precise, the electric powertrain can be modelled as a flat system

because all the powertrain components can be modelled as a function of the velocity profiles and their derivatives except battery SOC.

The battery SOC, presented in the Section 6.3.3, is a component that cannot be included in the system. This is because the SOC is a function of the SOC itself and it is not possible to model only as a function of velocity and its derivatives. However, the objective of this model aims to study the components sizing and use for optimisation. As a result, size of the battery affects powertrain by its mass, losses in the battery is considered to be a small number in this study as discuss in the Section 5.3 and then energy consumption can be estimated by the energy used at the motor.

One assumption which is defined in this study is to use a DC motor to represent the electric machine for the electric powertrain. In general, the BEV is usually equipped with two types of electric motor. The induction motor, such the Tesla EV [14] and the permanent magnet motor which is mostly used in the Japanese EV, such as the Nissan Leaf [12] and the Mitsubishi I-MIEV [13]. The DC motor which uses a permanent magnet to create magnetic flux is, in some ways, similar to the permanent magnet motor. The differences are in the power electronics and method to drive this machine, where the invertor efficiency is already included in the motor efficiency map, while the induction motor is modelled differently to the permanent magnet motor because it requires additional power to create the magnetic flux [25],[114]. A model of the induction motor as a component of the differentially flat system is not included in this study but it may be useful for further investigation.

The method of motor parameterisation was introduced in this chapter to make an adjustment to the motor model in order to be as accurate as possible compared to a real-world motor. The motor information obtained for this study is available only from the manufacturer’s website; however, a better level of accuracy of motor parameterisation can be performed later in the laboratory by using a physical machine and measurement apparatus. The raw data can be analysed

and estimated using a similar technique to that presented in this chapter to obtain accurate motor parameters.

Finally, I was proved that the differential flatness is possible to apply to electric powertrain modelling. This technique uses the same idea of signal flow as the quasi-static backward simulation and inversion of the dynamical model simulation, which from the family of backward simulation. This study emphasises the idea the inverse dynamical system in the powertrain design of the road vehicle, which was presented earlier in [92] and introduces the connection between designing the EV powertrain and differential flatness property, which is already used in the area of automatic guided vehicles.

6.6 Chapter conclusion

This chapter shows that the EV powertrain can be modelled as a differentially flat system. This allows the dynamics to be inverted and simulation to be performed without iteration. The comparison between existing methods to model the EV powertrain, such as the forward-facing simulation, quasi-static backward simulation and inversion of the dynamical model simulation were presented. Then, the details of the differentially flat system method and the implementation of this method to the EV powertrain modelling and the limitations of battery SOC modelling were explained. The implementation and results were included, which are similar to the quasi-static backward simulation solution but include transient behaviour, which is missing from the quasi-static backward simulation.

Even though differential flatness and BEV modelling have already existed for many decades, the link between them is small in number. This study claims that differential flatness is possible to be used for the purpose of modelling BEV to design their powertrain size and to optimisation them. The technique of applying this flatness design for BEV powertrain optimisation as the energy consumption is the goal objective will be presented in the next chapter. Finally, for those researchers who are familiar with the differential flatness technique, this study presents a connection to extend their knowledge of flatness properties and then apply them to BEV powertrain applications.

7 Multi-disciplinary design in BEV powertrain optimisation

7.1 Introduction

This chapter presents an alternative method of constrained optimisation for the BEV powertrain. The new optimisation processes developed in this study use a new computational tool, Chebfun, and apply it to BEV powertrain sizing and optimisation. Chebfun is an open-source, MATLAB based software for computing functions of real and complex variables. The idea of Chebfun is to approximating functions with Chebyshev polynomials interpolation [115]. This computational tool provides a feeling of symbolic calculation, such as some well-known Maple and Mathematica symbolic computational software, but with the speed of floating-point numerics. In other words, Chebfun is not a symbolic calculator but it does provide sufficiently enough accuracy for engineering application such as simulating the BEV powertrain energy estimation. The key that make Chebfun different from ordinary MATLAB is that Chebfun store data points as Chebyshev polynomial rather than data points, as a result, Chebfun computes function faster and require less memory. However, there are some limitations for being used Chebfun solely for BEV powertrain design and optimisation, details will be discussed later in the chapter.

The method of SA and differential flatness for BEV application, which are described in the previous chapters, are integrated with Chebfun and the multi-disciplinary optimisation (MDO) process to develop this alternative way of BEV powertrain optimisation as presented in Figure 7-1.

Figure 7-1 MDO is a bridge connection between the Chebfun mathematical tool and the application of BEV powertrain constraints optimisation.

This chapter begins with the introduction of Chebfun, multi-disciplinary optimisation and sensitivity analysis which are the key fundamental components of this system. Then the implementation of Chebfun with sensitivity analysis and integrated Chebfun with multi-disciplinary optimisation for optimisation will be presented. Finally, a case study of BEV powertrain constraints optimisation using Chebfun and multi-disciplinary optimisation will be examined and discussed.

7.2 Fundamentals

Chebfun, multi-disciplinary optimisation and sensitivity analysis are key fundamentals in this study. This section presents the background of these techniques, explains their merits and limitations, finally demonstrates points at which to apply these fundamentals for optimisation.

7.2.1 Chebfun

Chebfun is a software system that extends MATLAB object-oriented functions and operators to work with continuous and piecewise continuous functions on a real or complex variable. The command 'chebfun' in MATLAB provides an approximation of a smooth function $f: [-1,1] \rightarrow \mathbb{C}$ by interpolating Chebyshev polynomial of degree N, where N is selected adaptively by the Chebfun system to be accurate close to the machine precision (close to 10^{-13} digits accuracy).

Chebfun was initially created from the Oxford University during 2002-2004 [26]. The very first idea was to overload MATLAB vectors to functions. This first Chebfun version was implemented only with smooth functions on [-1,1] intervals. The second version of Chebfun was started in 2006 and extended the Chebfun to piecewise continuous functions and arbitrary intervals. Some other applications were added, such as solving differential and integral equations, finding eigenvalues of matrices etc. Chebfun version 2 was released in June 2008. The third and fourth versions were released in 2009 and 2010. At this time, the developers decided to create Chebfun as open-source software as they aimed to make this tool available and up-to-date, to help people to solve other scientific problems. The current version was started in 2012 and released in 2014,

this fifth version includes Chebfun2 which breaks the restriction of the one-dimensional function and enables Chebfun to compute with a 2D smooth function. Chebfun2 provides important functions which are used in this study, including global optimisation and root finding. The 3D extension in Chebfun3 is being developed (at the time this thesis is being written) and they expect to release this version in 2016 [26].

- **Chebyshev points**

Any interval $[a, b]$ can be scaled to [-1,1]. And this scaled interval can be divided into a positive integer N of equally spaced angles $\theta_j$from 0 to π. Then there are $N + 1$ Chebyshev points between interval [-1,1]. The Chebyshev points are the real values of these points.

$$x_j = Re(z_j) = \frac{1}{2}(z_j + {z_j}^{-1}), \qquad 0 \le j \le N \tag{7-1}$$

These Chebyshev points can also be defined by their original angle as:

$$x_j = \cos\left(\frac{j\pi}{N}\right), \qquad 0 \le j \le N \tag{7-2}$$

For example, if N = 16, there are 16 intervals and 17 points between [-1,1] as presented in Figure 7-2.

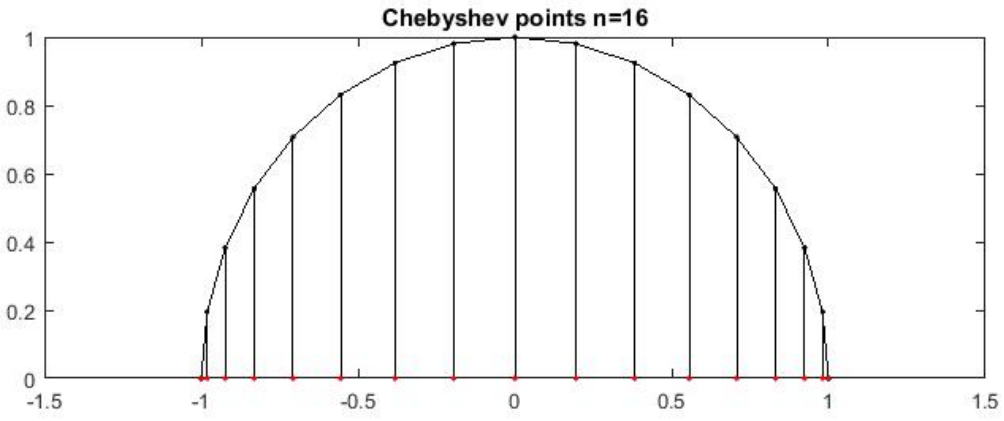

Figure 7-2 Example of 17 Chebyshev points on the [-1,1] interval.

- **Chebyshev polynomials**

Chebyshev points are defined as the real parts of equally spaced points on the unit circle, as shown in Figure 7-2. Similarly, the k^{th} Chebyshev polynomial can be defined as the real part of function z^k on the unit circle.

$$T_k(x) = Re(z^k) = \frac{1}{2}(z^k + z^{-k}) = \cos(k\theta), when\ x = cos\theta$$
$$x \in [-1,1], \theta \in [0,\pi] \tag{7-3}$$

When the range of the variable x is in the interval $[-1,1]$, then the range of the corresponding variable θ can be represented as $[0,\pi]$. But the range is in an opposite direction, as presented in Figure 7-2, when $x = -1$, then $\theta = \pi$ and $x = 1$ which corresponds to $\theta = 0$

The Chebyshev polynomials are presented in Table 7-1.

Table 7-1 Chebyshev polynomial

$\cos 0\theta = 1$	$T_0(x) = 1$
$\cos 1\theta = \cos\theta$	$T_1(x) = x$
$\cos 2\theta = 2\cos^2\theta - 1$	$T_2(x) = 2x^2 - 1$
$\cos 3\theta = 4\cos^3\theta - 3\cos\theta$	$T_3(x) = 4x^3 - 3x$
$\cos 4\theta = 8\cos^4\theta - 8\cos^2\theta + 1$	$T_4(x) = 8x^4 - 8x^2 + 1$
$\cos 5\theta = 16\cos^5\theta - 20\cos^3\theta + 5\cos\theta$	$T_5(x) = 16x^5 - 20x^3 + 5x$
	$\vdots \quad \vdots$
	$T_{k+1}(x) = 2xT_k(x) - T_{k-1}(x), n \geq 1$

Similarly, Figure 7-3 plots the Chebyshev polynomial from $k = [0:5]$.

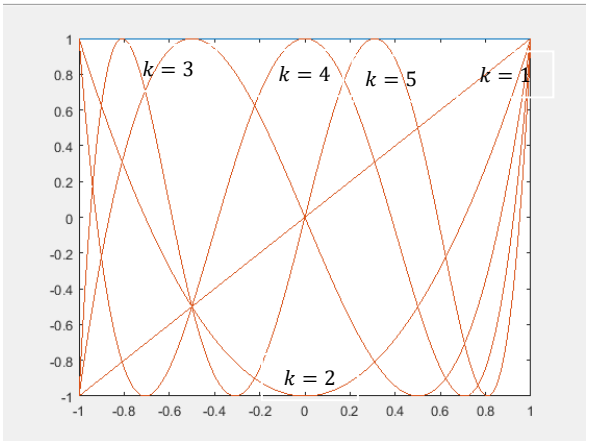

Figure 7-3 Chebyshev polynomial from $k = [0{:}5]$.

- **Chebyshev series expansion**

If $f(x)$ is continuous on $[-1,1]$, this function can be represented as a Chebyshev series

$$f(x) = \sum_{k=0}^{\infty} a_k T_k(x) \tag{7-4}$$

where $T_k(x)$ is the Chebyshev polynomial defined as:

$$T_0(x) = 1, T_1(x) = x$$
$$T_k(x) = 2xT_{k-1}(x) - T_{n-2}(x) \tag{7-5}$$

and a_k is a Chebyshev coefficient

$$a_k = \frac{2}{\pi}\int_{-1}^{1} \frac{f(x)T_k(x)}{\sqrt{1-x^2}}dx, k \geq 1 \tag{7-6}$$

If $k = 0$, the factor of $\frac{2}{\pi}$ is changed to $\frac{1}{\pi}$ [116]

In Chebfun, the infinite series in (7-4) can be approximated by truncating its Chebyshev expansion into a finite N series expansion. The exact Chebyshev coefficients a_k in (7-6) are not computed by Chebfun. However, the approximation of Chebyshev coefficients c_k in (7-7) are computed back and forth in between Chebyshev point grid by using the Clenshaw-Curtis quadrature

implemented with the fast Fourier transform (FFT) [117]. The polynomial p_n is an approximation to $f(x)$ without evaluating the integral of (7-6) [116].

$$p_n(x) = \sum_{k=0}^{N} c_k T_k(x) \qquad \textbf{(7-7)}$$

For a numerical method, a finite number N has to be defined; however, each coefficient c_k and polynomial p_n will converge to a_k and f respectively as $N \to \infty$.

Chebfun works within the MATLAB structure by overloading original MATLAB variables and commands. Continuous functions will be created as Chebfun objects and computed slightly differently from the original MATLAB functions. For example, the *sum* command in MATLAB adds up elements of vectors; however, if $f(x)$ is a Chebfun object and the specific range of x is $[a, b]$, then $f(x)$ evaluates the value of f at point x and $\mathrm{sum}(f)$ evaluates the finite integral of $f(x)$ over the range $[a, b]$. There are about 200 Chebfun operators which are overloaded from original MATLAB commands and functions. More details of Chebfun functions can be obtained from the Chebfun guide [118].

Chebfun works based on storing Chebyshev coefficients of function rather than storing discrete points of data, as has been done in normal MATLAB. Then if f and g are Chebfun, the operation such as $+, -, \times, /$ can be performed over these functions rather than its points in the function. Consequently, Chebfun can reduce the use of computational memory and time by operating numerical computing with functions. As a result, numerical operation can be computed to an accuracy close to machine precisions (10^{-13} accuracy). Hence, it can be said that symbolic calculating in Chebfun can be performed numerically [119].

The freeware Chebfun toolbox and instruction manual are available from the Chebfun website [26]. In this section some examples will be presented to introduce the basic idea behind this MATLAB toolbox. Firstly, Chebfun can be run from the MATLAB command windows as;

```
x=chebfun('x');
f =x.^5;
plot(f);  hold on;
plot(f, '.r','markersize',20);
grid on;
```

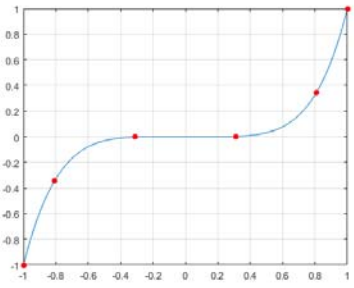

Figure 7-4 Chebfun command example.

The 'chebfun' command constructs a Chebfun object from a specification such as string 'x'. By default, the interval is specific at $[-1,1]$, but the user can select other ranges $[a,b]$ by giving a range input with the chebfun command such as: x=chebfun('x'),[-5,5] .Figure 7-4 shows a plot of $y = x^5$ over a $[-1,1]$ .This result shows that $f(x)$ is represented by a polynomial interpolant through 6 Chebyshev points as presented by the red dots.

The Chebfun command "chebpoly" returns Chebyshev polynomial $T_k(x)$ as;

```
p = chebpoly(f)        p =

                       0.0625    0    0.3125    0    0.6250    0
```

The example below shows the summing of the Chebyshev polynomial as in equation (7-7).

$$= 0.0625T_5(x) + 0T_4(x) + 0.3125T_3(x) + 0T_2(x) + 0.625T_1(x) + 0T_0(x)$$

$$= 0.0625(16x^5 - 20x^3 + 5x) + 0.3125(4x^3 - 3x) + 0.625(x)$$

$$= (x^5 - 1.25x^3 + 0.3125x) + (1.25x^3 - 0.9375x) + 0.625x$$

$$= x^5$$

The result is similar to using the MATLAB command "poly"

```
r = poly(f)        r =

                   1    0    0    0    0    0
```

The accuracy of the Chebfun approximation is dependent on the number of Chebyshev points (degree of Chebyshev interpolation). By default, Chebfun determines these numbers by their adaptive process to obtain results of the required accuracy. Figure 7-5 shows the results if this number of Chebyshev points is adjusted manually.

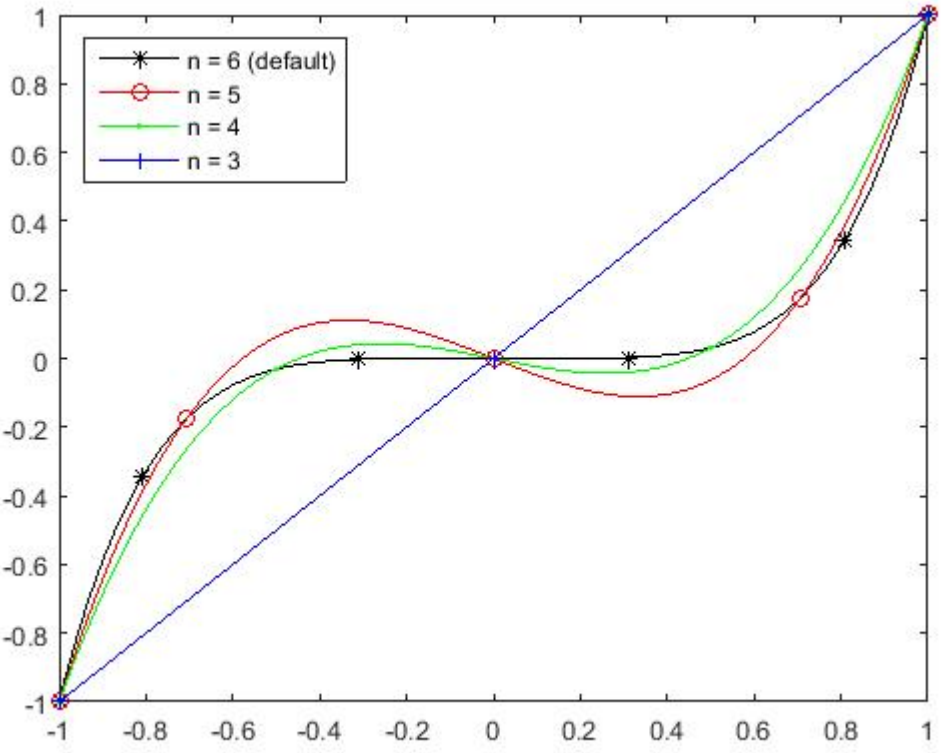

Figure 7-5 The manual selection of Chebyshev points.

- **Chebfun2**

Chebfun2 is an extension of Chebfun that is able to work with smooth functions of two variables on a rectangular $[a, b] \times [c, d\,]$ matrix. The method for two variables is similar to a single variable by extending Chebyshev polynomials into 2D. In a similar manner to equation (7-7), the Chebfun2 algorithm computes the expansion coefficients as:

$$f(x,y) = \sum_{i=0}^{m-1}\sum_{j=0}^{n-1} a_{ij}T_i(y)T_j(x) \tag{7-8}$$

and the $m \times n$ matrix returned represents these coefficients. The command of 'chebpoly2 (f)' in this Chebfun2 is represented by

$$\text{Chebpoly2(f)} = \sum_{j=1}^{k} d_j \text{chebpoly}(c_j)^T \text{chebpoly}(r_j) \tag{7-9}$$

The low rank function approximation will be used to fit the data with a given matrix. Details of this algorithm are presented by Townsend [120].

Two-dimensional global optimisation

Chebfun2 provides functionality for global optimisation. The command of 'minandmax2' gives results of minimisation and maximisation (red dots in Figure 7-6 [118]) of two variables over a specific parameter boundary.

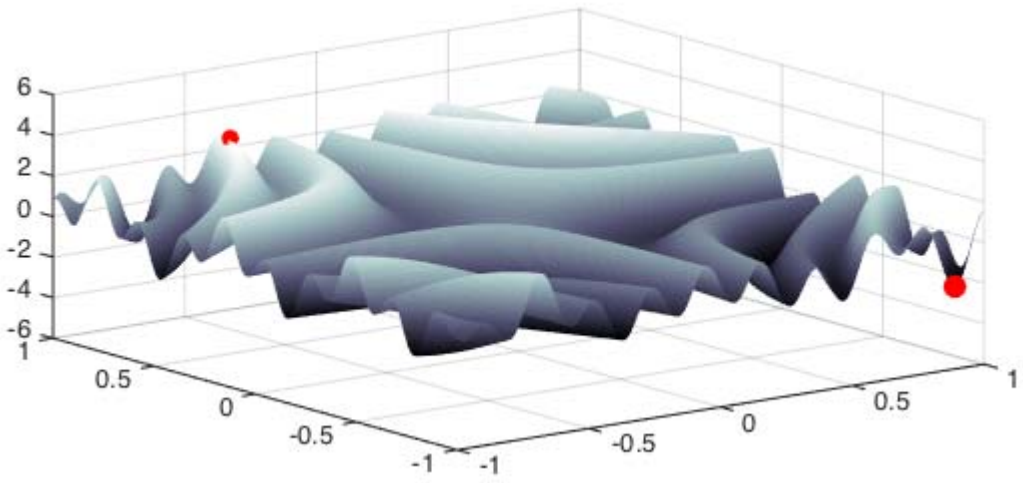

Figure 7-6 Global minimisation and maximisation of function

$$\boldsymbol{f(x,y) = \sin(30 \cdot x \cdot y) + \sin\left(10 \cdot x^2 \cdot y\right) + e^{(-x^2-(y-8)^2)}}$$

Chebfun uses different optimisation algorithms to locate minimum and maximum points depending on the rank of the Chebfun2 object.

Roots finding

The capability of finding zeros is provided by the "roots" command in Chebfun2. This command computes the zero contours of that function. The roots finding is an important tool for finding boundary constraints between variables. More examples will be presented in the implementation section. Details of this command can be further consulted in the Chebfun guide [118].

7.2.2 Multi-disciplinary optimisation

The objective of this chapter is to propose an alternative method of BEV powertrain constraints optimisation using the Chebfun computational tool and to critically analyse its strengths weakness. The multi-disciplinary optimisation technique has to be applied as a bridge connection between these two fields. This section aims to introduce the multi-disciplinary optimisation as a tool to overcome the limitations of Chebfun2 which can optimise a system with limited design parameters. The background of multi-disciplinary optimisation will be briefly described to introduce the roots and application of multi-disciplinary optimisation both in the aerospace and automotive industries. Two non-hierarchical multi-disciplinary optimisation methods will be introduced, with explanations, then the comparison will be presented at the end of this section.

This study does not intend to describe details of multi-disciplinary optimisation methods in the automotive application but the authors' intention is to elaborate on the technique of optimisation and to maximise the use of Chebfun in BEV powertrain application using the multi-disciplinary optimisation technique. Readers who are interested in the possibility of using multi-disciplinary optimisation in the former application are referred to the technical report that presents a critical review of multi-disciplinary optimisation in automotive application at [121].

- **Background**

multi-disciplinary optimisation is a well-known method in the aerospace industry; in fact, the concept of multi-disciplinary optimisation was originally developed for

structural optimisations [122]. The reason behind this is that structure is a subsystem that is attached to other engineering fields. The weight of the structure is usually an objective function to minimise and satisfy constraints (e.g. maximum stress, safety factor). Design variables usually include a cross section and thickness of the structure of beams. Eventually, multi-disciplinary optimisation was introduced into the aerospace industry where structure and aerodynamics interact and optimise together.

One of the most common multi-disciplinary optimisation applications in the aerospace industry is the simultaneous optimisation between aerodynamics, structure of aircraft wings and aircraft configurations [123]. A design conflict between slender and stubby shaped aircraft exists. A slender shape benefits from its lower drag force and results in better fuel consumption, while the stubby shape is lighter and has a lower manufacturing cost. A trade-off between drag and structure weight involves the solving of problems between different disciplines. The weight of a structure affects the power required for both a lifting force and drag force, whilst structure deformation causes the aerodynamic shape to be changed. The optimal design results in the design of a structure that deforms to the desired aerodynamic shape and the structural deformation is approximately constant during the flight time [123]. This is an example where the multi-disciplinary design is used for designing a system that requires parameter coupling between different disciplines.

The development of multi-disciplinary optimisation was described by Kroo and Manning KrMa00 [124]. There are three generations of multi-disciplinary optimisation system: integrated, distributed analysis and distributed design as presented in Figure 7-7. The first generation was to integrate all systems in a single optimisation loop. Then, a second generation was developed as the problem size increased. In this generation, subsystems were distributed by system analyser and coordinated by a single optimiser. These two generations are classified as a single-lever MOD. The third generation is called a multi-level multi-disciplinary optimisation and this method is used with large scale problems where subsystems are distributed and require their own optimiser.

Single-level methods, for example, Multidisciplinary Feasible (MDF) and Individual Disciplinary Feasible (IDF), have a non-hierarchical structure and a single optimiser. These methods work effectively with a strong interaction system but do not perform well in large dimension problems. On the other hand, multilevel methods include a hierarchical structure and each level has an optimiser. Concurrent subspace optimisation (CSSO), bi-level integrated system synthesis (BLISS) and collaborative optimisation (CO) are examples of multilevel methods [125].

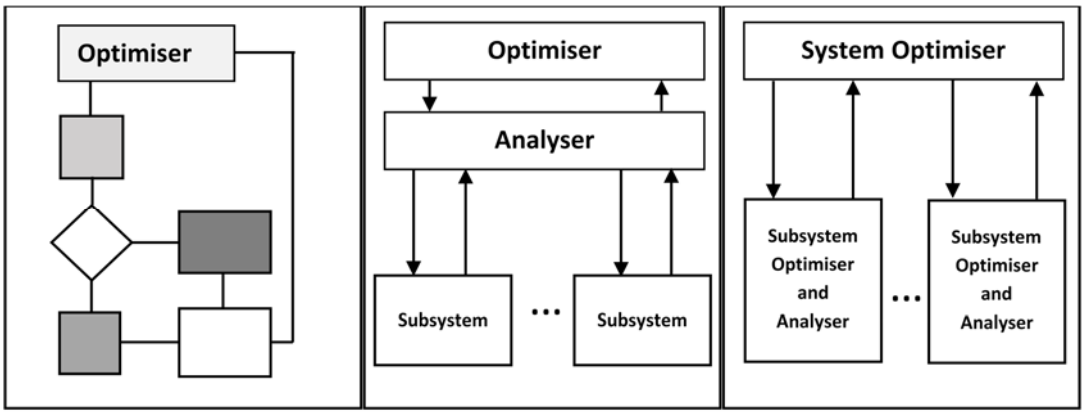

Figure 7-7 Three generations of multi-disciplinary optimisation system (a) integrated, (b) distributed analysis and (c) distributed design

- **Multi-disciplinary optimisation method in automotive applications**

Multi-disciplinary optimisation techniques were analysed and evaluated for the automotive industry, as described in a technical report presented by Ryberg et al. [121]. This report presents a comprehensive summary of multi-disciplinary optimisation with a focus on structural optimisation for automotive application. One interesting topic presented in this report is to compare the method of multi-disciplinary optimisation between aerospace and automotive applications. There are some interesting key points that make the multi-disciplinary optimisation in automotive different from aerospace:

- **Product cycle**

The aerospace industry has fewer in number but more expensive products than the automotive one. It takes a longer time for a design cycle and this is usually funded by a government organisation such as the military. Through both the available time and resources, the development of new processes and methods are likely to be possible. However, there are many more large automotive manufacturers than aerospace ones and this is leading to a competition in producing better, shorter and less expensive products rather than focusing on process development.

- **Rules and regulations**

The methods and processes in aerospace development are ruled by standards and regulations; they have to be approved by governmental safety agencies such as the FAA (Federal Aviation Administration) and EASA (European Aviation Safety Agency). However, the design of passenger cars is controlled by legislative requirements such as CO_2 emissions and safety. The competitiveness in automotive design is focused on market requirements, such as vehicle performance, and price.

- **Coupling between disciplines**

Structure is a good example of comparing the multi-disciplinary optimisation method for automotive and aerospace applications. The wings and fuselage of the aeroplane are compared to the body of the car. In a normal operation, deformation of the aeroplane wings affects their aerodynamic properties while the body of the car is likely to be more rigid or have only a small deformation compared to the aeroplane body. This indicates that multi-disciplinary optimisation in the automotive design process is therefore simpler than for aerospace application because of its loose coupling between disciplines. And it can be said that multi-disciplinary optimisation in automotive applications, such as in crashworthiness, are created in a multi-attribute environment (shared system variables) rather than in a truly multi-disciplinary design.

This study concludes that the multi-disciplinary optimisation which is developed in the aerospace industry is unsuitable for the automotive industry because of the disciplines in the automotive application being loosely coupled. Also, the computational cost of multi-level multi-disciplinary optimisation methods is greater than the benefits. The authors in this study, Ryberg et al. [121], suggest using a single-level method in most automotive applications. In addition, they also recommended using a metamodel, which is a detailed model simplification with a smooth gradient function to increase optimisation efficiency.

- **Multi-disciplinary optimisation methods for Chebfun optimisation**

This study is not intended to classify the multi-disciplinary optimisation design for automotive application but it aims to use the properties of the multi-disciplinary optimisation design and apply them to connect Chebfun with the BEV powertrain optimisation. The author shares the view of Agte et al. [122] that multi-disciplinary optimisation for the BEV powertrain is more likely to be a multi-attribute environment rather than a multi-disciplinary design; however, there are some properties of multi-disciplinary optimisation that are useful to use. A single-level multi-disciplinary optimisation method is used in this study because of its simple processes and because it is sufficient for this BEV powertrain application. The following section will present the single-level multi-disciplinary optimisation, MDF and IDF methods.

- **Multidisciplinary Feasible Method**

The MDF method is the most common formulation and is demonstrated more frequently than other non-hierarchical multidisciplinary methods; it is also called “nested analysis and design” or “All-in-one” [126],[127]. The MDF method consists of an optimiser and a multidisciplinary design analyser, as shown in Figure 7-8. The vector of design variables X_D, is supplied from the optimiser to the multidisciplinary design analyser, where the analyser has a role to manage the data flow between optimiser and subsystems. Variables between subsystems are shared between those subsystems in order to compute the objective function $f(X_D, U(X_D))$ and the constraints $C_D(X_D, U(X_D))$. These cost functions and

constraints are returned from the analyser as vector $U(X_D)$. This optimisation process will be repeatedly calculated in every iteration, keeping all constraints within the feasibility space until they reach the optimum [128].

$$\begin{aligned} &\text{Minimise} && f(X_D, U(X_D)) \\ &\text{with respect to} && X_D \\ &\text{and subject to} && C_D(X_D, U(X_D)) \geq 0 \end{aligned} \tag{7-10}$$

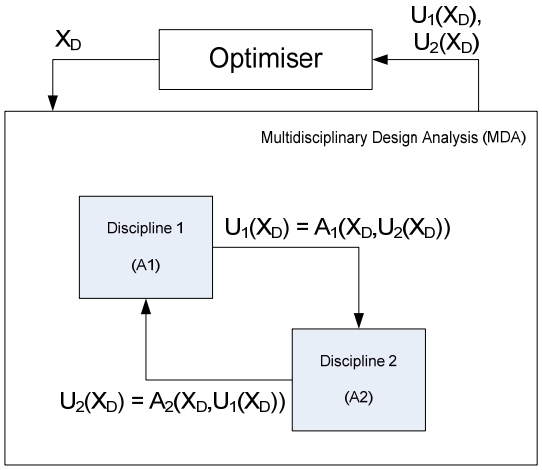

Figure 7-8 Multidisciplinary Feasible (MDF) Method

- **Individual disciplinary feasible (IDF) method**

The IDF method is in some ways similar to the MDF method as both of them are non-hierarchical multi-disciplinary optimisations, using a single optimiser and required multidisciplinary design analyser. However, there is a main difference that makes IDF more flexible than MDF. A drawback of the MDF method is that a complete multidisciplinary analysis at every optimisation iteration is required, which results in computational expense. In contrast, the IDF method maintains an individual disciplinary feasibility and the multidisciplinary design analyser is included in the subsystem. An optimiser drives the individual discipline to obtain multidisciplinary feasibility by controlling the interdisciplinary variables. Coupling variables between disciplines are promoted to become optimisation variables and are replaced by surrogate variables. Auxiliary equality constraints are created in

an optimiser to ensure that surrogate variables are equal to the interdisciplinary coupling variables [127], [129]. The IDF method equations can be written by

$$\begin{aligned} &\text{Minimise} && f(X_D, U(X)) \\ &\text{with respect to} && X = (X_D, X_\mu) \\ &\text{subject to} && g(X_D, U(X)) \leq 0 \\ & && C(X) = X_\mu - \mu = 0 \end{aligned} \quad \textbf{(7-11)}$$

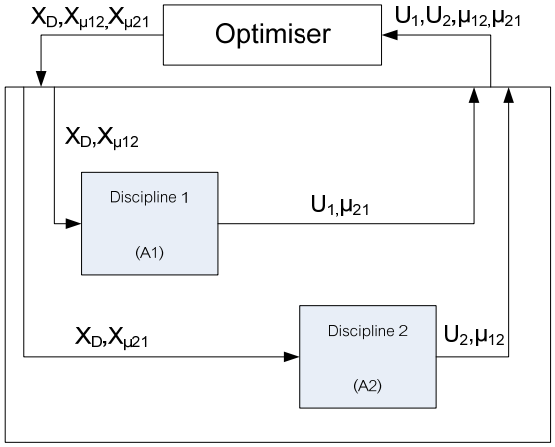

Figure 7-9 Individual disciplinary feasible (IDF) method

Figure 7-9 shows the data flow in the IDF method, where X, X_D are the vector of design variable, X_μ are the interdisciplinary coupling variables that are promoted to become optimisation variables, $f(X_D, U(X))$ and $g(X_D, U(X)) \leq 0$ represent the objective function and system constraints, respectively. The interdisciplinary coupling variables are converted to auxiliary equality constraints, as presented in $C(X) = X_\mu - \mu = 0$. Auxiliary constraints are required to enforce subsystem consistency at convergence [130].

- **Comparison between MDF and IDF Methods**

In terms of disciplinary feasibility methods, the IDF requires only individual feasibility at each optimisation iteration, while the MDF requires complete multidisciplinary feasibility. In other words, every constraint has to satisfy the MDF

optimisation before moving to a new optimum point while IDF requires only a feasibility of each subsystem but does not require system feasibility. As a result, the overall cost of simulation and number of functions that are called for the IDF method are less than those for the MDF method. Figure 7-10 (a) shows that the shared variables in the MDF are linked between subsystem to make whole system feasibility, while the variables of IDF in Figure 7-10 (b) are independent and only require subsystem feasibility.

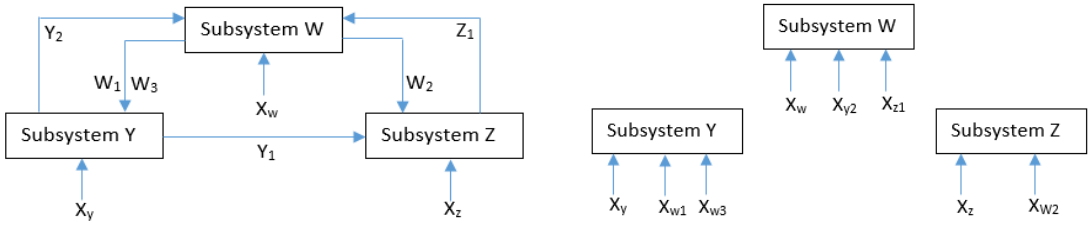

(a) (b)

Figure 7-10 Optimisation variable for the MDF (a) and IDF (b) methods [131]

It can be seen from Figure 7-11 [127] (a) that the MDF method may take longer to find the optimum point because it always stays in the feasible design space (or keeps returning to the feasible space) before driving the analysis to the optimum point. On the other hand, Figure 7-11 (b) shows the method of IDF that requires only individual subsystem feasibility and runs directly towards the optimum point at the first feasible space [129]. In addition, as the IDF subsystems are independent, optimisation task of different subsystem can be spit and computed separately. This IDF method is suitable for a parallel computing system.

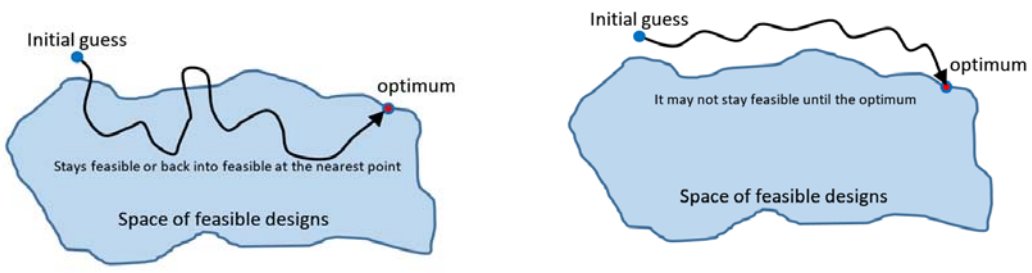

(a) MDF (b) IDF

Figure 7-11 Comparison of MDF and IDF methods

The MDF is slower to find the optimum but it can make sure that the solution is feasible; on the other hand, the IDF, which is faster than MDF, may be trapped outside a feasible space and fail to find the optimum feasible solution.

7.2.3 Sensitivity analysis

Sensitivity analysis is defined as a mathematical technique (numerical or otherwise) to study how uncertainty in the output of a system (model) can be apportioned by the different sources of uncertainty in the model input [78]. Two approach techniques can be performed for calculating sensitivity analysis: local and global. Sensitivity analysis initially started with the local sensitivity method using the derivative-based technique [132]. This technique finds the partial derivative at a point of the design parameter and cost function to obtain the sensitivity solution. If there are many input design parameters, this local technique changes one variable at a time while keeping other parameters fixed; this technique is also called one-at-a-time. Another approach method is global sensitivity analysis; instead of using a single data point, as in local sensitivity analysis, global sensitivity analysis uses a set of input factors to explore the output space. Some examples are Variance-based methods and Screening technique.

There are some benefits of the global technique that provide an opportunity to explore the sensitivity of the model in a wider range of inputs and are also possible to be used with a discontinuities function. However, the local method has an advantage in its efficient calculation time. This study has limited the scope by using the local method and extended it for BEV powertrain application. However, the use of the global technique can be explored more in [133] and a comparison between these methods is presented in [134].

In the optimisation context, sensitivity analysis can be used either before, after or both, such as[135]:

- Using sensitivity analysis before optimisation – When a large number of model parameters influences the optimisation problems. sensitivity

analysis can be used for determining the most significant parameter to the objective function or prioritize a set of input parameters. This technique helps to obtain the initial guesses of parameters in order to estimate the cost function before running the optimisation and also to reduce computational costs for optimisation.

- Using sensitivity analysis after optimisation – sensitivity analysis can be used after optimisation to test the robustness of the cost function to both design and fixed parameters.

o **Derivative-based sensitivity analysis for vehicle energy estimation**

The literature [25] demonstrates examples of using local sensitivity analysis for a road vehicle. The energy equation, which is an initial stage of finding sensitivity analysis, can be expressed as the algebraic equations presented by

$$\bar{E} = E_{\text{Aero}} + E_{\text{Rolling}} + E_{\text{Inertia}}$$
$$\bar{E}_{NEDC} = 1.9 \cdot 10^4 \cdot A_{fCd} + 8.4 \cdot 10^2 \cdot M_v \cdot C_r + 10 \cdot M_v \quad \textbf{(7-12)}$$

This equation contains three design parameters to estimate energy over a predefined driving cycle where, A_{fCd} is an aerodynamic drag area, C_r is a rolling resistant coefficient and M_v is a vehicle mass. Average energy consumption over a specific distance, $\bar{E}$, can be calculated based on these product of vehicle parameters and coefficients which vary for each driving cycle. For this example, the coefficients $\{1.9 \cdot 10^4, 8.4 \cdot 10^2, 10\}$ are used to calculate energy estimation for NEDC in kJ/100km.

- **First order sensitivity analysis**

Sensitivity analysis of parameters to energy consumption can be expressed as:

$$S_{p_i} = \lim_{\delta p_{\text{i-nom}} \to 0} \frac{[\bar{E}(p_{\text{i-nom}} + \delta p_{\text{i-nom}}) - \bar{E}(p_{\text{i-nom}})]/\bar{E}(p_{\text{i-nom}})}{\delta p_{\text{i-nom}}/p_{\text{i-nom}}} \quad \textbf{(7-13)}$$
$$p = [A_{fCd}, C_r, M_v]$$

This derivative-based method compares the rate of change of energy consumption with a change of a specific parameter at a particular point. In other

words, the sensitivity analysis value gives information on how much energy changes (as a percentage) if a parameter value is changed by a percentage. When there is more than one parameter in the equation, one parameter can be analysed at a time while other parameters are kept constant at their nominal points. Deriving three partial derivatives, the sensitivity analysis of each parameter can be expressed as

$$
\begin{aligned}
SA_{\mathrm{f}}C_{\mathrm{d}} &= \frac{\partial \bar{E}}{\partial\, A_{\mathrm{f}}C_{\mathrm{d}}}(A_{\mathrm{f}}C_{\mathrm{d}})_{\text{-nom}} \cdot \frac{(A_{\mathrm{f}}C_{\mathrm{d}})_{\text{-nom}}}{\bar{E}(A_{\mathrm{f}}C_{\mathrm{d}}, C_r, M_v)_{\text{-nom}}} = 1.9 \cdot 10^4 \cdot \frac{(A_{\mathrm{f}}C_{\mathrm{d}})_{\text{-nom}}}{\bar{E}(A_{\mathrm{f}}C_{\mathrm{d}}, C_r, M_v)_{\text{-nom}}} \\
S_{Cr} &= \frac{\partial \bar{E}}{\partial\, C_r}(C_r)_{\text{-nom}} \cdot \frac{(C_r)_{\text{-nom}}}{\bar{E}(A_{\mathrm{f}}C_{\mathrm{d}}, C_r, M_v)_{\text{-nom}}} = 840 \cdot (M_v)_{\text{-nom}} \cdot \frac{(C_r)_{\text{-nom}}}{\bar{E}(A_{\mathrm{f}}C_{\mathrm{d}}, C_r, M_v)_{\text{-nom}}} \\
S_{M_v} &= \frac{\partial(\bar{E})}{\partial\, M_v}\,(M_v)_{\text{-nom}} \cdot \frac{(M_v)_{\text{-nom}}}{\bar{E}(A_{\mathrm{f}}C_{\mathrm{d}}, C_r, M_v)_{\text{-nom}}} \\
&= (840 \cdot (C_r)_{\text{-nom}} + 10) \cdot \frac{(M_v)_{\text{-nom}}}{\bar{E}(A_{\mathrm{f}}C_{\mathrm{d}}, C_r, M_v)_{\text{-nom}}}
\end{aligned}
\qquad \textbf{(7-14)}
$$

If a compact class vehicle is considered, parameters of $\{A_{fCd}, C_r, M_v\}$ can be easily substituted by $\{0.6, 0.012, 1000\}$ and give the sensitivity value of $\{0.36, 0.32, 0.64\}$ respectively. This first order sensitivity analysis technique shows the different impacts when each parameter changes over an energy consumption; however, they do not provide any insight information of cross-coupling between parameters.

- **Second order sensitivity analysis**

Analysis of cross-coupling parameters in the BEV powertrain is presented in the Chapter 5 . This technique was extended from first order sensitivity analysis and by performing a further partial derivative between two design parameters. This second order sensitivity analysis of a simplified road vehicle powertrain is presented by

$$
\begin{aligned}
S'_{A_{fCd},\, C_r} &= \frac{\partial^2(\bar{E})}{\partial\, A_{fCd} \cdot \partial\, C_r} \cdot \frac{(A_{\mathrm{f}}C_{\mathrm{d}})_{\text{-nom}} \cdot (C_r)_{\text{-nom}}}{\bar{E}(A_{\mathrm{f}}C_{\mathrm{d}}, C_r, M_v)_{\text{-nom}}} = 0 \\
S'_{A_{fCd},\, M_v} &= \frac{\partial^2(\bar{E})}{\partial\, A_{fCd} \cdot \partial\, M_v} \cdot \frac{(A_{\mathrm{f}}C_{\mathrm{d}})_{\text{-nom}} \cdot (M_v)_{\text{-nom}}}{\bar{E}(A_{\mathrm{f}}C_{\mathrm{d}}, C_r, M_v)_{\text{-nom}}} = 0 \\
S'_{C_r,\, M_v} &= \frac{\partial^2(\bar{E})}{\partial\, C_r \cdot \partial\, M_v} \cdot \frac{(C_r)_{\text{-nom}} \cdot (M_v)_{\text{-nom}}}{\bar{E}(A_{\mathrm{f}}C_{\mathrm{d}}, C_r, M_v)_{\text{-nom}}} = 840
\end{aligned}
\qquad \textbf{(7-15)}
$$

Sensitivity analysis has been used for analysing the uncertainty of mathematical models and is also used in the optimisation process. This section gives a general idea of how to apply derivative-based sensitivity analysis in road vehicle powertrain analysis. Examples of energy equations using three general design parameters have been presented. The first order sensitivity analysis gives us the information on the most important parameters at the particular point of interest, and the second order sensitivity analysis tells us about the interaction between them.

From the above example, in the design parameters of a compact road vehicle, the mass of the vehicle is the most sensitive parameter for energy consumption. This can be easily observed from the value of the first order sensitivity analysis as presented earlier. Then if the cross-coupling parameters are considered, the second order sensitivity analysis will give the information that which parameters are cross-coupling to the mass. The above example shows that the aerodynamic drag area is not cross-coupled to other parameters. In other words, the aerodynamic part can be improved alone without affecting other parameters, but improving the mass and rolling resistance may significantly improve energy consumption.

7.3 Implementations

7.3.1 Sensitivity analysis of BEV using Chebfun

The previous sections have given some general ideas of using sensitivity analysis in BEV powertrain application and Chebfun was introduced in a very early section. Partial derivation can be calculated by using analytical techniques, as presented in the previous example; however, for a complex equation when many design parameters are involved, an analytical solution may not be a flexible technique for this computation. This section aims to present a numerical technique for first and second order sensitivity analysis using Chebfun and then apply this method to the existing energy equation of the BEV powertrain from the Chapter 5. The energy equation of full parameters for the BEV powertrain is

$$\bar{E} = E_{\text{Aero}}(A_{\text{f}}C_{\text{d}}) + E_{\text{Rolling}}(C_r) + E_{\text{Inertia}}(M_v) - E_{\text{ReGen}}(\eta_{\text{ReGen}}) + E_{\text{GearLoss}}(\eta_{\text{Gear}}) + E_{\text{MotorLoss}}(\eta_{\text{Motor}}) + E_{\text{BatteryDischargeLoss}} + E_{\text{BatteryChargeLoss}} \quad \textbf{(7-16)}$$

This equation provides most of the influential sources of energy dissipated by the BEV powertrain. The details and fundamentals have been clearly explained in the literature. This section will treat the equation as a function with six design parameters and seven fixed parameters

$$\bar{E} = f(A_{\text{f}}C_{\text{d}}, C_r, M_v, \eta_{\text{ReGen}}, \eta_{\text{Gear}}, \eta_{\text{Motor}}) \quad \textbf{(7-17)}$$

Details of this equation are presented in the Chapter 5.

Figure 7-12 shows plots of the energy consumption of vehicle mass and aerodynamic drag area on their possible operated ranges. As the plot is linear, Chebfun approximate three Chebyshev points and approximately two intervals between them.

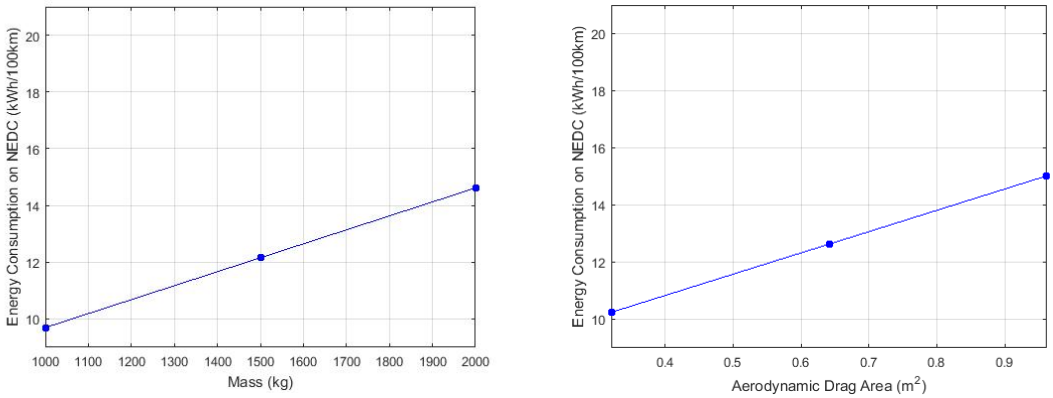

Figure 7-12 Energy consumption (kWh per 100 km) on the selected range of vehicle mass and aerodynamic drag area. Both of these plots are simulated using the NEDC.

Figure 7-13 shows the Chebfun2 capability to operate two variables of a smooth function simultaneously. A surface and contour of energy consumption has been plotted against two selected parameters: vehicle mass and aerodynamic drag

area. Since these parameters are not cross-coupling to each other, then a linear surface and contour can be observed in these figures.

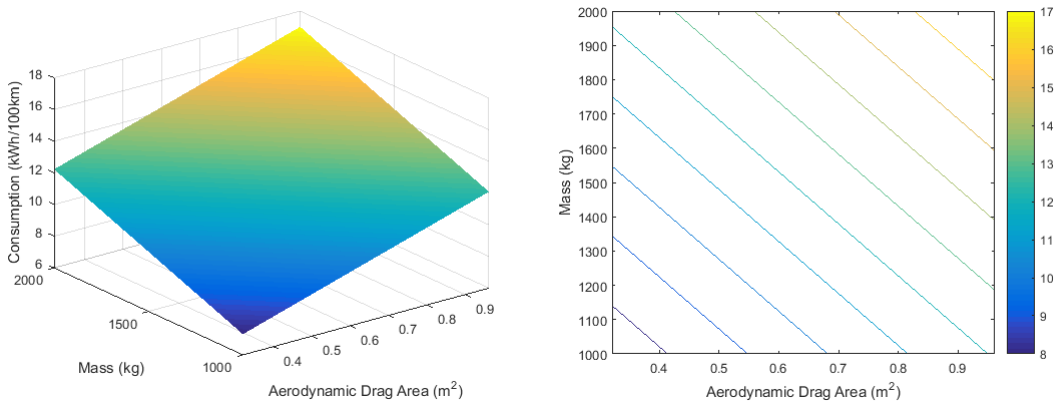

(a) **(b)**

Figure 7-13 Linear surface plot (a) and contour (b) of energy consumption between variables.

- **First-order sensitivity analysis using Chebfun**

Chebfun (one variable) is capable of operating both smooth and piecewise smooth functions [118]. In this case, the energy equation in equation (7-16) is a smooth function and differentiable at every point. Using the Chebfun provided function 'diff( )' for a numerical differentiation. Figure 7-14 shows plots of sensitivity values of vehicle mass and average gear efficiency over a selected operating range. The nominal value of vehicle mass at 1590 kg (2012 model weight plus rotational inertia and loads) and average gearbox efficiency at 97% are presented. Positive sensitivity analysis shows a direct proportionality of energy consumption and vice versa.

- **Second-order sensitivity analysis of cross-coupling variables**

Cross-coupling effect between two BEV variables can be visualised as a smooth surface or contour by using Chebfun2. This section presents a sample using Chebfun to plot the second order sensitivity analysis on the BEV powertrain variables.

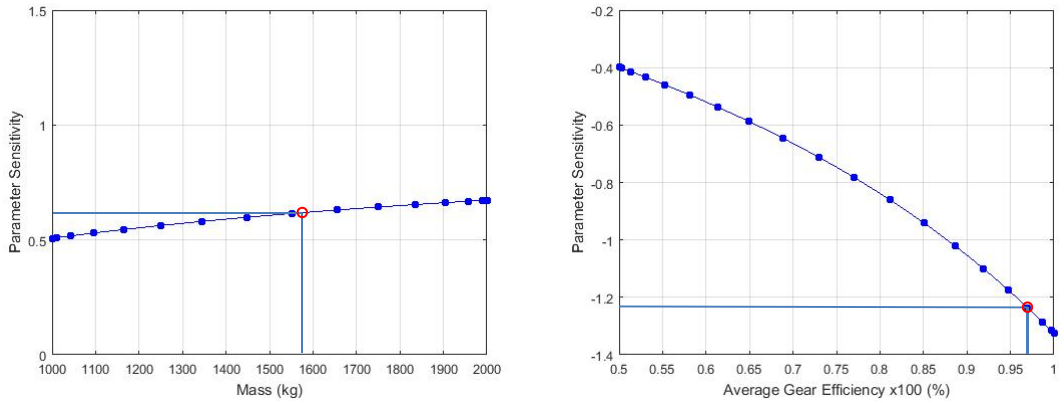

Figure 7-14 First order sensitivity analysis of mass and average gear efficiency on the selected range.

- **Cross coupling between variables**

Figure 7-15 shows the cross-coupling between two parameters of the BEV powertrain. Figure 7-15 (a) shows the coupling between vehicle mass and the aerodynamic drag area. The points in these figures illustrate the nominal variables of the vehicle which are 1590 kg vehicle mass, 0.64 m^2 drag area and 97% (0.97) average gearbox efficiency. Based on the results from the Chapter 5, the cross-coupling effect between aerodynamic and vehicle mass is almost negligible (~0, no coupling) while the cross-coupling effect between average gear efficiency and vehicle mass is indicated as a very strong coupling (value of -8.8 as presented in the Section 5.3.4). These figures present similar results to those presented in the Chapter 5; however, the use of Chebfun helps to present a better visualisation of how the cross-coupling values between two variables change over the variables domain instead of only a snapshot of cross-coupling values at those particular powertrain parameters, as in the Chapter 5.

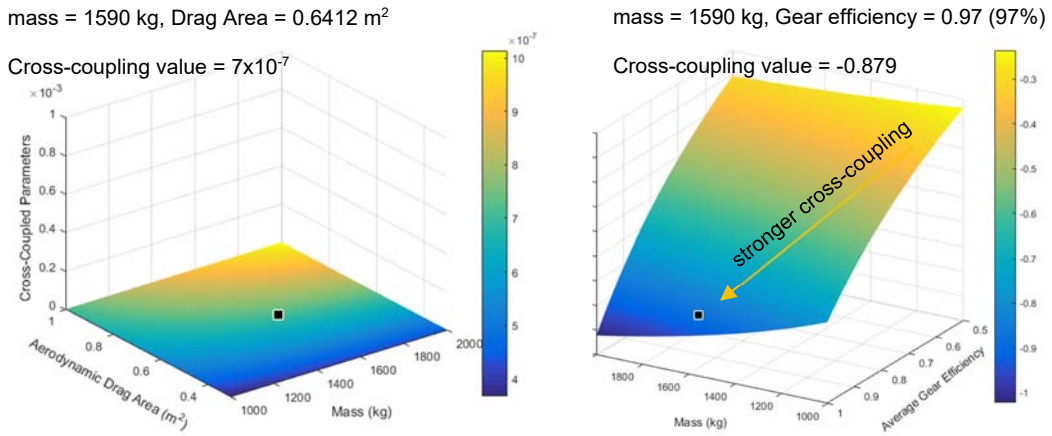

(a) **(b)**

Figure 7-15 Plots of 2nd order cross-coupling effect between BEV powertrain variables.

Results from these figures conclude that there are very small (almost negligible) cross-coupling effects between the aerodynamic drag area and vehicle mass, as presented in Figure 7-15 (a), and the cross-coupling effect between average gear efficiency and vehicle mass is very strong and they will be a stronger coupling when the value of mass and gear efficiency increases, as presented in Figure 7-15 (b).

Figure 7-16 shows the confirmation results of the cross-coupling effect between variables presented in Figure 7-15. The contours in Figure 7-16 visualise the energy consumption increase between powertrain variables. In Figure 7-16 (a) the straight line contour indicates a linear slope between these variables, as they are not cross-coupled to each other, while the curved contour in Figure 7-16 (b) presents a clear result of the non-linear increase of energy consumption due to the strong cross-coupling effect between variables.

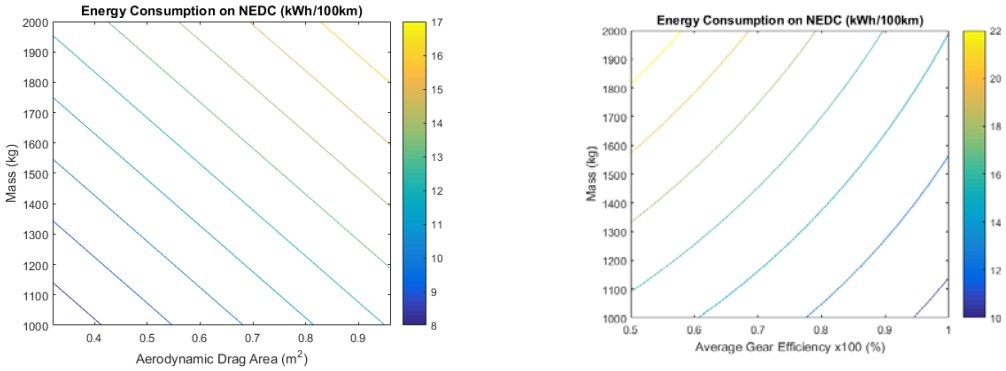

(a) (b)

Figure 7-16 Energy consumption contours between selected BEV powertrain variables.

7.3.2 Multi-disciplinary design procedure for BEV optimisation using Chebfun

In the previous section, the energy balance equation is associated with the following elements: aerodynamic drag force, rolling friction force, inertial force, transmission losses, losses in the motor and losses in the battery. These elements can be considered as fundamental elements of the energy estimation for the BEV powertrain; however, for optimisation purposes, a different set of design parameters, which affect the fundamental elements, is required. This section aims to introduce the BEV model for an optimisation purpose. The cost function and constraints will be indicated, and this section will explain how the multi-disciplinary optimisation process integrated with Chebfun and the BEV model.

- **Model of BEV powertrain optimisation**

This study selects three system-level design variables for this BEV powertrain optimisation: motor size, gear ratio and battery size. The objective function of this model is the energy consumption over a unit distant (in kWh/km). Constraints in this optimisation are range, motor maximum speed and vehicle acceleration.

Energy consumption of a road vehicle starts from a fundamental balance equation of vehicle traction and environmental losses. Vehicle traction force F_t in

$$\text{Force}_{\text{Traction}} = \text{Force}_{\text{Aerodynamic}} + \text{Force}_{\text{Rolling resistance}} + \text{Inertia}$$
$$F_t(v(t)) = 0.5\rho_{air} C_d A_f v(t)|v(t)| + C_{\text{r}} \cdot M_v \cdot g + M_v \cdot \dot{v}(t) \quad \textbf{(7-18)}$$

results from the force needed to overcome aerodynamic resistances, tyre rolling resistance, vehicle climbing a slope and inertia. However, the vehicle is simulated on a flat road; consequently losses from hill climbing are ignored. In equation (7-18), ρ_{air} is air density, C_d is the drag coefficient, A_f is the vehicle frontal area, C_{r} is the rolling resistant coefficient, M_v is the vehicle mass and g is the gravitational acceleration. Vehicle traction force is a function of a vehicle speed profile. The speed profile, also called a driving cycle, is an input to the equation as parameter v (m/s) and its derivative, $\dot{v}$ (m/s^2). These parameters are a function of time along the driving cycle.

Vehicle mass M_v is a parameter that affects overall energy consumption of the vehicle and is composed of mass from gliding body M_B, motor M_m, battery M_b and loads M_L, as described by

$$\text{Mass}_{\text{Vehicle kg}} = M_v = M_B + M_m + M_b + M_L \quad \textbf{(7-19)}$$

Since motor size and battery size are the design parameters, these variables will affect the energy consumption by increasing vehicle mass as their size increases. The relationship between motor, battery size and mass of the BEV powertrain are presented in

$$\text{Mass}_{\text{Motor kg}} = M_m = 0.532\ (\text{Motor size}_{\text{kW}}) + 21.6 \quad \textbf{(7-20)}$$

$$\text{Mass}_{\text{Battery kg}} = M_b = 7.8\ (\text{Battery size}_{\text{kWh}}) \quad \textbf{(7-21)}$$

These powertrain mass equations are based on a long-term scenario of motor mass and battery mass estimation, as in [46]. Changes in gear ratio may affect a small change in powertrain weight but they will be assumed to be a uniform weight over their different ratio which will be included in the weight of a gliding body.

The electric machine is an energy converter which acts as a motor/generator. In motor mode, it provides torque for acceleration and keeps the vehicle moving at a constant cruising speed, while it captures kinetic energy that would otherwise be lost during braking. The motor current I_m is proportional to the motor torque, as presented in

$$I_m(v) = \frac{T_m(v)}{K_m} = \frac{r_w}{K_m \cdot i_g \cdot n_g} F_t(v(t)) \quad \textbf{(7-22)}$$

and is also related to the vehicle traction force described previously. The motor's stator current, the rate of motor current $\dot{I}_m(v, \ddot{v})$ and motor rotational speed $\omega_m(v)$, which are a function of the driving cycle $v(t)$, are described by

$$\dot{I}_m(v, \ddot{v}) = \frac{r_w}{K_m i_g n_g} (\rho_{air} C_d A_f \cdot v(t) + M\ \ddot{v}(t)) \quad \textbf{(7-23)}$$

$$\omega_m(v) = \frac{i_g}{r_w} v(t) \quad \textbf{(7-24)}$$

where $I_m(v)$ is the motor's internal current, $\dot{I}_m(v, \ddot{v})$ is a change of motor current, $T_m(v)$ is motor torque, K_m is motor constant, r_w is wheels' radius, i_g is gear ratio and n_g is gear efficiency. The $\omega_m(v)$ is a rotational speed of the motor.

Energy consumption is calculated by the total energy that drives the electric machine. These electric machine equations are based on the fundamentals of a DC motor. Power consumption of the motor is a product of motor current $I_m(v)$ and motor voltage $V(v, \ddot{v})$. Energy consumption can be calculated from summing of the powertrain during a driving cycle of the motor. Battery losses, which are small in number, have been safely assumed to be negligible as was verified in the Chapter 5. The cost function will be the energy over a unit distance as presented by

$$V(v, \ddot{v}) = L\dot{I}_m(v, \ddot{v}) + R \cdot I_m(v) + K_m \cdot \omega_m(v) \quad \textbf{(7-25)}$$

$$P = I_m(v) \cdot V(v, \ddot{v}) \quad \textbf{(7-26)}$$

$$E_{\text{per cycle}} = \sum_{t_0}^{t_n} P \cdot \Delta t$$

$$E_{\text{per km}} = \frac{E_{\text{per cycle}}}{\sum_{t_0}^{t_n} v(t) \cdot \Delta t} \quad \textbf{(7-27)}$$

where $V(v, \ddot{v})$ is a motor voltage, P is motor power and E is an energy consumption of a vehicle.

- **Constraints for BEV powertrain optimisation**

Constraints help designers force the optimiser to select optimal results within a desired feasible area. For example, the minimum energy consumption of the powertrain is the objective function in this study. However, the designers want a powertrain that provides the greatest energy efficiency but still provides enough driving range, satisfactory acceleration time and is within the limits of the motor's capability. This section describes three constraints which are used in this study.

- **Range constraints**

One of the major issues of concern of a BEV is that the vehicle may have an insufficient range to reach the destination. The range of the BEV can be defined as the distance that the vehicle can travel electrically without having to be recharged. The range estimation in this study is based on two factors, energy consumption per a unit distance and size of the battery, as described in

$$\text{Range}_{\text{Estimation}} = \text{Battery size}_{\text{kWh}} \times 1000 / \text{E}_{\text{per kilometre}} \quad \textbf{(7-28)}$$

Increased battery capacity results in increases in travel range but requires more energy per unit distance. Range constraint is a factor to balance the minimum sufficient amount of battery capacity and keeping as low an energy consumption as possible.

- **Max speed constraints**

Equations (7-22) and (7-25) show that losses in the motor are due to electrical losses (coil resistance) and mechanical friction losses. However, electrical losses are the only ones of concern for this study. Losses in the motor are due to the amount of electric current in the motor coil and proportional to the amount of motor torque. It can be concluded that operating the motor at high speeds to maintain sufficient necessary power results in lower torque being required and a saving of energy, since the power is a product of torque and speed. This is possible if a high ratio gearbox is available. However, the losses due to operating the gearbox at high speeds are assumed to be negligible since the gearbox efficiency is modelled on an average value. The simple rule applied to this simulation as described in the following condition

$$\begin{aligned} \text{motor constraint} = 1 = \quad & \text{feasible if } \omega_{motor} \leq \omega_{m\ max}(v) \\ \text{motor operation} = 0 = & \text{ infeasible if } \omega_{motor} \geq \omega_{m\,max}(v) \end{aligned} \tag{7-29}$$

This constraint prevents the optimiser from selecting too high a gear ratio, since the higher gear ratio results in lower torque and energy saving. This factor is dependent on the maximum vehicle speed which is also dependent on different driving cycles.

- **Acceleration constraint**

This constraint affects the BEV in terms of the marketing aspect, rather than engineering practices and energy efficiency, since higher acceleration reflects how much fun driving the vehicle is and how enjoyable. This restriction keeps the motor size sufficiently large enough for driving to be a pleasure and avoids the optimiser selecting too small a motor. The acceleration time from rest to 100 km/h can be computed by

$$\text{Time}_{\text{Acceleration}} = \text{T}_{100} = \sum_{v=0}^{v=27.78} \frac{M_v}{F_t(v)}\,\Delta v \tag{7-30}$$

where v is vehicle velocity in m/s and T_{100} is in second.

- **BEV powertrain optimisation as multi-disciplinary optimisation technique**

Components of the multi-disciplinary optimisation method, as presented in [123], include a mathematical model, approximation concept, system sensitivity analysis, optimisation procedures with decomposition, and human interface. These components were deduced from various literature surveys in multi-disciplinary optimisation developments. For a particular multi-disciplinary optimisation application, all these components may not be used but most of them may be included. This study requires most of their properties except for the approximation concept. The following section will give some explanations and examples of how these concepts will be integrated in this Chebfun - multi-disciplinary optimisation method for BEV powertrain constraints optimisation.

- **Optimisation procedures with decomposition**

System decomposition and associated optimisation is one key component of the multi-disciplinary optimisation technique [123]. This may somehow make the multi-disciplinary optimisation different to the conventional optimisation technique. A conventional optimisation algorithm usually considers the model to be a black box. The optimiser responds to the cost function and constraints which are the results of the optimiser selecting the model input and calculating the results of the model. The optimiser, such as Genetic Algorithm, will select a new set of variables and then continue searching until an optimum is found [35]. It can be seen from the optimisation toolbox [136] that the optimisation algorithm can be developed separately to the model and can perform correctly, as long as the interface between them is correct.

Multi-disciplinary optimisation tries to break the system synthesis into smaller tasks and it is possible to execute these concurrently. In most cases, it can reduce the computational effort. Multi-disciplinary optimisation divides a large system into many disciplines and lets disciplines communicate (exchange parameters and results). In this study the discipline in the multi-disciplinary optimisation

method is called a subsystem and these subsystems can be coordinated by the system analyser.

In this particular case, the BEV powertrain model is divided into smaller subsystems, as presented in Figure 7-17. Variables and solutions are exchanged between subsystems. The multidisciplinary design analyser is a coordinator for the system. The powertrain system is separated into five subsystems, each of which has its own communication routine. Most subsystems require results from the others; for example, the result of energy consumption $Y_E(X_2, Y_m)$ requires the result of vehicle mass $Y_m(X_1, X_3)$. It can be seen that to calculate energy consumption, the motor and battery variables (X_1, X_3) may not be directly required; however, these variables are required to compute the vehicle mass solution, $Y_m(X_1, X_3)$, beforehand. This is an example of cross-coupling design variables in the powertrain simulation. Moreover, the motor speed constraint subsystem does not require any results from the previous subsystem. Only the gear ratio X_2 affects this maximum motor speed Y_S. Furthermore variable X_2 in the motor speed constraint subsystem has no cross-coupling effect on other design variable

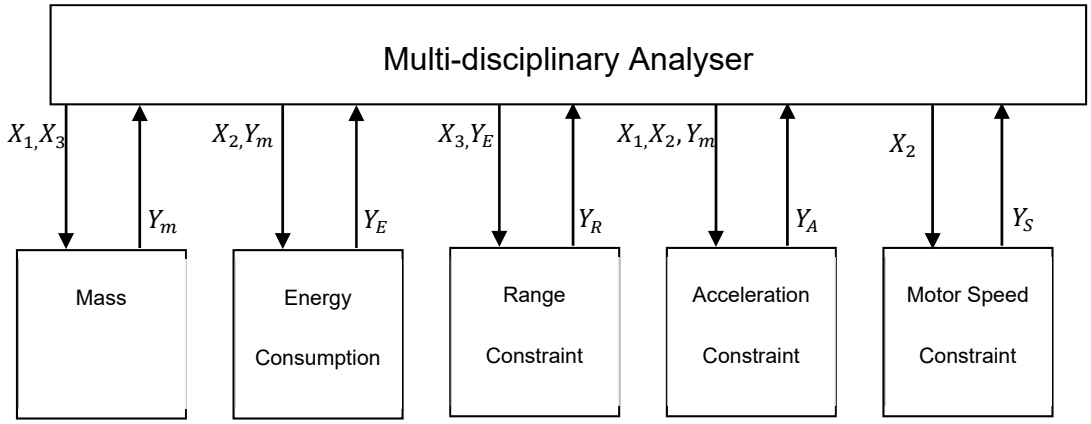

Figure 7-17 Variables and solutions are exchanged between subsystems. The multidisciplinary design analyser is a coordinator of the system.

where X_1, X_2, X_3 in the Figure 7-17 are design variable (motor size [kW], gear ratio [-] and battery size [kWh]) and Y_m, Y_E, Y_R, Y_A, Y_S , in the same figure, are results from each subsystem.

- **Parameter sensitivity in the BEV model**

This section presents the sensitivity values of design variables (motor, gear and battery) for the cost function and constraints. In other words, this sensitivity values present the importance of each variable to the cost function and constraints.

- **First order sensitivity analysis**

Table 7-2 presents the 1st order sensitivity analysis values of each parameter to the cost function and constraints. These sensitivity analysis values were calculated using a similar method to that presented in the previous section, except that these results were calculated from the BEV model used for powertrain optimisation as presented in the previous section.

Table 7-2 First order sensitivity analysis between variables and optimisation function.

	First Order Sensitivity Analysis		
(parameters: motor, gear, battery)	Motor	Gear	Battery
Energy cost function @ (80,8,24)	0.0202	0.0510	**0.0887**
Range constraint @ (80,8,24)	0.0202	0.0510	**0.9113**
Motor speed constraint @ (80,8,24)	0.0	**1.0**	0.0
Acceleration constraint @ (80,8,24)	**0.9**	0.6	0.5

It can be seen that for a particular powertrain size (80 kw motor, 8:1 gear ratio and 24 kWh battery), battery size is the most sensitive parameter in both energy consumption and range, while motor size is very sensitive to acceleration performance. The gear ratio is the only parameter that affects the maximum motor speed. These results provide an insight into the complex equation of how the parameters are effected by the cost function and constraints of the model.

- **Second order sensitivity analysis**

Table 7-3 shows the cross-coupling value between each pair of variables for cost function and constraints. These results were obtained by using 2nd order sensitivity analysis with the BEV model for optimisation. The sensitivity values show how much each pair of variables are cross-coupling with each other. This table demonstrates only a particular design variable, such as at this particular point of the powertrain's selected variables (80,8,24). Chebfun can calculate sensitivity analysis for a range of variables (instead of a single set of variables) as the results presented in the previous section.

Table 7-3 Cross-coupling effect between design parameters.

Energy @ (80,8,24)	Gear	Battery
Motor	**0.0025**	0.0001
Gear	-	0.0111
Range @ (80,8,24)	Gear	Battery
Motor	0.0005	0.0167
Gear	-	**0.0531**
Motor Max Speed @ (80,8,24)	Gear	Battery
Motor	0	0
Gear	-	0
Acceleration @ (80,8,24)	Gear	Battery
Motor	0.0025	0.0001
Gear	-	**0.0111**

Results from 2nd order sensitivity analysis presented in Table 7-3 indicate that motor-gear is the strongest coupling parameter pair at this design variables (80,8,24), then gear-battery is the strongest coupling in range constraint. In the maximum motor speed constraint, there are no coupling effects between variables and gear-battery is the strongest coupling variable pair for the acceleration constraint.

- **Multi-disciplinary feasible for BEV optimisation using Chebfun**

MDF is a single layer multidisciplinary method consisting of system analyser and optimiser. The optimiser is responsible for finding the optimal design parameters by requesting cost and constraints functions from the subsystem (model), while the system analyser has a role to enforce multidisciplinary consistency. In this example, both optimisation and system analyses have been undertaken using Chebfun. Figure 7-18 shows a diagram of the MDF technique in this example. The optimiser, as presented at the top level in this diagram, manages the role of finding the minimum cost function and adjusting the parameters to satisfy the constraints, while the system analyser manages the interaction between the optimiser and models (subsystem). A hierarchical structure can be seen in this system; however, in the multi-disciplinary optimisation system, this MDF method is a non-hierarchical (single layer) system because there is a single optimiser. In addition, this MDF method requires a feasible solution in every iteration, which is different from the IDF method that only requires feasibility at the optimum. In the next section, the optimiser and system analyser will be explained in more detail with examples.

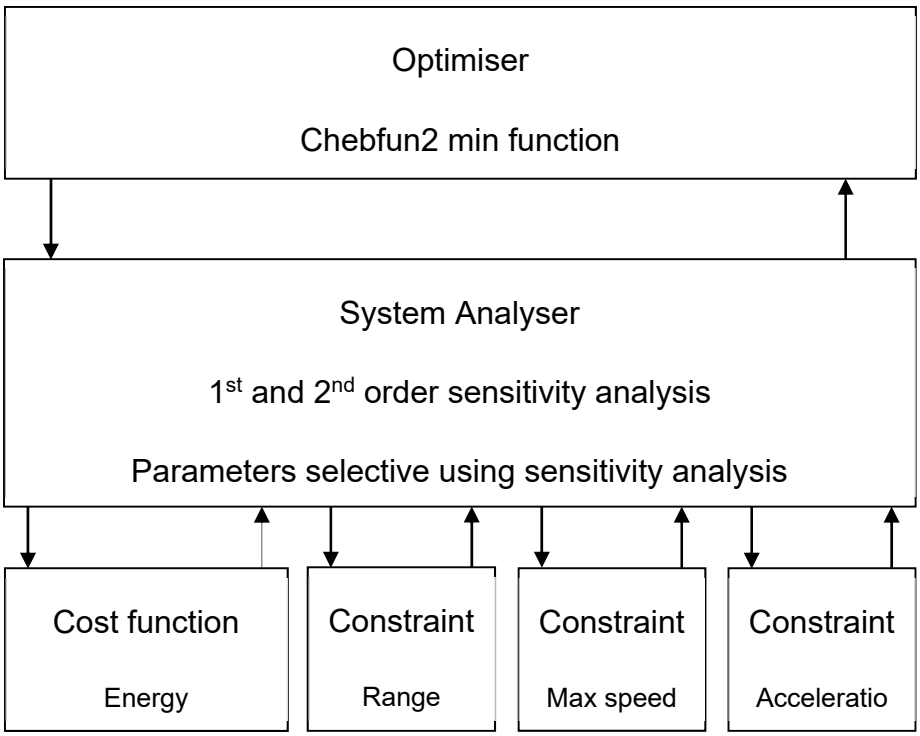

Figure 7-18 Using MDF method with the BEV powertrain optimisation

- **Multi-disciplinary system analyser**

The system analyser has an important role in this multi-disciplinary optimisation system. And this is one of the important features of the multi-disciplinary optimisation system that provides an additional capability beyond ordinary optimisation techniques. Normally, optimisers are directly connected to the model. This routine often starts with initial parameters then the optimisation algorithm will select a design variable that improves the cost function and satisfies the constraints until the termination criteria are met. However, the system analyser can make the ordinary optimiser deal with more complex tasks, such as using Genetic Algorithm with the multi-disciplinary optimisation system, or overcome the optimiser limitation such as using Chebfun optimisation in this study.

- **Selecting optimisation parameters using sensitivity analysis**

The limitation of Chebfun2 is that it can manipulate only two parameters at a time, while the BEV optimisation in this study required three parameters to optimise. This system analyser has a role to select a pair of design variables to optimise.

This procedure can be done by using the sensitivity analysis to rank the sensitivity parameters for the cost function and constraints, then choosing two variables to optimise at a time.

Figure 7-19 presents a flow chart of this optimisation procedure, starting from selecting the initial design variables, after which the constraints are checked to make sure that the solution is within the feasible space. If any of constraints criteria are unsatisfied, the constraint adjustment process will be performed by using the 1st order sensitivity analysis to select the most sensitive parameter to that constraint and using 2nd order sensitivity analysis to rank and find the cross-coupling variable. After that the design variables will be adjusted.

After making sure that all design variables are in the feasible space, the optimisation process will be performed by using the 1st order sensitivity analysis to rank the sensitive parameters, and repeating the steps until the termination criteria are satisfied.

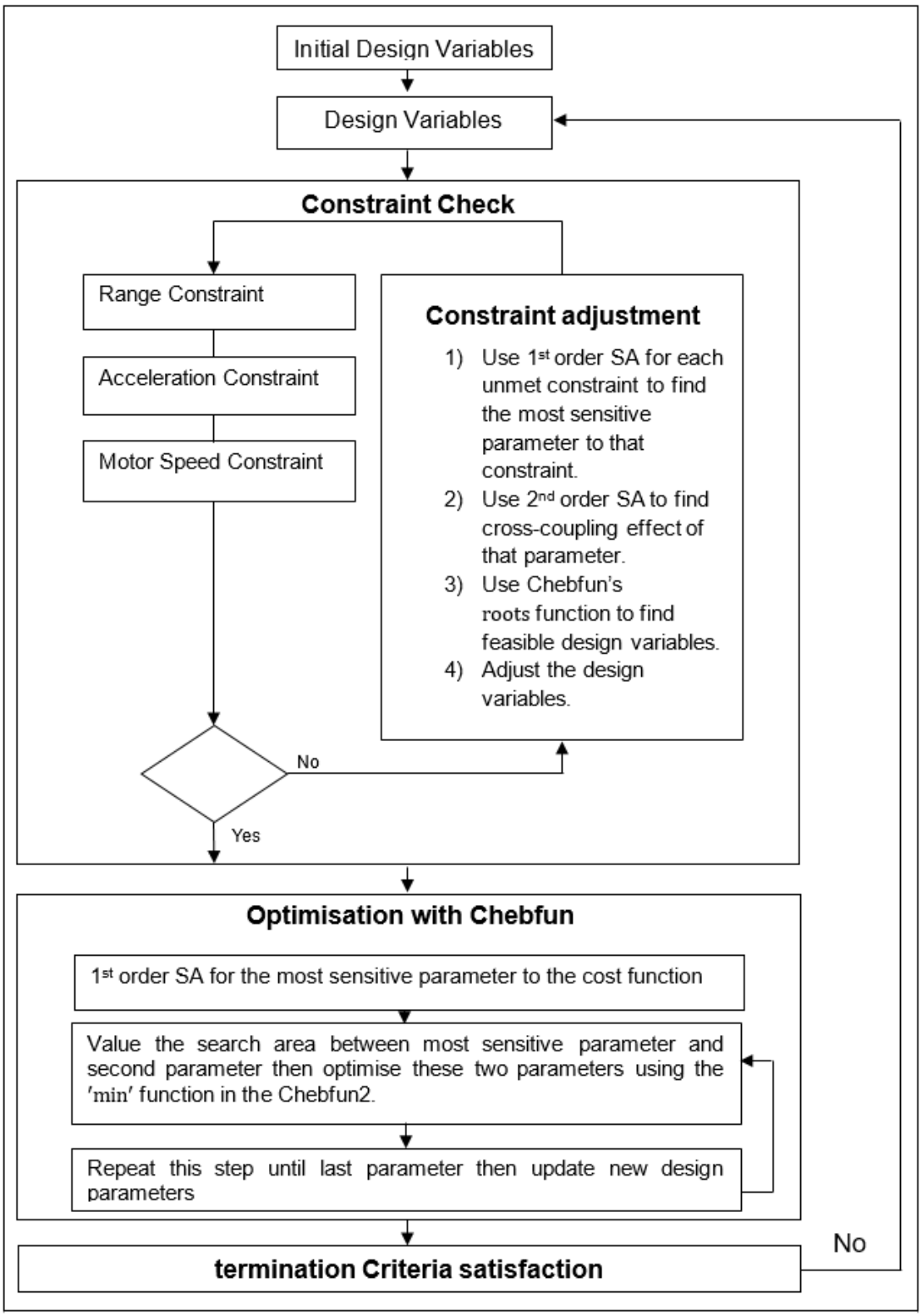

Figure 7-19 The procedure of BEV optimisation using Chebfun and multi-disciplinary optimisation methods.

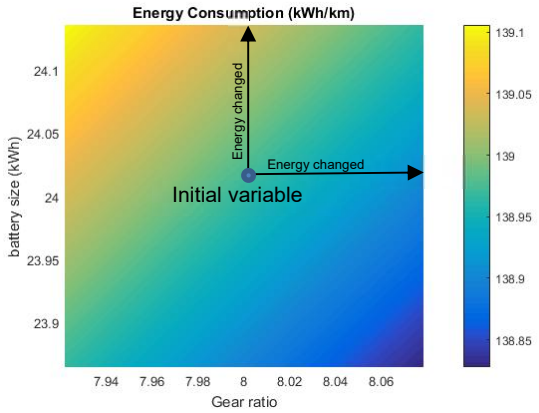

Figure 7-20 Search area of the Chebfun is located by a range of difference cost function (calculated from sensitivity analysis) at each side of the two variables.

- **Optimisation of two parameters at a time using Chebfun**

Chebfun2 is possible to use as a global optimisation tool for a system with two parameters. However, if the number of design parameters is greater than two then the methods of multi-disciplinary optimisation and gradient based optimisation will be implemented. Recalling the Steepest Descent method, a procedure for finding the minimum point is described briefly by [137]:

> Start with $\boldsymbol{x}_k$ as current design variable vector at kth iteration. A downhill direction $\boldsymbol{d}$ and a step size $\alpha > 0$ will be selected. A new point will be $\boldsymbol{x}_k + \alpha\boldsymbol{d}$. And it is expected that the new point will improve cost function $f(\boldsymbol{x}_k + \alpha\boldsymbol{d}) < f(\boldsymbol{x}_k)$. In the gradient optimisation method, it is required that $\boldsymbol{d}$ is a descent search direction as $\nabla f(\boldsymbol{x}_k)^{\mathrm{T}}\boldsymbol{d} < 0$. For a descent direction, it can be seen that $\boldsymbol{d}_k = -\nabla f(\boldsymbol{x}_k)$. After the descent direction is chosen, a step size α will be selected for the next better cost function. It can be seen that when the search direction is fixed as $\boldsymbol{d}$, the objective function depends only on α as $\boldsymbol{x}_k + \alpha\boldsymbol{d}_k \equiv \boldsymbol{x}(\alpha)$ and $f(\boldsymbol{x}_k + \alpha\boldsymbol{d}_k) \equiv f(\alpha)$. The optimisation can be presented by
>
> $$minimize_{\alpha \geq 0} \quad f(\alpha) \equiv f(\boldsymbol{x}_k + \alpha\boldsymbol{d}_k) \qquad \textbf{(7-31)}$$
>
> And the design variable vector will update for a new minimum point as $\boldsymbol{x}_{k+1} = \boldsymbol{x}_k + \alpha_k\boldsymbol{d}_k$.

Chebfun2 provides a $'\min'$ function to find a minimum point over a search area, as presented in Figure 7-21 (a). These procedures are compared with the search direction in the Steepest Descent optimisation method, as presented in Figure 7-21 (b).

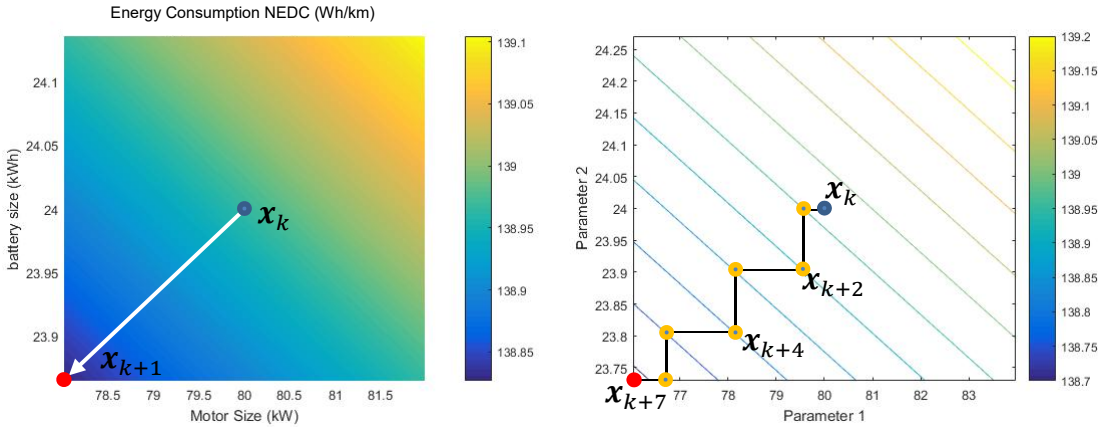

(a) **(b)**

Figure 7-21 Comparison between Chebfun minimisation global search method and the Steepest Descent minimisation method.

Instead of finding the gradient vector ∇f, direction $\boldsymbol{d}$ and step size α as in the Steepest Descent method, Chebfun2 finds a new lowest objective function instantly. This makes Chebfun2 fast and accurate for optimisation with two parameters in a specific search area. The algorithm behind Chebfun2 is a grid search and some optimisation procedures, the details are addressed in [120].

- **Constraint optimisation using Chebfun**

For the MDF method, all optimised parameters have to be selected in the feasible area before continuing to the next iteration. The method of keeping parameters in the feasible region in Chebfun is by using the rootsfinding function in the Chebfun tools. For example, the range calculated at (80,8,24) is 172 km, if the minimum range constraint is greater than 170 km, battery size selection can be varied by either motor size or gear ratio. Figure 7-22 (a) shows that if the range constraint is greater than or equal to 170 km, gear ratio and motor size are 8:1 and 80kW respectively, and battery size selection should be at least, or above, the line and position in the feasible area.

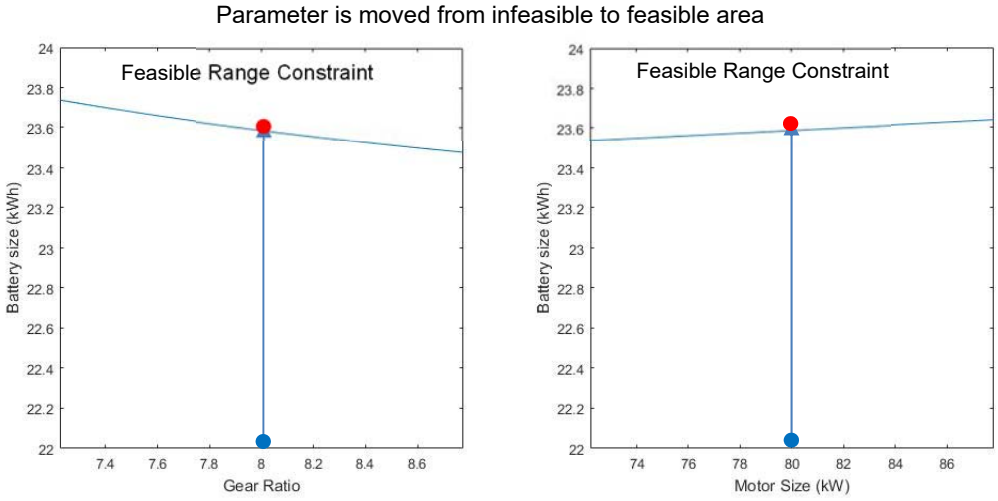

(a) **(b)**

Figure 7-22 Constraints adjustment process using 'rootsfinding' function in Chebfun

System analysers also have a role in selecting parameters for adjusting these constraints. The previous example of constraint adjusting is looking at the parameters close to (80,8,24) and the most sensitive parameter to the range constraint is the battery size, as presented in Table 7-2; this shows that the battery size can be adjusted to a minimum to obtain the maximum effort for range constraint. The cross-coupling effect also helps to select the second pair of parameters to adjust together with battery size. The results from Table 7-3 that show that gear ratio is the most sensitive coupling parameter for the battery and it is clear that adjusting the battery with the gear ratio will satisfy the range constraint.

Figure 7-23 shows a 3-D plot between battery size and motor size against energy consumption. The selected search area will be chosen from the initial variable. Range and acceleration constraints which are functions of motor and battery, are also plotted.

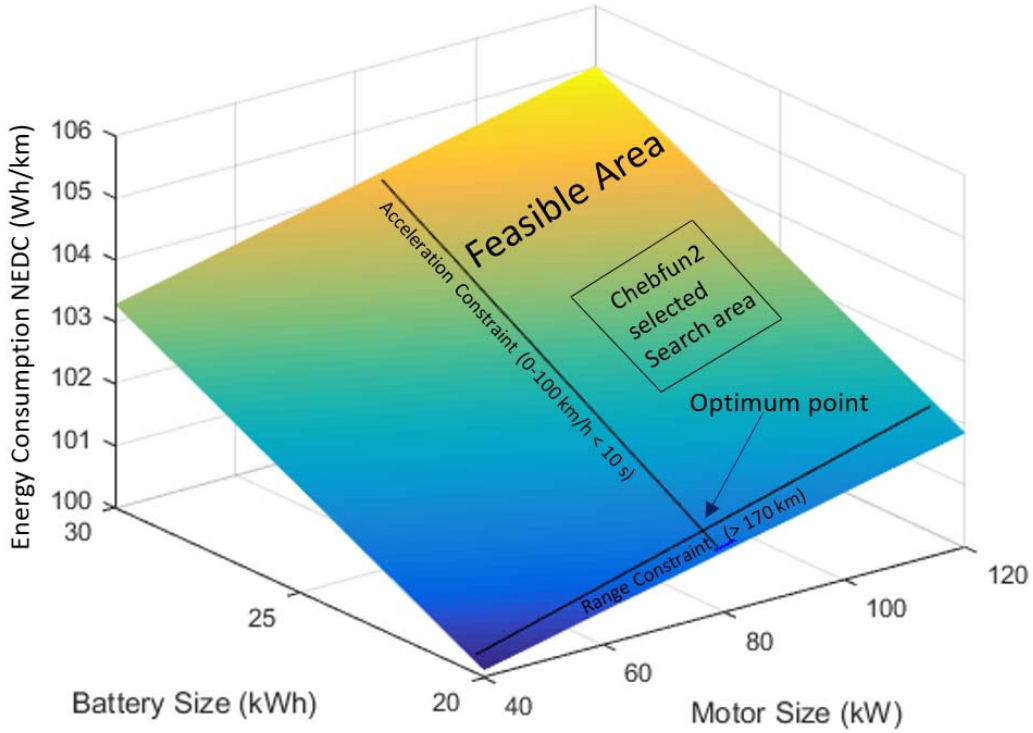

Figure 7-23 A 3-D plot of Chebfun optimisation

It can be seen that BEV powertrain model is a smooth function. This smooth function is compatible to be used with Chebfun2. This shows that over the design parameters domain the minimum battery size and motor size will give the minimum objective function. However, this optimum point is bounded by constraints. The selected search area is created as a square region as presented in Figure 7-20 and Figure 7-23 to search for a global minimum in that area and move along with the new optimum parameter until the optimum point is reached. However, this methodology works based on the gradient based optimisation method which is limited to finding the solution in a convex set only [137]. In this study, the BEV powertrain model is a convex set that is appropriate to this method and the initial point has to be in the feasible area only.

7.4 Case study in powertrain optimisation with Chebfun

In the previous section, the optimisation method using Chebfun and multi-disciplinary optimisation has been introduced. In this section, the optimisation technique will be applied to a BEV case study and compared to the traditional optimisation methods. The Nissan Leaf (2012 model), a well-known production C-segment BEV, is used as the case study and benchmark. This vehicle is a SM-SA BEV and the powertrain layout is presented in Figure 7-24.

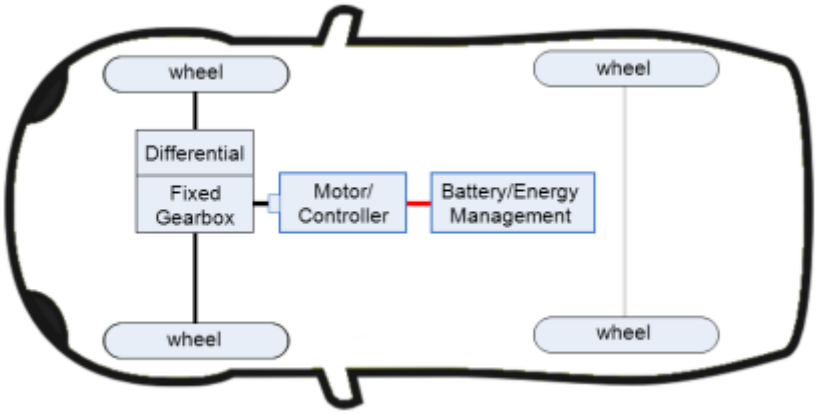

Figure 7-24 The SM-SA BEV powertrain.

The original Nissan Leaf vehicle is driven by a single front wheel drive 80 kW motor with a 7.9:1 fixed ratio transmission and 24 kWh lithium battery. In this study, the selected design parameters are motor size, gear ratio and battery size while all other constant and dependent parameters are based on publically available data [37] and are otherwise based on the author's assumptions. Table 7-4 shows the selected design parameters and their boundary constraints.

Table 7-4 Design variables for BEV optimisation

Parameters	Range of parameters optimisation
Motor Size (kW)	40 – 120
Gear Ratio	1:1 – 11:1
Battery Size (kWh)	20 – 30

Table 7-5 Constant and dependent parameters	
Vehicle Body	
Aerodynamic Area $(A_{\mathrm{f}}C_{\mathrm{d}}), (m^2)$	0.6412
Rolling resistant coefficiency $(C_r), (-)$	0.007
Vehicle mass $(M_v), (kg)$	Dependent on motor and battery size as equation (7-19)
Wheel radius $(r_w), (m)$	0.15
Transmission	
Transmission efficiency $(n_g), (-)$	97%
Electric Machine	
Motor efficiency $(n_m), (-)$	Dependent on motor torque and speed
Motor constant (K_m)	0.4
Motor resistance $(R), (\mathrm{ohm})$	0.02

Objective function and constraints

Minimize: $$E(\boldsymbol{x})$$

$$\boldsymbol{x} \in \{motor\ size, gear\ ratio, battery\ size\}$$

Subject to: $$170 - g_{Range}(\boldsymbol{x}) \leq 0 \quad \textbf{(7-32)}$$

$$g_{Motor\ Speed}(\boldsymbol{x}) - 1000 \leq 0$$

$$g_{Acceleration\ time}(\boldsymbol{x}) - 10 \leq 0$$

$$x_{iL} \leq x_i \leq x_{iU}, i = 1,3$$

where $E(\boldsymbol{x})$ represents the objective function which is the energy consumption of the BEV powertrain (Wh/km) over the NEDC. This objective function is restricted

by inequality constraints g_n which are limited to the vehicle travelling at least 170 km, motor max speed less than 1000 rad/s and acceleration time from 0 to 100 km per hour, for less than 10 sec. The $\boldsymbol{x}$ vector represents the three design variables: motor size, gear ratio and battery size. These variables are modified during the optimisation process to obtain the optimum. The design space is defined by the lower and upper bounds (side constraints), x_{iL} and x_{iU}, of the design variables.

7.5 Chapter discussion

Chebfun provides a set of powerful computational tools that give high digits of accuracy while also providing fast calculation. This system has been developed for more than a decade from a single dimension with restricted to continuous functions and it is currently developed for piecewise smooth 1D and then smooth multi-dimension functions (Chebfun2 and Chebfun3). As the Chebfun developed to a 2D function, some useful tools such as global optimisation and rootsfinding are possible to apply to many branches of science and engineering applications. Chebfun has the ability to find the global minimum of a complicated function [138] in just less than 0.2 sec with 12 correct digits [120]. However, there are some limitations to applying this tool to some engineering applications, such as the EV. Firstly, a BEV powertrain simulation usually requires a study of multi-variable optimisation with more than two variables. This study tries to apply a very simplified BEV powertrain but it still consists of at least three variables to compute. This limitation is possible to be solved by the future Chebfun3 but currently Chebfun2 cannot solve it on its own. Secondly, smooth function restriction is another constraint when using Chebfun2.

Multi-disciplinary optimisation was introduced in this study to unlock this restriction and, as described earlier, multi-disciplinary optimisation is used as a bridge to connect between Chebfun and BEV powertrain constraints optimisation. The composition of multi-disciplinary optimisation was defined broadly as it was applied in a number of different applications. However, the components of the multi-disciplinary optimisation method were concluded by Sobieski in 1997 as

presented in [123]. Some of the multi-disciplinary optimisation components which it is possible to use to overcome the Chebfun restriction, are the optimisation procedures with decomposition. By breaking down the cost function and constraints of this BEV optimisation into different subsystems (disciplines), it is possible to optimise the BEV variables (two variables at a time) by using Chebfun.

Sensitivity analysis which is another multi-disciplinary optimisation component that is broadly used in many multi-disciplinary optimisation applications [123]. The sensitivity analysis in this study was used as a decision making tool to decide which variables are suitable to optimise. The local method sensitivity analysis was calculated in both 1^{st} order and 2^{nd} order by using Chebfun. Sensitivity analysis in this study is located in the multidisciplinary design analyser to coordinate the information flow between the optimiser and the model subsystem.

Mathematical modelling of a system and the approximation concept are other multi-disciplinary optimisation components [123]. Since Chebfun2 was restricted to smooth functions, in this study, a concept of differential flatness was introduced and evaluated for the BEV powertrain application. Research in [121] encouraged the use of a metamodel to increase optimisation efficiency. However, by using the differentially flat system, a detailed model of the BEV powertrain components exists and also performed fast enough for optimisation. For example, the model of the electric machine in this study was created by inverting the simulation of a DC electric motor. The differential flatness model contains information at transient response while other backward simulation techniques used looked-up table and eliminated this system transient behaviour, such as the model presented in the following literatures: [9],[30],[139].

7.5.1 Interesting points of the limitations

With Chebfun2 it is possible to locate the global minimum and maximum of two variables over a selected search area, but for use in this study, at least three variables are required for the powertrain optimisation. By using the process of multi-disciplinary optimisation, global optimisation cannot be guaranteed because only two variables can be optimised at a time. The idea of the Steepest Descent

optimisation method, which is adapted with the Chebfun optimisation, is used and then this optimisation may somehow be limited to the convex set of solution space only.

The historical background of multi-disciplinary optimisation indicated that the first generation of multi-disciplinary optimisation in aerospace was to integrate all systems in a single optimisation loop as presented in the Figure 7-7 (a) [124], and as the problems become more complex, the 2nd and 3rd multi-disciplinary optimisation generation were applied to decompose the systems as in Figure 7-7 (b) and the system decomposition using a multi-optimiser as in Figure 7-7 (c). Compared to road vehicle powertrain optimisations recently, most of them optimise the powertrain in a single loop with different types of optimisation algorithms. Then, the report in [121] predicted the trend of multi-disciplinary optimisation in the automotive industry as using a global optimisation method with single-lever multi-disciplinary optimisation. This may somehow point out that the model for road vehicles will become more complex in the near future and multi-disciplinary optimisation will extend the ability of the optimisation tools to deal with a complex automotive system.

This study does not aim to upgrade mature optimisation algorithms, such as the Genetic Algorithm, to deal with a problem of electric road vehicle design. Instead, the aim of this study is to investigate the potential of Chebfun to deal with an ordinary BEV powertrain constraints optimisation. As a result, it is difficult to compare this Chebfun - multi-disciplinary optimisation with the well-known global optimisation tools such as Genetic Algorithm or NSGA2 in terms of robustness and flexibility. Chebfun - multi-disciplinary optimisation requires a custom-made algorithm to suit each application. The push-button design procedure may not be applicable when applied to this multi-disciplinary optimisation system. This circumstance is already explained as one of the multi-disciplinary optimisation components presented in [123].

This Chebfun - multi-disciplinary optimisation technique presents a modification method of Chebfun2 which is restricted by two variables, and extends its ability

to solve three variables optimisation. It is possible to extend Chebfun2 to work with more than three variables optimisation; however, this algorithm may not be very efficient, since the computational cost of sensitivity analysis may be too high to compare with traditional optimisation algorithms.

Chebfun3 which is aimed at computing functions in a 3D cube $[a,b]\times[c,d]\times[e,g]$ is being developed [26], so the global optimisation function in Chebfun3 is not currently available. In the author's opinion, if the Chebfun3 optimisation function is available, the three variables optimisation as presented in this study will be easily solved. However, the four variables optimisation can be extended by using Chebfun3 and the method presented in this study.

7.6 Chapter conclusion

The work presented in this study constructs a new idea and method for BEV powertrain optimisation. A combination of existing knowledge, the Chebfun and multi-disciplinary optimisation, are combined for solving problems in a new application, the BEV powertrain constraint optimisation. Multi-disciplinary optimisation properties which were used in other applications are introduced, analysed for their cost/merit and adapted in this study. The method of optimisation procedures with system decomposition is a key process to overcome the restrictions of the Chebfun with more than two variables in BEV powertrain optimisation. The system sensitivity analysis for the BEV powertrain in both first and second order, as introduced in the previous chapter, is judiciously applied to make a decision and it is presented as the system analyser for this new optimisation technique. Finally, this method has already been tested and the results verified against the conventional optimisation technique. In conclusion, the author does not claim that the Chebfun - multi-disciplinary optimisation technique is a universal optimisation tool; however, the contribution of this work is to introduce two existing processes, the Chebfun and multi-disciplinary optimisation, break the restriction between them and then introduce this idea to researchers in the author's field which is EV Powertrain Optimisation.

8 Thesis conclusions

This final chapter concludes the thesis by summarising thesis chapters in the Section 8.1, states the thesis keys finding in the Section 8.2, emphasises the contribution in the Section 8.3 and introduces the future works in the Section 8.4.

8.1 Chapter summarise

Two main objectives of this thesis are presented in two groups of chapters. The Chapter 2 to the Chapter 4 response to the first objective to evaluate possible BEV powertrain topologies using existing computational tool. Then, the Chapter 5 to the Chapter 7 are elaborated from the second objective to develop new computation techniques for the BEV powertrain components sizing and optimisation.

8.1.1 Traditional tools for BEV powertrain optimisation

- **Chapter 2**

This chapter gives an introduction to the modelling and simulation the powertrain of a road vehicle for the purpose of powertrain sizing and optimisation. Fundamentals of the powertrain were described by mathematical equations. Then, the computational tool, the quasi-static toolbox, was modified and used in this simulation and focus for modelling powertrain of a battery electric vehicle (BEV). A model of powertrain weight and cost are also included in this study. In summary, this chapter uses the simulation technique from the quasi-static toolbox to construct a powertrain model for a single motor front-wheel drive BEV. Consequently, this model is used for the optimisation purpose in the later chapters.

- **Chapter 3**

The Chapter 3 demonstrates the application of the quasi-static backward simulation technique on the case study BEV. The Nissan Leaf was selected because of its position as an affordable family car which is similar to vehicle segment considered in this study. In the author’s opinion, the vehicle’s properties

suggest that the Nissan Leaf was initially designed and optimised as a BEV rather than modified from an internal combustion engine platform. As it can be seen that the high speed motor as presented in Figure 3-2 and single gear ratio were originally designed for the vehicle. The optimisation results of the BEV powertrain using the Leaf as a case study were presented. In addition, two-speed gearbox was also introduced to investigate the beneficial of multi-ratio gearbox in the BEV. Finally, these results of the single-motor single-axle (SM-SA) BEV were used as a benchmark for developing different powertrain topologies as they were presented in the Chapter 4

- **Chapter 4**

This chapter presents a motivation to examine a system level BEV powertrain in some selected topologies and analyse the trade-off between them. The study assumed some possible vehicle topologies based on the benchmark vehicle used scenario and evaluates their performances. The selected BEV topologies include the SM-SA, which is similar to the benchmark vehicle; DM-DA which extends the first topology by adding a motor at the rear axle to perform a 4WD BEV vehicle; IWM-SA which uses two in-wheel motors at the front wheels; and IWM-DA where all four wheels are equipped with in-wheel motor.

Then, the global optimisation technique which was initially applied to the SM-SA, was extended to include multi-objective optimisation and compare results using Pareto-front plots. Three objectives: energy consumption, acceleration time and powertrain cost were applied. Finally, this chapter evaluated costs and benefits of the three objective functions for four BEV powertrain topologies. This study provides guide line assumptions for researchers and manufacturers to design the BEV powertrains for different applications.

8.1.2 Alternative possible tools for BEV powertrain optimisation

- **Chapter 5**

The method of sensitivity analysis for a powertrain of a road vehicle has already been presented in the literatures [25]. However, this study aimed to extend the

method by elaborating the technique for a BEV powertrain application. More parameters, which are specific to the BEV, were added including motor efficiency, gearbox efficiency and regenerative braking parameters. Compare to the literature, the new results were more application specific.

Moreover, the cross-coupling effect between different parameter sensitivities of a BEV powertrain was first introduced in this study. The second order sensitivity analysis is a key method of this application. The results presented some new outcomes that provide insight into powertrain design.

- **Chapter 6**

In the Chapter 6, the result shows that most of the BEV powertrain can be modelled as a differentially flat system. Even though the differential flatness and inverse of dynamic system are somehow a similar approach and the literature [92] presented the model of powertrain using a stable inverse of dynamic system, however, nothing in the literature has considered modelling of a BEV powertrain for the purpose of component sizing and optimisation as a differentially flat system.

This chapter explains existing modelling techniques of BEV powertrains such as forward-facing simulation, quasi-static backward simulation and inversion of the dynamical model simulation. Then, the BEV powertrain modelled as a differentially flat system was introduced and were evaluated its possibilities and limitations.

The results indicate that the differential flatness can be exploited for modelling this application. However, there are some limitation on battery state of charge (SOC) modelling through flatness, as presented in Section 6.3.3. Despite its limitation, flatness can be exploited for estimating energy consumption for the optimisation purpose.

- **Chapter 7**

This chapter introduces an alternative methodology for a BEV powertrain components sizing and optimisation by applying the multi-disciplinary

optimisation procedures and the Chebfun computational tool. The methodologies in this chapter overcome some limitations of the Chebfun and make it possible to apply for this application. Another key achievement is the formulation of an multi-disciplinary optimisation by decomposing optimisation tasks and optimise them within the Chebfun capability. Finally, the use of Chebfun and multi-disciplinary optimisation is firstly applied to a BEV powertrain optimisation and illustrating the potential of this technique. This methodology gives another computational tool for the application of BEV powertrain modelling and optimisation.

8.2 Findings

- In Chapter 3, a single-objective (for energy consumption) optimisation of the SM-SA vehicle was performed. The optimisation results show that the vehicle parameter set that provides the minimum energy consumption while satisfying all constraints is very close to the benchmark Nissan Leaf (the 2012 model). This result gives confidence in modelling and assumptions on the powertrain parameters. The results also show that the model was likely to be a valid representation of the case study vehicle, and also providing experience and insight for further BEV modelling work.
- The use of a multi-ratio transmission with the SM-SA configuration was considered in Chapters 2 and 3. This study introduces an additional gear ratio with a speed-dependent shift-point and used optimisation to find values for these. The results show that additional gear ratio makes only a very small improvement in energy consumption; although the machines are running in more favourable conditions, this is largely offset by decreased transmission efficiency and increased weight. It also makes the powertrain more complex. This observation was supported by the sensitivity analyses of Chapter 5, which showed that energy consumption is very sensitive to transmission efficiency and additional transmission ratio is less beneficial compared to a better efficiency gearbox. This finding supports the current trends in production BEVs, where most vehicles are equipped with a single-ratio transmission.

- The result from the Chapter 3 shows that the production SM-SA BEV is already near-optimal. This study considered another three BEV topologies: double-motor double-axle (DM-DA), in-wheel motor single-axle (IWM-SA) and in-wheel motor double-axle (IWM-DA). Simulation to represent these were developed and used to optimise the parameters and then compare the topologies to the baseline SM-SA topology.
- The selected topologies were compared in terms of energy efficiency, acceleration performance and powertrain cost. Multi-objective optimisation was performed to compare the design spaces for the selected topologies. The results show that in-wheel drive vehicles with two axles are the winner in energy performance and also acceleration time but due to the numbers of motors, this topology's drawback is higher cost.
- In the final conclusion, the SM-SA, the current production BEV, has a positive aspect in simplified powertrain by using a large electric motor with mechanical transmission. This results in lower powertrain cost and maintenance compared to other topologies. However, due to the limitation of this powertrain's degree of freedom, further improvements should be focussed on the vehicle body such as vehicle weight and improve aerodynamics. This topology is the early generation of production BEVs and this topology will introduce more attentions of using BEV as an everyday vehicle.
- DM-DA BEV is a good candidate as a near future BEV configuration and is already produced by some BEV manufacturers. The results indicate that two motors give an extra degree of freedom to operate motors in an efficient way. Moreover, two traction motors provide a powerful traction force with better vehicle stability on 4WD. The result has shown that the topology added almost 100 kg weight of additional motor but consumed only around 1% extra energy. The only drawback compare to the SM-SA is the additional cost of the extra motor and gearbox. This BEV topology

is suitable for a high performance BEV or off-road EV that need extra power with similar consumption to SM-SA.

- For the in-wheel BEV, one of the most critical issues is the vehicle dynamic performance and torque-speed control between motors; this was not included in this study. However, for the energy consumption aspect the in-wheel motor has several benefits: the transmission efficiency is 100% (because it has no gearbox, etc.) and the powertrain weight is reduced. This matches with the results from the sensitivity analysis, which showed that the results are sensitive to transmission efficiency and powertrain weight. The disadvantage will be the higher cost of the powertrain, so this topology is less-suited to low-cost mass-consumer vehicles, and more suited to the premium performance sector.
- The results show costs and benefits of each BEV powertrain topologies on the selected objective functions which are energy efficiency, vehicle performance and powertrain cost. It is clear to see that each topology has its own positive aspect and cost. The trade–off are discussed and this informs choices for the manufacturer to select possible BEV powertrain topologies for production EVs.
- In chapter 5, the author has performed a sensitivity analysis of the SM-SA configuration using analytical methods, using the case study vehicle as an example. The author considered powertrain parameters, and it was found that the greatest parameter sensitivity was to the transmission efficiency, then motor efficiency. In addition, The author investigated cross-coupling effects by changing two parameters at the same time. A second order sensitivity analysis showed that transmission efficiency-vehicle mass and transmission efficiency-motor efficiency are the most sensitive cross-coupled parameter pairs for the SM-SA BEV.
- Chapter 6 introduced a model of BEV powertrain as a differentially flat system which combine advantages of the forward-facing simulation and quasi-static backward simulation technique. Differential flatness is a

property of the system dynamics and when adapted to the BEV application, powertrain simulation is fast as the quasi-static backward simulation and provide system transient behaviour as the forward-facing simulation. The work by Froberg et al. presented similar idea of this study by adapting a technique of stable inversion of nonlinear systems however, the main difference between their work and this thesis is that the work in the Chapter 6 explicitly considered differential flatness. Moreover, this work also confirms the ideas of using inverse dynamic system for the road vehicle's powertrain.

- Chebfun, a useful freeware numerical computational tool, was applied to recalculate the analytical solution of sensitivity analysis in the Chapter 5. The results show that Chebfun calculates sufficiently accurate solutions as the solution from analytical technique but requiring less setup time. In addition, Chebfun2 visualises clear 3D smooth plots functions of two parameters which were used to present the energy consumption and sensitivity values of parameters in the Chapter7.

- The use of Chebfun2 for the optimisation purpose was demonstrated in Chapter 7. There are two main limitations on the Chebfun2: it requires smooth function and only two parameters can be performed simultaneously. The first requirement is resolved by exploiting differential flatness and the associated continually differentiable functions. Differential flatness provided the smooth function within selected boundaries. Secondly, Chebfun2's limitation to two parameters was overcame by using an multi-disciplinary optimisation technique. The technique was originally designed for solving complex tasks such as the optimisation of aircraft systems. Similar ideas were applied in this thesis by breaking a complex task into many small simplified objects. The technique of sensitivity analysis presented in the Chapter 6 is one of the methodologies of these simplification processes. Finally, the Chapter 7 elaborates an alternative optimisation method for designing the BEV powertrain.

8.3 Overall objectives

Finally, this thesis delivers solutions of the objectives mentioned in the Section 1.3 as:

- to develop a methodology to evaluate different powertrain topologies of the BEV and
- to construct and evaluate alternative modelling and optimisation methodologies for BEV powertrain design

through these chapters of the thesis. Lastly, author would like to re-mention the thesis novelty as:

Main thesis contributions

- The thesis evaluated the costs and benefits of different powertrain topologies of the BEVs.
- The thesis developed the 2nd order sensitivity analysis technique to investigate the cross-coupling parameters in the BEV powertrain.
- The thesis determined that the differential flatness property is useful for modelling a BEV powertrain for the purpose of components sizing and optimisation, and indicate its merits and limitations.
- The thesis developed an alternative methodology of BEV powertrain sizing and optimisation using the Chebfun computational tool and the multi-disciplinary optimisation methods.

8.4 Further Works

This section presents the purpose of future works which are extending the study from this thesis and cover some limitations presented earlier. The further works can be described in two stages, near-term studies which can be extended promptly from this thesis and a long-term one which is likely to be another research project.

8.4.1 Near-term study

- **Hybrid optimisation technique using Chebfun**

A global optimisation for more than two variables cannot be performed in Chebfun2; however, using the multi-disciplinary optimisation technique as presented in this study is to extend the ability of Chebfun2 for optimisation of more than bivariable problems. BEV powertrain optimisation for three variables is possible using this technique but it cannot guarantee a global solution. The expected release of Chebfun3 provides the possibility of dealing with three parameters simultaneously but the optimisation tool for Chebfun3 has not yet been released at the time of writing this thesis. The work is not aimed at developing the Chebfun computational tool but at applying the Chebfun for this BEV simulation. It is likely to be possible to apply the future Chebfun3 optimisation tool to globally optimise these three variable BEV powertrains; however, as with Chebfun2, there might be some solutions to the problems.

To achieve the global optimisation using Chebfun2 and the multi-disciplinary optimisation for BEV powertrain optimisation, the technique of hybrid optimisation may be introduced. Combining some global optimisation techniques, such as evolutionary algorithms and the Chebfun. Evolutionary algorithms can be used for locating possible areas of global optimum and the Chebfun local search can be performed to detect a local optimum inside a selected area. From this idea, the powerful global searching of evolutionary algorithms will be combined with the speed of the local Chebfun optimisation technique. In addition, a key strength of the multi-disciplinary optimisation technique is to give greater insight of the powertrain, so the evolutionary optimisation technique will be more powerful if it is integrated and adapted with the multi-disciplinary optimisation.

- **Multi-objective optimisation using Chebfun-MDO-IDF technique**

The Chebfun- multi-disciplinary optimisation technique presented in Chapter 7 used the MDF technique (these multi-disciplinary optimisation techniques were explained in Section 7.2.2). However, there are numbers of multi-disciplinary optimisation techniques available for a specific application. The IDF technique,

which is a single level multi-disciplinary optimisation, has its benefits and limitations. The IDF does not depend on the feasibility of the objective function but it will continue to search for optimal feasibility in each discipline, then combine optimal solutions in each discipline to gain an optimum solution of the system.
For this short-term future work, it will be possible to modify the algorithm in Figure 7-19 to be capable of being used with the IDF method. Then it is likely that this IDF may improve the efficiency of the single-objective optimisation and extend the multi-objective optimisation in this BEV powertrain application.

8.4.2 Long-term study

- **Optimisation of multi-dimensional dynamics for BEV topologies**

One of the scopes of this study was to consider the powertrain for the longitudinal dynamics only. As a result, performances of BEV powertrain topologies presented in Chapter 4 are representing only the energy consumption aspect. This has led to a limitation that some topologies are providing excellent energy consumption but may give a poor result for the vehicle dynamics. For example, the in-wheel motor gives a good energy consumption because of its weight reduction and gearbox elimination, and all energy can be transferred by wire instead of mechanical devices. However, a drawback of this in-wheel motor which is not considered in this study is its un-sprung mass. This un-sprung mass may cause vehicle instability, especially when the vehicle is used at high speeds.

Long-term future work could optimise the BEV powertrain topologies together with the effects of a two-dimensional vehicle dynamics. These results will indicate a more realistic solution for designing BEVs. The multi-objective cost functions will include the effect of energy consumption, the 2-D vehicle dynamic behaviour and the powertrain cost. This work can initially be started with the global evolutionary algorithms, quasi-static backward simulation and/or forward-facing simulation as presented in Chapter 4 of this thesis. Then the technique of multi-disciplinary optimisation, Chebfun and sensitivity analysis as presented in Chapters 5 to 7 can be performed to evaluate insight of the powertrain and to understand their constraints and behaviours clearly.

REFERENCES

1. *Electric Vehicle*. 2010; Available from: http://www.parliament.uk/, Accessed 8 October 2016.

2. Chellaswamy, C. and R. Ramesh, *Future renewable energy option for recharging full electric vehicles.* Renewable and Sustainable Energy Reviews, 2017. **76**: p. 824-838.

3. Manzetti, S. and F. Mariasiu, *Electric vehicle battery technologies: From present state to future systems.* Renewable and Sustainable Energy Reviews, 2015. **51**: p. 1004-1012.

4. *Tax benefits for ultra low emission vehicles*. 2016; Available from: https://www.gov.uk/, Accessed 8 October 2016.

5. *Free electric vehicle parking space for thousands in Milton Keynes*. 2016; Available from: https://www.gov.uk/, Accessed 8 October 2016.

6. *Electric Vehicle Homecharge Scheme, Guidance for customers*. 2016; Available from: https://www.gov.uk/, Accessed 8 October 2016.

7. Chan, C.C., *The Rise and Fall of Electric Vehicles in* Proceedings of the IEEE, 2013. **101**(1): p. 206-212.

8. Chan, C.C., A. Bouscayrol, and K. Chen, *Electric, Hybrid, and Fuel-Cell Vehicles: Architectures and Modeling.* IEEE Transactions on Vehicular Technology, 2010. **59**(2): p. 589-598.

9. Pourabdollah, M., N. Murgovski, A. Grauers, and B. Egardt, *Optimal Sizing of a Parallel PHEV Powertrain.* IEEE Transactions on Vehicular Technology, 2013. **62**(6): p. 2469-2480.

10. Itani, K., A. De Bernardinis, Z. Khatir, and A. Jammal, *Comparative analysis of two hybrid energy storage systems used in a two front wheel driven electric vehicle during extreme start-up and regenerative braking operations.* Energy Conversion and Management, 2017. **144**: p. 69-87.

11. Leitman, S. and B. Brant, *Build Your Own Electric Vehicle*. 2009: McGraw-Hill, Inc. 327.

12. *The Nissan Leaf, 100% electric family car*. 2016; Available from: https://www.nissan.co.uk/, Accessed 31 October 2016.

13. *The Mitsubishi i-MiEV, the modern world of electric car*. 2016; Available from: http://www.mitsubishi-cars.co.uk/, Accessed 31 October 2016.

14. *The Tesla Motors*. 2016; Available from: https://www.tesla.com/en_GB/, Accessed 31 October 2016.

15. *BMW i, Born Electric*. 2016; Available from: http://www.bmw.co.uk/, Accessed 31 October 2016.

16. *The Smart Fortwo Electric Drive.2016;* Available from: http://int.smart.com/ Accessed 31 October 2016.

17. *The BYD e6*. 2016; Available from: http://bydeurope.com/, Accessed 31 October 2016.

18. Lorf, C.F., *Optimum Battery Capacity for Electric Vehicles with Particular Focus on Battery Degradation*, in *Department of Mechanical Engineering*. 2014, Imperial College London: London.

19. *The Lightning GT*. 2016; Available from: http://www.lightningcarcompany.co.uk/, Accessed 31 October 2016.

20. *The Lightning GT.* 2016; Available from: https://en.wikipedia.org/wiki/Lightning_GT, Accessed 31 October 2016.

21. Chen, G.H. and K.J. Tseng. *Design of a permanent-magnet direct-driven wheel motor drive for electric vehicle*. in *Power Electronics Specialists Conference, 1996. PESC '96 Record., 27th Annual IEEE*. 1996.

22. Qian, H., G. Xu, J. Yan, T.L. Lam, Y. Xu, and K. Xu. *Energy management for four-wheel independent driving vehicle*. in *Intelligent Robots and Systems (IROS), 2010 IEEE/RSJ International Conference on*. 2010.

23. Caricchi, F., F. Crescimbini, A.D. Napoli, and M. Marcheggiani. *Prototype of electric vehicle drive with twin water-cooled wheel direct drive motors*. in *Power Electronics Specialists Conference, 1996. PESC '96 Record., 27th Annual IEEE*. 1996.

24. Chan, C.C., *Advances in Electric Vehicle.* HKIE Transactions, 2003. **10**(4): p. 1-13.

25. Guzzella, L. and A. Sciarretta, *Vehicle Propulsion Systems, Introduction to Modeling and Optimization*. 2005: Springer-Verlag Berlin Heidelberg.

26. *Chebfun - numerical computing with function*. 2016; Available from: http://www.chebfun.org/, Accessed 15 August 2016.

27. Gao, D.W., C. Mi, and A. Emadi, *Modeling and Simulation of Electric and Hybrid Vehicles.* Proceedings of the IEEE, 2007. **95**(4): p. 729-745.

28. Alegre, S., J.V. Míguez, and J. Carpio, *Modelling of electric and parallel-hybrid electric vehicle using Matlab/Simulink environment and planning of charging stations through a geographic information system and genetic algorithms.* Renewable and Sustainable Energy Reviews, 2017. **74**: p. 1020-1027.

29. Wipke, K.B., M.R. Cuddy, and S.D. Burch, *ADVISOR 2.1: a user-friendly advanced powertrain simulation using a combined backward/forward approach.* IEEE Transactions on Vehicular Technology, 1999. **48**(6): p. 1751-1761.

30. Guzzella, L. and A. Amstutz, *CAE tools for quasi-static modeling and optimization of hybrid powertrains.* IEEE Transactions on Vehicular Technology, 1999. **48**(6): p. 1762-1769.

31. Galvin, R., *Energy consumption effects of speed and acceleration in electric vehicles: Laboratory case studies and implications for drivers and policymakers.* Transportation Research Part D: Transport and Environment, 2017. **53**: p. 234-248.

32. *Emission Test Cycle for European*. 2013; Available from: https://www.dieselnet.com/standards/cycles/ece_eudc.php, Accessed 6 October 2016.

33. *Concerning the Adoption of Uniform Technical Prescriptions for Wheeled Vehicles, Equipent and Parts which can be Fitted and/or be Used on Wheeled Vehicle and the Conditions for Reciprocal Recognition of Approvals Granted on the Basic of these Prescriptions;*, United Nations: Herndon, VA, USA, 2005.

34. André, M., *The ARTEMIS European driving cycles for measuring car pollutant emissions.* Science of The Total Environment, 2004. **334–335**: p. 73-84.

35. *Common Artemis Driving Cycle*; Available from: https://www.dieselnet.com/standards/cycles/artemis.php, Accessed 6 October 2016.

36. Mohan, G., F. Assadian, and S. Longo. *Comparative analysis of forward-facing models vs backwardfacing models in powertrain component sizing*. in *Hybrid and Electric Vehicles Conference 2013 (HEVC 2013), IET*. 2013.

37. *Lightweight, compact and high-efficiency powertrain for EVs, The Nissan Leaf*; Available from: http://www.nissan-global.com/, Accessed 8 October 2016.

38. Ehsani, M., Y. Gao, and A. Emadi, *Modern Electric, Hybrid Electric, and Fuel Cell Vehicles: Fundamentals, Theory, and Design*. 2nd ed. 2009: CRC Press

39. Sorniotti, A., M. Boscolo, A. Turner, and C. Cavallino. *Optimization of a multi-speed electric axle as a function of the electric motor properties*. in *2010 IEEE Vehicle Power and Propulsion Conference*. 2010.

40. Xi, J.-q., G.-m. Xiong, and Y. Zhang. *Application of automatic manual transmission technology in pure electric bus*. in *2008 IEEE Vehicle Power and Propulsion Conference*. 2008.

41. Roozegar, M. and J. Angeles, *The optimal gear-shifting for a multi-speed transmission system for electric vehicles.* Mechanism and Machine Theory, 2017. **116**: p. 1-13.

42. Ehsani, M., K.M. Rahman, and H.A. Toliyat, *Propulsion system design of electric and hybrid vehicles.* IEEE Transactions on Industrial Electronics, 1997. **44**(1): p. 19-27.

43. Larminie, J. and J. Lowry, *Electric Vehicle Technology Explained*. 2003: John Wiley & Sons, Ltd

44. Hayes, J.G., R.P.R.d. Oliveira, S. Vaughan, and M.G. Egan. *Simplified electric vehicle power train models and range estimation*. in *2011 IEEE Vehicle Power and Propulsion Conference*. 2011.

45. *Battery cell, module, and pack for EV application*. 2014; Available from: http://www.eco-aesc-lb.com, Accessed 18 June 2014.

46. Simpson, A., *Cost-Benefit Analysis of Plug-In Hybrid Electric Vehicle Technology*, in *22th International Battery, Hybrid and Fuel Cell Electric Vehicle Symposium and Exhibition*. 2006: Yokohama, Japan.

47. *Electric vehicle and hybrid electric vehicle safety.* 2012; Available from: http://www.nhtsa.gov/, Accessed 27 August 2014.

48. Gao, Y., L. Chen, and M. Ehsani, *Investigation of the Effectiveness of Regenerative Braking for EV and HEV*. 1999, SAE International.

49. Lv, C., J. Zhang, Y. Li, and Y. Yuan, *Novel control algorithm of braking energy regeneration system for an electric vehicle during safety–critical driving maneuvers.* Energy Conversion and Management, 2015. **106**: p. 520-529.

50. Jang, S., H. Yeo, C. Kim, and H. Kim, *A study on regenerative braking for a parallel hybrid electric vehicle.* KSME International Journal, 2001. **15**(11): p. 1490-1498.

51. Wang, F., H. Zhong, X.-j. Mao, L. Yang, and B. Zhuo. *Regenerative braking algorithm for a parallel hybrid electric vehicle with continuously variable transmission*. in *Vehicular Electronics and Safety, 2007. ICVES. IEEE International Conference on*. 2007.

52. Yeo, H., D. Kim, S. Hwang, and H. Kim, *Regenerative Braking Algorithm for a HEV with CVT Ratio Control During Deceleration*, in *International Continuously Variable and Hybrid Transmission Congress*. 2004.

53. Qin, D., M. Ye, and Z. Liu, *Regenerative braking control strategy in mild hybrid electric vehicles equipped with automatic manual transmission.* Frontiers of Mechanical Engineering in China, 2007. **2**(3): p. 364-369.

54. McCulloch, M., H. Spowers, N.D. Vaughan, and J. Marco, *Modelling the acceleration and braking characteristics of a fuel-cell electric sports vehicle equipped with an ultracapacitor.* Part D: Journal of Automobile Engineering, 2007. **221**(1): p. 67-81.

55. *Nissan delivers first Leaf in San Francisco*. 2010; Available from: http://www.independent.co.uk/, Accessed 27 August 2016.

56. Lukic, S.M. and A. Emado. *Modeling of electric machines for automotive applications using efficiency maps*. in *Electrical Insulation Conference and Electrical Manufacturing & Coil Winding Technology Conference, 2003. Proceedings*. 2003.

57. Sato, Y., S. Ishikawa, T. Okubo, M. Abe, and K. Tamai, Development of High Response Motor and Inverter System for the Nissan LEAF Electric Vehicle. 2011, SAE International.

58. Jain, M. and S.S. Williamson. *Suitability analysis of in-wheel motor direct drives for electric and hybrid electric vehicles*. in *Electrical Power & Energy Conference (EPEC), 2009 IEEE*. 2009.

59. Wang, R., Y. Chen, D. Feng, X. Huang, and J. Wang, *Development and performance characterization of an electric ground vehicle with independently actuated in-wheel motors.* Journal of Power Sources, 2011. **196**(8): p. 3962-3971.

60. Qian, H., T.L. Lam, W. Li, C. Xia, and Y. Xu. *System and design of an Omni-directional vehicle*. in *Robotics and Biomimetics, 2008. ROBIO 2008. IEEE International Conference on*. 2009.

61. Rahman, K.M., N.R. Patel, T.G. Ward, J.M. Nagashima, F. Caricchi, and F. Crescimbini, *Application of Direct-Drive Wheel Motor for Fuel Cell Electric and Hybrid Electric Vehicle Propulsion System.* IEEE Transactions on Industry Applications, 2006. **42**(5): p. 1185-1192.

62. Tao, G., Z. Ma, L. Zhou, and L. Li. *A novel driving and control system for direct-wheel-driven electric vehicle*. in *Electromagnetic Launch Technology, 2004. 2004 12th Symposium on*. 2004.

63. Yang, Y.P. and T.H. Hu. *A New Energy Management System of Directly-Driven Electric Vehicle with Electronic Gearshift and Regenerative Braking*. in *2007 American Control Conference*. 2007.

64. Schalkwyk, D.J.V. and M.J. Kamper. *Effect of Hub Motor Mass on Stability and Comfort of Electric Vehicles*. in *2006 IEEE Vehicle Power and Propulsion Conference*. 2006.

65. Tie, S.F. and C.W. Tan, *A review of energy sources and energy management system in electric vehicles.* Renewable and Sustainable Energy Reviews, 2013. **20**: p. 82-102.

66. Dejun, Y. and H. Yoichi. *A novel traction control of EV based on maximum effective torque estimation*. in *2008 IEEE Vehicle Power and Propulsion Conference*. 2008.

67. Hori, Y., *Future vehicle driven by electricity and Control-research on four-wheel-motored "UOT electric march II".* IEEE Transactions on Industrial Electronics, 2004. **51**(5): p. 954-962.

68. Sakai, S., H. Sado, and Y. Hori, *Motion control in an electric vehicle with four independently driven in-wheel motors.* IEEE/ASME Transactions on Mechatronics, 1999. **4**(1): p. 9-16.

69. Wang, J., Q. Wang, L. Jin, and C. Song, *Independent wheel torque control of 4WD electric vehicle for differential drive assisted steering.* Mechatronics, 2011. **21**(1): p. 63-76.

70. De Novellis, L., A. Sorniotti, and P. Gruber, *Driving modes for designing the cornering response of fully electric vehicles with multiple motors.* Mechanical Systems and Signal Processing, 2015. **64–65**: p. 1-15.

71. Weissinger, C., D. Buecherl, and H.G. Herzog. *Conceptual design of a pure electric vehicle*. in *2010 IEEE Vehicle Power and Propulsion Conference*. 2010.

72. *Global Optimization Toolbox*. 2016; Available from: https://uk.mathworks.com/, Accessed 08 November 2016.

73. Bashash, S., S.J. Moura, J.C. Forman, and H.K. Fathy, *Plug-in hybrid electric vehicle charge pattern optimization for energy cost and battery longevity.* Journal of Power Sources, 2011. **196**(1): p. 541-549.

74. Auger, D., M. Groff, G. Mohan, S. Longo, and F. Assadian, *Impact of Battery Ageing on an Electric Vehicle Powertrain Optimisation.* Journal of Sustainable Development of Energy, Water and Environment Systems, 2014. **2**(4).

75. Ribau, J.P., J.M.C. Sousa, and C. Silva, *Multi-Objective Optimization of Fuel Cell Hybrid Vehicle Powertrain Design - Cost and Energy*. 2013, SAE International.

76. Ribau, J., R. Viegas, A. Angelino, A. Moutinho, and C. Silva, *A new offline optimization approach for designing a fuel cell hybrid bus.* Transportation Research Part C: Emerging Technologies, 2014. **42**: p. 14-27.

77. Leis, J.R. and M.A. Kramer, *Sensitivity analysis of systems of differential and algebraic equations.* Computers & Chemical Engineering, 1985. **9**(1): p. 93-96.

78. Saltelli, A., S. Tarantola, F. Campolongo, and M. Ratto, *Sensitivity Analysis in Practice: A Guide to Assessing Scientific Models*. 2004: John Wiley & Sons Ltd,.

79. Brevault, L.ı., M. Balesdent, N. B´erend, and R.L. Riche. *Comparison of different global sensitivity analysis methods for aerospace vehicle optimal design*. in *10th World Congress on Structural and Multidisciplinary Optimization*. 2013. Orlando Florida, USA.

80. Tomlin, A.S., *The role of sensitivity and uncertainty analysis in combustion modelling.* Proceedings of the Combustion Institute, 2013. **34**(1): p. 159-176.

81. Huang, X. and J. Wang, *Lightweight Vehicle Control-Oriented Modeling and Payload Parameter Sensitivity Analysis.* IEEE Transactions on Vehicular Technology, 2011. **60**(5): p. 1999-2011.

82. Kim, C.J., Y.J. Kang, B.H. Lee, and H.J. Ahn, *Sensitivity analysis for reducing critical responses at the axle shaft of a lightweight vehicle.* International Journal of Automotive Technology, 2012. **13**(3): p. 451-458.

83. Avalle, M., G. Belingardi, and A. Ibba, *Stochaatic Crash Analysis of Vehicle Model for Sensitivity Analysis and Optimization* in *20th International Technical Conference on the Enhanced Safety of Vehicles (ESV)*. 2007: Lyon , France.

84. Pagerit, S., P. Sharer, and A. Rousseau, *Fuel Economy Sensitivity to Vehicle Mass for Advanced Vehicle Powertrains*. 2006, SAE International.

85. Othaganont, P., F. Assadian, and D. Auger, *Cycle-based optimisation of multi-speed transmission for battery electric vehicles*, in *Future Powertrain Conference*. 2014: National Motorcycle Museum, Solihull, UK.

86. Stubbs, B. and P.M. Fracchia. *eDCT: 4 speed seamless-shift technology for electric vehicles*. in *Hybrid and Electric Vehicles Conference 2013 (HEVC 2013), IET*. 2013.

87. Bosgra, O., *Physical Modelling for Systems and Control*. 2006-2007, Eindhoven University of Technology.

88. Hofman, T., D.V. Leeuwen, and M. Steinbuch, *Analysis of modelling and simulation methodologies for vehicular propulsion systems.* International Journal of Powertrains, 2011. **1**(2): p. 117-136.

89. Ogata, K., *System Dynamics*. 4th ed. 2003: Pearson, pp. 85-104.

90. Nise, N.S., *Control System Engineering*. 5th ed. 2008: John Wiley & Sons.

91. Astrom, K.J. and R.M. Murray, *Feedback Systems: An Introduction for Scientists and Engineers*. 2012.

92. Froberg, A. and L. Nielsen, *Efficient Drive Cycle Simulation.* IEEE Transactions on Vehicular Technology, 2008. **57**(3): p. 1442-1453.

93. Petit, N. and A. Sciarretta, *Optimal drive of electric vehicles using an inversion-based trajectory generation approach.* IFAC Proceedings Volumes, 2011. **44**(1): p. 14519-14526.

94. Murray, R.M., M. Rathinam, and W. Sluis. *Differential Flatness of Mechanical Control Systems: A Catalog of Prototype Systems*. in *Proceedings of the 1995 ASME International Congress and Exposition*. 1995.

95. Fliess, M., J. Lévine, and P. Rouchon, *Flatness and defect of nonlinear systems: Introductory theory and examples.* International Journal of Control, 1995. **61**: p. 1327-1361.

96. Cowling, I.D., O.A. Yakimenko, J.F. Whidborne, and A.K. Cooke, *Direct Method Based Control System for an Autonomous Quadrotor.* Journal of Intelligent & Robotic Systems, 2010. **60**(2): p. 285-316.

97. Ferrin, J., R. Leishman, R. Beard, and T. McLain. *Differential flatness based control of a rotorcraft for aggressive maneuvers*. in *2011 IEEE/RSJ International Conference on Intelligent Robots and Systems*. 2011.

98. Chamseddine, A., Y. Zhang, C.A. Rabbath, C. Join, and D. Theilliol, *Flatness-Based Trajectory Planning/Replanning for a Quadrotor Unmanned Aerial Vehicle.* IEEE Transactions on Aerospace and Electronic Systems, 2012. **48**(4): p. 2832-2848.

99. Tang, C.P., P.T. Miller, V.N. Krovi, J.C. Ryu, and S.K. Agrawal, *Differential Flatness Based Planning and Control of a Wheeled Mobile Manipulator 2014;Theory and Experiment.* IEEE/ASME Transactions on Mechatronics, 2011. **16**(4): p. 768-773.

100. Nieuwstadt, M.J.v. and R.M. Murray. *Approximate trajectory generation for differentially flat systems with zero dynamics*. in *Decision and Control, 1995., Proceedings of the 34th IEEE Conference on*. 1995.

101. Rigatos, G., *Nonlinear Control and Filtering Using Differential Flatness Approaches; Applications to Electromechanical Systems*. 2015: Springer International Publishing.

102. Thounthong, P., S. Pierfederici, and B. Davat, *Analysis of Differential Flatness-Based Control for a Fuel Cell Hybrid Power Source.* IEEE Transactions on Energy Conversion, 2010. **25**(3): p. 909-920.

103. Martin, P., R. Murray, and P. Rouchon, *Control system, Robotics and automation; Fault Analysis and Control; Encyclopedia of Life Support Systems* in *Flatness Based Design*. 2009, EOLSS.

104. Chapuis, C., E. Bideaux, X. Brun, and N. Minoiu-Enache. *Comparison of feedback linearization and flatness control for anti-slip regulation (ASR) of an hybrid vehicle: From theory to experimental results*. in *Control Conference (ECC), 2013 European*. 2013.

105. Alt, B., F. Antritter, and F. Svaricek. *Flatness based control for electric and hybrid electric vehicle drivetrains*. in *Control & Automation (MED), 2012 20th Mediterranean Conference on*. 2012.

106. Benaouadj, M., A. Aboubou, R. Saadi, M.Y. Ayad, M. Becherif, M. Bahri, and O. Akhrif. *Flatness control of batteries/supercapacitors hybrid sources for electric traction*. in *Power Engineering, Energy and Electrical Drives (POWERENG), 2013 Fourth International Conference on*. 2013.

107. Kahaner, D., C. Moler, and S. Nash, *Numerical Methods and Softward*. 1989, Englewood Cliffs, New Jersey: Prentice Hall, Inc.

108. MathWorks. *Piecewise Cubic Hermite Interpolating Polynomial*. 2016; Available from: https://uk.mathworks.com/, Accessed 8 October 2016.

109. Sire-Ramirez, H. and S.K. Agrawal, *Differentially Flat Systems*, ed. F.L. Lewis. 2004: Marcel Dekker, Inc.

110. YASA. *YASA 750 R Axial Flux Electric Motor Data Sheet*. 2016; Available from: http://www.yasamotors.com/, Accessed 9 November 2016

111. Chaturvedi, D.K., *Modeling and Simulation of systems Using MATLAB and Simulink*. 2010: CRC Press.

112. Sung Chul, O., *Evaluation of motor characteristics for hybrid electric vehicles using the hardware-in-the-loop concept.* IEEE Transactions on Vehicular Technology, 2005. **54**(3): p. 817-824.

113. Joeri, V.M., M. Gaston, and V.d.B. Peter *Simulation methodologies for innovative vehicle drive systems*.

114. Rippel, W. *Induction Versus DC Brushless Motors*. 2007; Available from: https://www.tesla.com/, Access 04 October 2016.

115. Battles, Z. and L.N. Trefethen, *An Extension of MATLAB to Continuous Functions and Operators.* SIAM Journal on Scientific Computing, 2004. **25**(5): p. 1743-1770.

116. Trefethen, L.N., *Approximation Theory and Approximation Practice (Other Titles in Applied Mathematics)*. 2012: Society for Industrial and Applied Mathematics. 318.

117. Clenshaw, C.W. and A.R. Curtis, *A method for numerical integration on an automatic computer.* Numerische Mathematik, 1960. **2**(1): p. 197-205.

118. Driscoll, T.A., N. Hale, and L.N. Trefethen (2014) *Chebfun Guide, 1st Edition, For Chebfun version 5*

119. Trefethen, L.N., *Computing numerically with functions instead of numbers.* Commun. ACM, 2007. **58**(10): p. 91-97.

120. Townsend, A. and L.N. Trefethen, *An Extension of Chebfun to Two Dimensions.* SIAM Journal on Scientific Computing, 2013. **35**(6): p. C495-C518.

121. Ryberg, A.-B., R.D. Bäckryd, and L. Nilsson, *Metamodel-Based Multidisciplinary Design Optimization for Automotive Applications*. 2012, Linköping University: Linköping.

122. Agte, J., O. de Weck, J. Sobieszczanski-Sobieski, P. Arendsen, A. Morris, and M. Spieck, *MDO: assessment and direction for advancement—an opinion of one international group.* Structural and Multidisciplinary Optimization, 2009. **40**(1): p. 17-33.

123. Sobieszczanski-Sobieski, J. and R.T. Haftka, *Multidisciplinary aerospace design optimization: survey of recent developments.* Structural optimization, 1997. **14**(1): p. 1-23.

124. Kroo, I. and V. Manning. *Collaborative optimization - Status and directions* in *8th Symposium on Multidisciplinary Analysis and Optimization Conferences*. 2000. Long Beach,CA,U.S.A.: American Institute of Aeronautics and Astronautics.

125. Yi, S.I., Shin,J.K., and Park, G.J., *Comparison of MDO methods with mathematical examples*. 2008.

126. Allison, J.T., M. Kokkolaras, and P.Y. Papalambros, *On selection of single-level formulations for complex system design optimization.* Journal of Mechanical Design, Transactions of the ASME, 2007.

127. Hulme, K.F. and C.L. Bloebaum, *A simulation-based comparison of multidisciplinary design optimization solution strategies using CASCADE.* Structural and Multidisciplinary Optimization, 2000. **19**(1): p. 17-35.

128. Cramer, E.J., J. J. E. Dennis, P.D. Frank, R.M. Lewis, and G.R. Shubin, *Problem Formulation for Multidisciplinary Optimization.* SIAM Journal on Optimization, 1994. **4**(4): p. 754-776.

129. Cramer, E.J., P.D. Frank, and G.R. Shubin, *On Alternative Problem Formulation for Multidisciplinary Design Optimisation*. 1992.

130. Allison, J., M. Kokkolaras, and P. Papalambros. *On the impact of coupling strength on complex system optimization for single-level formulations.* in *Proceedings of the ASME International Design Engineering Technical Conferences and Computers and Information in Engineering Conference - DETC2005*. 2005. Long Beach, CA, United States.

131. Hulme, K.F., and Bloebaum,C.L., *A Simulation-based comparison of multidisciplinary design optimisation solusion strategies using CASCADE*. 2000.

132. Cacuci, D.G., *Sensitivity and Uncertainty Analysis*. Vol. 1: Theory. 2003: Chapman and Hall/CRC Press, Boca Raton, FL.

133. Saltelli, A. (2005) *Global Sensitivity Analysis: An Introduction*. 27-43.

134. Wainwright, H.M., S. Finsterle, Y. Jung, Q. Zhou, and J.T. Birkholzer, *Making sense of global sensitivity analyses.* Computers & Geosciences, 2014. **65**: p. 84-94.

135. *What is Sensitivity Analysis? 2016*; Available from: http://uk.mathworks.com/, Accessed 21 Aug 2016.

136. *Global Optimization Toolbox*. *2016*; Available from: https://uk.mathworks.com/, Accessed 21 Aug 2016.

137. Kahaner, D., C. Moler, and S. Nash, *Numerical Methods and Software*. 1989: Prentice-Hall, Inc.

138. Trefethen, L.N., *A Hundred-dollar, Hundred-digit Challenge*, in *SIAM News*. 2002.

139. Rizzoni, G., L. Guzzella, and B.M. Baumann, *Unified modeling of hybrid electric vehicle drivetrains.* IEEE/ASME Transactions on Mechatronics, 1999. **4**(3): p. 246-257.

APPENDICES

Appendix A

Vehicle specification of Nissan Leaf

Motors	80	kw rate
type	synchronous motor	
Max torque	280	Nm
Max torque at	0-2730	rpm
Max Power at	2730 - 9800	rpm
Max speed	10390	rpm
Body		
Wheelbase	2690	mm
Curb weight	1,521	kg
coefficient of drag	0.29	
Frontal area	2.27	m^2
Transmition		
type	Single speed direct drive	
Final drvie ratio	7.94:1	
tire	P205/55R16	
Tire diameter	0.632	m
Performance		
Top speed	145	km/h
0-60 mph acceleration time	9.9	s
range	117 (EPA)	km
	175 (NEDC)	km
Battery		
Type	lithium ion battery	
	48 modules, 192 cells	
Capacity	24	kW·h
Specific energy	140	W·h/kg

Table A-1 Published vehicle specification of Nissan Leaf